Development and Application of a Chemical Degradation Model for Reinforced Electrolyte Membranes in Polymer Electrolyte Membrane Fuel Cells

by

Sumit Kundu

A thesis

presented to the University of Waterloo

in fulfillment of the

thesis requirement for the degree of

Doctor of Philosophy

in

Chemical Engineering

Waterloo, Ontario, Canada, 2008

Authors Declaration

I hereby declare that I am the sole author of this thesis. This is a true copy of the thesis, including any required final revisions, as accepted by my examiners.

I understand that my thesis may be made electronically available to the public.

_____

ABSTRACT

Fuel cells are electrochemical devices being developed for a variety of consumer applications including homes and vehicles. Before customers will accept this technology fuel cells must demonstrate suitable durability and reliability. One of the most important parts of a fuel cell stack is the polymer electrolyte membrane (PEM). This layer is responsible for conducting protons from anode to cathode and acting as a gas barrier, while operating in a harsh electrochemical environment. In order to develop better and more durable membranes researchers must understand the linkage between the causes of degradation, such as specific material properties and operational conditions.

One significant mode of degradation of the electrolyte membrane is through chemical degradation caused by the crossover of reactant gases leading to the formation of peroxide and ultimately radical species. These radicals are able to attack vulnerable groups in the polymer structure of the membrane. The result is membrane thinning, increased gas crossover, fluoride ion release, and voltage degradation. Considerable experimental work has been done to understand these mechanisms, although there has been no attempt to model the connection between the causes of degradation and the physical effects of degradation on the electrolyte membrane. Such a model can be used as a valuable tool when evaluating different degradation mechanisms, developing stronger materials, and enable estimation of the influence of fuel cell operation and system design on degradation.

This work presents the development and application of a dynamic semi-mechanistic chemical degradation model for a reinforced membrane in a polymer electrolyte membrane fuel cell. The model was developed using single cell testing with Gore™ PRIMEA® series 5510 catalyst coated membranes under open circuit voltage (OCV) conditions. Such conditions are useful for accelerated testing since they are believed to enhance chemical degradation in membranes since reactant gas partial pressures are at their maximum. It was found that the electrolyte layer closer to the cathode catalyst

preferentially degraded. Furthermore, cumulative fluoride release curves for the anode and cathode began to reach plateaus at similar times. The developed model proposes that as the cathode electrolyte layer is degraded, fluoride release slows due to a lack of reactants since the inert reinforcement layer creates a barrier between the cathode and anode electrolyte layers. It is also believed that all fluoride release originates at the degradation site at the cathode. By fitting key parameters, the fluoride release trends were simulated. The proposed model links material properties such as the membrane gas permeability, membrane thickness, and membrane reactivity, as well as operating parameters such as hydrogen partial pressure and relative humidity to fluoride release, thickness change, and crossover.

Further investigation into degradation at OCV operation and different relative humidity conditions showed that initial hydrogen crossover measurements were a good indicator of degradation rate over long testing times. The proposed semi-mechanistic model was able to best model the results when using a second order dependence on the hydrogen crossover term. In all cases there was some discrepancy between the model and experimental data after long times. This was attributed to the onset and contribution of anode side degradation.

The effect of drawing current on fluoride release was also investigated. Experimental results showed that with increasing current density the fluoride release rate decreased. Using the developed semi-mechanistic model it was proposed that a decrease in hydrogen crossover was primarily responsible for the reduction in chemical degradation of the membrane. A macro-homogeneous model of the anode catalyst layer was used to show that a reduction in hydrogen concentration through the catalyst layer when a current is drawn is a possible reason for the reduction in degradation.

Finally the model was applied to three different dynamic drive cycles. The model was able to show that over different drive cycles, the fuel cell will experience different degradation rates. Thus the developed model can be used as a potential tool to evaluate degradation in systems.

ACKNOWLEDGEMENTS

There have been many people that have made my time as a PhD student successful and enjoyable. First, I would like to thank Dr. Michael Fowler and Dr. Leonardo Simon, two great influences and great supervisors. They have been tremendous in helping me develop professionally through sending me to conferences, research, and supporting my job searches. Dr. Fowler has even given me insight into women, telling me, "…you are the type of guy that women settle down with."

I would also like to thank my committee members, Xianshe Feng, Pearl Sullivan, Mark Pritzker, and Gullian Goward, for taking the time to read, comment on, and hopefully enjoy my thesis.

Everyone in the fuel cell lab has also been great to work with, particularly Jeff, without whom I would have gone insane years ago. Jeff was always around to bounce ideas off of, to hear my PhD woes, and to just hang out with. It's been a pleasure to have worked with such a great scientist and friend. Also Matt who has been a great inspiration to me. I can never figure out how Matt juggles so many interesting projects all at once but it is something that I strive to mimic. Incidentally, both Jeff and Matt have provided me with lots of advice about women.

I would also like to thank my family for supporting my decisions and always feeding me when I needed it and of course for advice on how to find a girlfriend.

Finally, I would like to thank Crista who was instrumental to finishing this thesis. I met you in my last year and thanks to all the hints and tips from the previous four years we will be settling down together.

TABLE OF CONTENTS

LIST OF FIGURES

LIST OF TABLES

NOMENCLATURE

a	Catalytic surface area per volume	$m^2\ m^{-3}$
$A_{Pt,el}$	Platinum surface area	$m^2\ g^{-1}$
C_{F-}	Fluoride ion concentration	$mol\ L^{-1}$
$C_{H_2}^{ref}$	Hydrogen reference concentration	$mol\ m^{-3}$
C_{H_2}	Hydrogen concentration	$mol\ m^{-3}$
$C_{H_2,0}$	Hydrogen concentration at GDL-catalyst interface	$mol\ m^{-3}$
$C_{H_2,\delta_{cat}}$	Hydrogen concentration at catalyst-electrolyte interface	$mol\ m^{-3}$
D_i	Diffusion coefficient	$m^2\ s^{-1}$, $cm^2\ s^{-1}$
D_i^{eff}	Effective diffusion coefficient of species "i"	$m^2\ s^{-1}$
E°	Nernst Potential	V
EAS	Electrochemically active surface area	$m^2_{pt}\ cm^{-2}_{geo}$
F	Faraday's constant (96485)	$C\ mol^{-1}$
f_I	Cathode ionomer fraction	
$H_{H_2,w}$	Henry's law constant	$atm\ cm^3\ mol^{-1}$
i	Current density	$A\ cm^{-2}$
i_o	Exchange current density	$A\ cm^{-2}$
i_{H_2}	Hydrogen crossover current	$A\ cm^{-2}$
K_1	Proportionality constant	mol^{-1}
K_2	Proportionality constant	$mol\ cm^{-2}$
L_{ca}	Platinum loading	$mg\ cm^{-2}_{geo}$
n	Number of electrons transferred in an electrochemical reaction	
N_A	Flux of species A	$mol\ cm^{-2}\ s^{-1}$
p_A	Partial pressure of species A	mmHg
$P'_{M,A}$	Permeability of gas species A through a membrane	$A\ cm\ cm^{-2}\ mmHg^{-1}$
R	Ideal gas constant (8.314)	$J\ mol^{-1}\ K^{-1}$
R_v	Reaction rate	$mol\ m^{-3}\ s^{-1}$
R_Ω	Membrane resistance	ohms
T	Temperature	K
V_{Cell}	Cell Voltage	V
$V_{Cell,OCV\,i}$	Cell voltage at OCV	V
α	Transfer coefficient	
α_{AB}	Membrane selectivity	
δ_m	Membrane thickness	cm

δ_{IA}	Anode ionomer thickness	cm
δ_{IC}^{o}	Initial cathode ionomer thickness	cm
δ_{cat}	Catalyst layer thickness	m
ε	Porosity	
γ	Constant	
η_{act}	Activation loss (overpotential)	V
η_{ohmic}	Ohmic Loss (overpotential)	V
$\eta_{concentration}$	Concentration Loss (overpotential)	V
η_{ix}	Crossover overpotential	V
$\eta_{reversible}$	Reversible voltage loss	V
$\eta_{irreversible}$	Irreversible voltage loss	V

ABBREVIATIONS

CC	"Crossover current" – A measure of hydrogen crossover.
CV	"Cyclic Voltammetry" – Used to estimate active surface area.
CCM	"Catalyst Coated Membrane" – electrolyte and catalyst layers together. No Gas diffusion layer.
Cumulative fluoride release	The total amount of fluoride release on either the anode or cathode side.
DI	"Deionised Water"
EAS	"Electrochemically active surface area"
Fluoride release rate	The rate of fluoride release on either the anode or cathode side.
GDL	"Gas Diffusion Layer"
HPHT	"High Pressure High Temperature" – A type of polarization curve.
Ionomer membrane	Also known as the electrolyte membrane.
LPLT	"Low Pressure Low Temperature" – A type of polarization curve.
LPM	"Litres per Minute"
MEA	"Membrane Electrode Assembly" – A CCM with GDL layers.
MTTF	"Mean Time to Failure"
OCV	"Open Circuit Voltage" – The voltage when no current is flowing.
PEM	"Polymer Electrolyte Membrane"
PEMFC	"Polymer Electrolyte Membrane Fuel Cell"
Polarization Curve	A voltage versus current plot used to assess fuel cell performance.
Pol Curve	*See polarization curve*
SLPM	"Standard Litres per Minute" – 0°C, 1 atm.
Stoichiometry	The amount of excess reactant fed to the anode or cathode.
Stoich	*See Stoichiometry*
Test station	The unit used to test fuel cell and assess fuel cell performance.
Total cumulative fluoride release	The sum of anode and cathode fluoride release.

CHAPTER 1 : INTRODUCTION

1.1 OVERVIEW AND OBJECTIVES

Understanding fuel cell material durability problems is recognized as an important requirement for its greater commercialization. There has recently been considerable research in this area covering a wide variety of degradation modes such as catalyst layer degradation, mechanical and chemical degradation of the electrolyte membrane, also called the electrolyte membrane, and bi-polar plate durability. The bulk of the reported work has focused on experimental studies to provide evidence and establish mechanisms of degradation. Currently there are only a limited number of material degradation models that have been developed. Degradation models offer researchers and fuel cell developers insight into how material properties and operational conditions affect the lifetime characteristics of a fuel cell material or system. They can also help analyse different possible degradation mechanisms depending on how well they fit experimental data. When degradation models are linked to parameters that affect performance, they also create a powerful tool to design more durable systems and control algorithms that minimise degradation.

The overall objective of this work is to present the development of a dynamic semi-mechanistic chemical degradation model for a reinforced fuel cell electrolyte membrane. The model links material properties and operating conditions to the rate of material

degradation by simulating degradation indicators such as fluoride ion release. Also, attempts to link the material degradation to performance degradation are explored. As such, this research has three objectives:

1) To establish a mechanism of electrolyte degradation for GORE membranes.
2) To create a model that describes the degradation.
3) To apply the model to dynamic situations.

The proposed model is based on experimental work using accelerated degradation tests of fuel cells conducted under different relative humidity conditions and current densities.

1.2 SCOPE

The scope of this work is the examination of chemical degradation of the polymer electrolyte membrane (PEM) trademarked as Gore PRIMEA 5510 when used in single cells. The effect of relative humidity and current density are explored at constant temperature. Temperature effects are not included in this work although some discussion on the subject will be offered. Furthermore, the contribution of mechanical degradation and degradation of the catalyst layer or other fuel cell materials other than the electrolyte membrane is not specifically addressed in this work.

1.3 THESIS LAYOUT

The following chapters of this work will be organized in the following way as summarized below:

Chapter 2: Background and Preliminary Experimental Work – In this chapter the relevant background information from the literature necessary to understand this study and its significance will be presented. More importantly, this chapter presents experimental results performed to gain a fundamental understanding of the mechanism of chemical degradation. Some of the contents of this chapter were published in 3 journal papers.

Chapter 3: Experimental - This chapter will describe the main measurements and experimental techniques used for the subsequent studies. Further, this chapter will also describe the different materials used and the different experiments that were pursued.

Chapter 4: Effect of crossover and surface area on OCV – In this chapter, fundamental measurements that are linked to material properties will be used to show how knowledge of these parameters can lead to performance estimates such as OCV. Also, by understanding how these parameters change with time irreversible voltage degradation can be estimated.

Chapter 5: Development of a Chemical Degradation Model - This chapter follows the degradation of a fuel cell membrane under open circuit voltage conditions. Further, a mechanism is proposed that attempts to explain the observed behaviour. Finally, a model of the proposed mechanism is developed and fitted to the experimental data. This model will then be used to explain fluoride release trends in a second set of data obtained in an experiment that had been interrupted several times throughout the experiment.

Chapter 6: Effect of RH - In this section, the ability of the model to predict degradation under different relative humidity conditions will be explored. The predictive limitation of the model in cases of severe degradation will also be explored. Finally, the links between key chemical degradation factors and voltage degradation will be explored to determine if there are potential correlations between the two.

Chapter 7: Model Parameter Sensitivity - Having developed a model for chemical degradation in Chapter 3, the sensitivity of the model to different parameters will be examined. Furthermore, key indicators of degradation will be discussed.

Chapter 8: Current Density Effects - This chapter explores the extension of the open circuit voltage degradation model presented in Chapters 4 – 6 to include the effects of current flow. Experimental degradation studies at three current densities will be used to propose a mechanism to explain the observed fluoride release trends.

Chapter 9: Degradation potential of different load cycles – Having developed a closed circuit membrane chemical degradation model, the model will be used to evaluate the impact of three different drive cycles on chemical durability of the membrane. The load cycles are based on drive cycles used to evaluate vehicles and their use shows how a dynamic model can be used.

Chapter 10: Conclusions and future work – This chapter will review the main conclusions and identify the contributions to the scientific literature offered by this work as well as areas of future study.

Some of the work presented here has been published in various journals. A complete summary of the Author's publications is available in Appendix A.

CHAPTER 2 : BACKGROUND

2.1 FUEL CELL BACKGROUND

A fuel cell is a device, similar to a primary battery, which uses an electrochemical reaction to generate electricity. The main components of a fuel cell are the same as any electrochemical cell consisting of an anode, cathode and electrolyte. Unlike primary batteries however, fuel cells are given a continuous supply of reactants and therefore can produce power as long as the reactants are available. For vehicle applications, theoretical fuel cell efficiencies are higher than combustion engines because a fuel cell is not restricted to the Carnot cycle and instead directly converts fuel into useable electricity. Also, since fuel cells have no moving parts, they are potentially more reliable than typical internal combustion engines. There are many types of fuel cells, each categorized by the type of fuel used or the composition of the electrolyte. This thesis focuses on the polymer electrolyte membrane fuel cell (PEMFC) which takes hydrogen and oxygen as reactants and uses a solid polymer as electrolyte. The basic set-up of a fuel cell is shown in Figure 2-1.

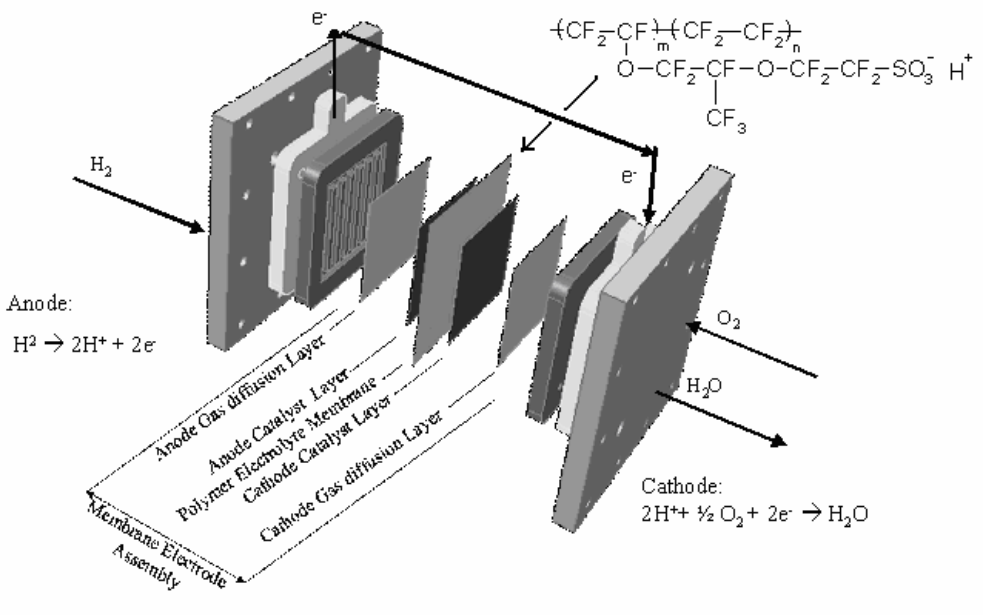

Figure 2-1: Schematic of a PEM fuel cell [1].

At the anode, hydrogen flows into the system through channels machined into the graphite bipolar plates. Hydrogen is transported from the channels, through a porous gas diffusion layer and a porous catalyst layer to react at platinum catalyst sites to produce hydrogen ions and electrons. The electrons flow through the external circuit and produce power while the protons are conducted through a solid polymer electrolyte. This polymer also serves as a gas barrier so that the reactant species can not freely combine together. The most common type of electrolyte used in fuel cell applications are perfluorosulfonic acid (PFSA) polymers. There are several different PFSA membranes available under different trade names, the most common one being Nafion^{TM} supplied by Dupont. The chemical structure of Nafion^{TM} is shown in Figure 2-1. The Teflon like backbone of Nafion^{TM} gives the membrane structural stability while the sulfonic acid groups allow Nafion^{TM} to act as a proton conductor when hydrated with water. At the cathode, the hydrogen ions, electrons, and oxygen (delivered by a second bipolar plate) combine on the cathode platinum catalyst to form water and heat. The composite material formed by the catalyst and electrolyte layers is typically called a catalyst coated membrane (CCM). When gas diffusion layers are included it is called a membrane electrode assembly (MEA).

The performance of a fuel cell is typically evaluated by using a polarization curve as shown in Figure 2-2. A polarization curve can be broken up into 4 parts each characterized by a loss from ideal Nernst voltage: a) open circuit voltage (OCV), b) an activation region, c) a linear ohmic loss region, and finally d) a mass transfer limited region. OCV, activation and ohmic regions of the polarization curve will be discussed with reference to a 0-Dimensional (0-D) fuel cell model to highlight the relevant material properties involved. Concentration polarization (or mass transfer limitation) is typically a function of gas diffusion layer properties and is beyond the scope of this project. The overall fuel cell performance equation is given in Equation (2-1)[2] which represents the cell voltage as the ideal Nernst voltage (E^0) minus different sources of voltage loss.

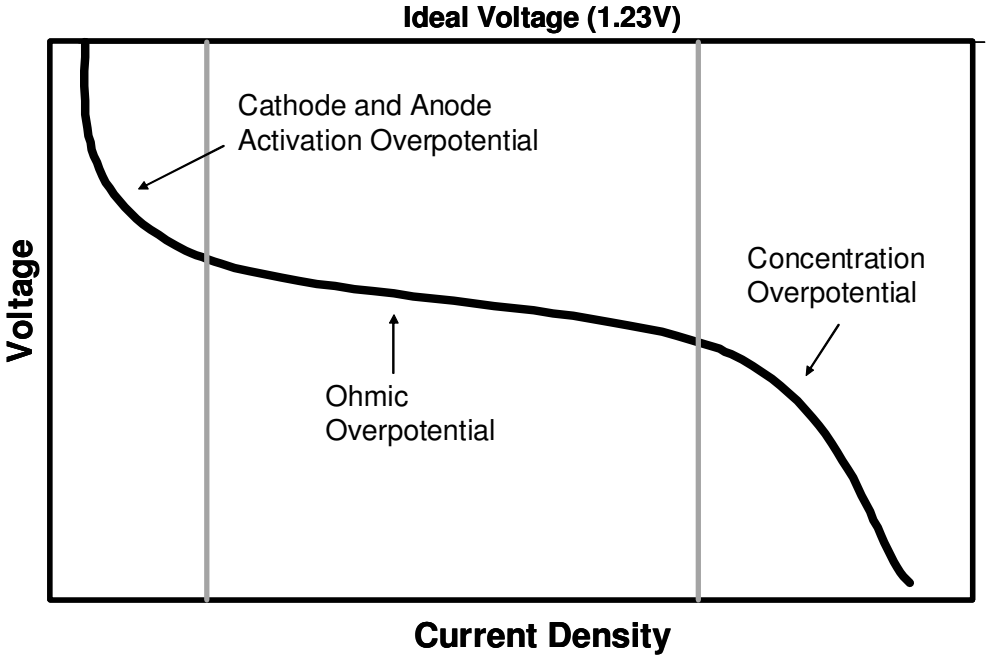

Figure 2-2: Regions of a polarization curve. Areas show where different losses are dominant.

$$V_{Cell} = E^{\circ} - \eta_{act} - \eta_{ohmic} - \eta_{concentration} \qquad \textbf{(2-1)}$$

When no current is flowing, cell voltage should approach the ideal equilibrium potential (E^0). However, internal currents caused by hydrogen crossover are believed to lower the open circuit potential below the Nernst potential. Activation loss (η_{act}) is a measure of how easily the hydrogen oxidation reaction (HOR) and oxygen reduction reaction (ORR) can proceed. Studies have shown that it is the ORR that causes the most voltage loss in a fuel cell and therefore the HOR contribution to activation overpotential is often neglected. The activation loss from the ORR is related to platinum surface area ($A_{Pt,el}$), platinum loading (L_{ca}), current and exchange current density (i_o) as well as the fuel cell current (i) using Equation (2-2)[3].

$$\eta_{act} = \frac{RT}{n\alpha F} \ln\left[\frac{i}{10 \cdot \left(L_{ca} A_{Pt,el}\right) \cdot i_o}\right] \tag{2-2}$$

where T is the absolute temperature, R is the universal gas constant, n is the number of electrons transferred (in this case 2), α is the transfer coefficient (taken to be 0.5), and F is Faraday's constant.

However, as will be discussed, due to the permeability of the electrolyte membrane some hydrogen is able to permeate, or "cross over", to the cathode. Once at the cathode, the hydrogen reacts at the cathode platinum catalyst sites with oxygen. In effect, the oxygen undergoes a reduction reaction at the cathode while hydrogen is oxidised at the same electrode and therefore activation losses for the ORR are incurred [4]. The voltage loss from hydrogen crossover can be estimated by modifying Equation (2-2) with a crossover current, i_{H_2}. The crossover current relates the molar flux of hydrogen permeating through the electrolyte membrane, N_{H_2}, to an equivalent current as shown in Equation (2-3). The flux is a mass transfer phenomenon and is independent of cell potential. The mechanism of hydrogen crossover is covered in section 2.3.1.

$$i_{H_2} = (N_{H_2})(2F) \tag{2-3}$$

Since hydrogen crossover to the cathode incurs activation losses Equation (2-2) becomes Equation (2-4) [3].

$$\eta_{act} = \frac{RT}{F} \ln\left[\frac{i + i_{H_2}}{10 \cdot \left(L_{ca} A_{Pt,el}\right) \cdot i_o}\right] \tag{2-4}$$

When no current is drawn, and thus only the hydrogen crossover causes voltage loss, the above term will be called the hydrogen crossover overpotential and denoted by η_{ix}.

Ohmic losses can also be modeled as a function of current using Ohm's law as shown in Equation (2-5)[3].

$$\eta_{ohmic} = iR_{\Omega} \tag{2-5}$$

R_{Ω} includes resistive contributions from proton flow through the electrolyte as well as protonic resistances through the catalyst layers. The conductivity and thickness of the electrolyte have a significant effect on this loss. Since water saturation of the membrane also plays a role, electrolyte conductivity is also a function of temperature and humidity as well as polymer structure including the presence, number, and size of proton-conducting sulfonic acid sites

The above description of fuel cell performance shows how fuel cell voltage is related to a number of different material parameters. When materials degrade in a fuel cell, these characteristics will inevitably change and consequently polarization characteristics will also change. For instance, loss of electrochemical surface area is typically seen as a downward translation of a typical polarization curve while increased proton resistance causes the slope in the linear region to become more negative [5]. Since modeling of fuel cell performance degradation can be done in this way, it then becomes important to understand and be able to predict how fast material properties change with time.

Not all losses to fuel cell performance are permanent, or irreversible. Instead, part of the voltage degradation over time can be attributed to reversible degradation and therefore is recoverable. Reversible degradation occurs often as a result of transient processes where the loss in voltage may be reversed by changing the operating conditions (or with the aid of an 'in-situ' recovery procedure) and consequently the cell performance may return to pre-degraded levels. An example of reversible degradation includes water retention in the GDL over time, commonly known as flooding. This process will reduce cell performance over time, although performance may be recovered by removing the excess water. Irreversible degradation includes irreversible changes to the fuel cell materials such as membrane thinning or loss of catalytic surface area from platinum migration or carbon corrosion. The type of mitigation strategy employed to minimize voltage degradation will be influenced by the cause and mode of degradation, and whether the degradation is reversible or irreversible. Therefore, it is important to understand if the observed voltage decay is due to reversible processes or due to irreversible materials degradation.

Understanding how material properties influence performance inevitably leads to the development of better materials. As discussed, membrane thickness has a significant effect on ohmic losses, thus state of the art membranes have become much thinner. In order to address mechanical stability problems inherent with thinner membranes, reinforcements have been added to the thin films. Some of these composite membranes use a porous polytetrafluoroethylene (PTFE) or an expanded PTFE (ePTFE) layer in the middle of the electrolyte membrane to provide mechanical strength [6-8]. Gore PRIMEA 5510 reinforced membranes (Figure 2-3) use such reinforcements sandwiched between two PFSA electrolyte layers.

Along with the role of conducting protons, the PEM must also act as a gas barrier between the anode and cathode and provide mechanical strength to the MEA. As such, it is important to employ a material that is durable and reliable in a fuel cell. As discussed, material properties such as the permeability, conductivity, and thickness all play a role in its effectiveness. In order to design new materials which can achieve these goals as well

as resist degradation it is necessary to understand how the electrolyte membrane degrades.

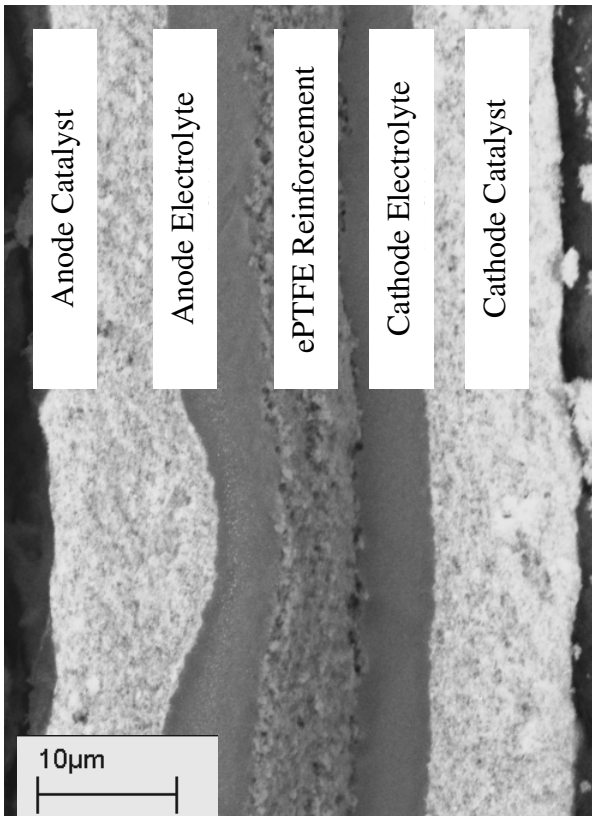

Figure 2-3: Gore PRIMEA 5510 reinforced catalyst coated membrane using PFSA for the anode and cathode electrolyte layers and an ePTFE reinforcement layer at the centre.

2.2 Introduction to Fuel Cell Degradation

Fuel cell degradation processes can be categorized according to causes, modes, and effects, as depicted in Figure 2-4 [9]. *Causes* include intrinsic material properties, material defects as well as assembly procedures, operational conditions and age, and maintenance procedures. These factors, once set, effectively determine how long a fuel cell will operate and by what modes the materials will degrade. For the most part, the fuel cell manufacturer or members of the supply chain have some measure of control over the causes, specifically membrane properties and quality. Manufacturers may select materials with certain properties, operate the fuel cells under certain conditions, and design special

maintenance procedures. However, some causes are more random and therefore difficult to control such as the appearance of defects in materials [9] or slight differences in assembly from fuel cell to fuel cell.

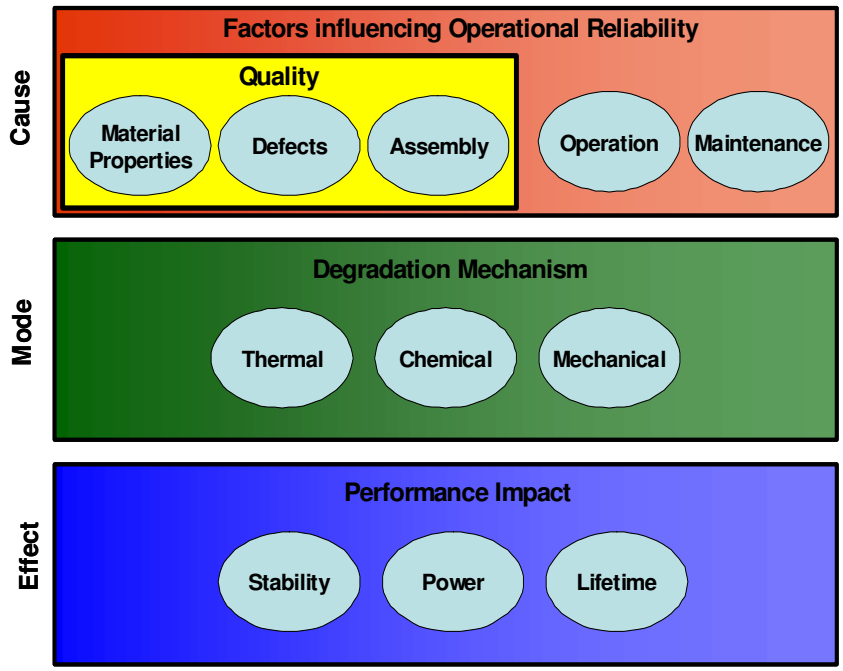

Figure 2-4: Degradation process schematic for a PEM fuel cell [9].

The *modes* of degradation for a fuel cell are determined by the causes. These modes can be broadly categorized as thermal, chemical, or mechanical in nature, though modes may also combine several aspects of these categories [9-11]. The final category contains the *effects* of degradation. These represent the influence that a degradation of fuel cell materials has on the final performance of the cell. The effects may be numerous, however, the most important ones are those defined by the end-user and by safety guidelines. The final effect that degradation has is often used to determine when fuel cell failure has occurred as in the case of increased hydrogen crossover and voltage loss [10,12].

In order to be suitable for commercialization, fuel cells must be able to operate for long periods of time. In the case of fuel cells for automotive applications, the time is over 5,000 hours [13] while for stationary applications the length of time could be over 40,000

hours [14]. As such, it is impractical and costly to run full lifetime tests. For this reason, fuel cell developers use accelerated durability test protocols. These tests attempt to increase the severity of the operating condition through the use of high temperatures, low relative humidity, and fast cycling. Often, accelerated tests also attempt to focus on one particular degradation mode to make it easier to study. Accelerated tests are often categorized by the main operating parameters which impact degradation. They typically focus on promoting degradation by a specific mode (i.e. either thermal, chemical, mechanical). These categories include reactant contamination [15-17] (chemical), load cycling [18] [19,20](chemical + mechanical), and freeze/thaw and temperature cycling [21-24] (mechanical), hydration cycling [12,25,26] (mechanical), high temperatures [27] (thermal).

2.3 Chemical Degradation of Fuel Cell Electrolytes

Although the electrolyte membrane in a fuel cell is one of the most important materials for successful operation, there are many causes and degradation modes related to failure of this layer [10]. One mode considered to be a leading factor for poor membrane life is chemical degradation. It has been proposed that carboxylic end groups left over from the Nafion™ manufacturing process may be susceptible to attack by radical species generated during fuel cell reactions [28].

The proposed mechanism is as follows:

Step 1: $R\text{-}CF_2COOH + OH\bullet \rightarrow R\text{-}CF_2\bullet + CO_2 + H_2O$

Step 2: $R\text{-}CF_2\bullet + OH\bullet \rightarrow R\text{-}CF_2OH \rightarrow R\text{-}COF + HF$

Step 3: $R\text{-}COF + H_2O \rightarrow R\text{-}COOH + HF$

The radical species, such as hydroxyl radicals, are thought to be formed by the decay of hydrogen peroxide which is an intermediate of the electrochemical oxygen reduction reaction; additionally it has been proposed that hydrogen or oxygen permeating to the anode catalyst layer may react to also produce peroxide species [10,28-31]. The result of

chemical degradation is membrane thinning as the electrolyte is consumed, increased gas crossover, the release of fluoride ions, and ultimately voltage degradation. The main parts of the degradation process can be summarized in three steps which will be discussed in detail:

1) reactant gas crossover;
2) peroxide and radical generation; and
3) polymer degradation leading to thinning, crossover, fluoride release, and voltage degradation.

2.3.1 Reactant gas Crossover

As with any polymer membrane, the polymer electrolyte of a fuel cell allows some gas to permeate across it. Crossover rates of different gases have been measured for Nafion™ membranes [32-34], and can be broadly described by Fick's law [35] as shown in Equation (2-6). P_M is the membrane permeability, p_I and p_{II} are the partial pressures of the gas of interest on either side of the membrane, N_A is the flux of the gas species across the membrane of thickness (δ).

$$N_A = \frac{P_{M,A}(p_I - p_{II})}{\delta} \tag{2-6}$$

The value of P_M depends on the type of permeation behaviour. For solution diffusion type behaviour, which is common for solid polymer membranes such as Nafion™, the permeability is related to the permeating gas and factors such as the molecular size, solubility, and affinity to the substrate [36]. In the case of Nafion™ 117, the permeability for five different gases was measured by Chiou and coworkers [34] to decrease in the following order: He, H_2, O_2, Ar, and N_2. Inspection of Equation (2-6) shows that if a membrane thins during chemical degradation (assuming no significant change in the permeability coefficient) the gas flux through the membrane (crossover rate) will increase.

The selectivity of the membrane to gas A relative to that for gas B, α_{AB}, can be defined using Equation (2-7).

$$\alpha_{AB} = \frac{N_A}{N_B} \tag{2-7}$$

The H_2/O_2 selectivity of Nafion^{TM} membranes has been reported to range between 2.1 [32,33] and 8.6 [34]. This means that hydrogen is at least twice as permeable as oxygen. Since the crossover rate is also related to the partial pressure of the gases, the crossover rate of hydrogen would be at least 10 times higher than the crossover rate of oxygen under fuel cell operation with air

The electrical current being drawn from a cell also has an effect on the crossover rates. As reactant gas diffuses through the porous catalyst layer it is consumed. As a result of this diffusion-reaction process, the concentration of reactant decreases from the GDL/catalyst interface to the catalyst/membrane interface. The final concentration of reactant at the catalyst/membrane interface is dependent on the rate of reaction. The higher reaction rates at higher currents reduce the gas concentration at the electrolyte membrane surface. Since this concentration is also the driving force for gas permeation, the rate of crossover is also reduced with increasing current. This effect has been modeled by two authors [37,38] showing that with increased current density the crossover will decrease.

2.3.2 Peroxide and radical generation

There are few studies in the literature that directly measure peroxide concentration or peroxide generation within the fuel cell. The primary reason for this is that peroxide is particularly difficult to measure because of its high reactivity and low concentrations. Studies therefore must infer information from secondary measurement when studying peroxide generation and radical attack. This section will review the current literature concerning in-situ and ex-situ testing.

Peroxide is thought to form in a fuel cell by several possible mechanisms.

1) electrochemically at the anode;
2) direct reaction between hydrogen and oxygen; and
3) electrochemically at the cathode as a by-product of the oxygen reduction reaction (ORR).

Ex-situ experiments studying the effect of hydroxyl radical attack on Nafion™ membranes have been carried out. Ex-situ accelerated chemical degradation experiments of fuel cell electrolytes most commonly employ Fenton's reagents. Fenton's reagents are made by combining hydrogen peroxide with Fe^{2+} ions in order to produce radicals as shown:

Fenton's Reaction: $H_2O_2 + Fe^{2+} \rightarrow Fe^{3+} + OH\bullet + OH^-$

Two main methods have been employed to study the degradation of Nafion™ membranes by Fenton's type reaction. The first method exposes the membrane to a solution of peroxide and metal ions (solution method) [31] [39] [40] [1] while the second method exchanges the metal ions with the acid sites of the polymer before exposure to peroxide (exchange method) [1] [14,30].

The results of ex-situ studies vary because of the wide range of experimental conditions used. Peroxide solution concentrations used in the experiments range from 12% to 30% and iron concentrations range between 4 and 280 ppm. In all cases fluoride ions were measured as a by-product [1,14,30,31,39,40]. Healy et al. [31] compared degradation products from samples of Nafion™ degraded with a Fenton's solution containing 4 – 16 ppm Fe^{2+} and 29% H_2O_2 with degradation products from an in-situ experiment. Using F^{19} NMR they found that degradation of the membrane released chemical compounds that shared many chemical signals as those released by membranes degraded during fuel cell testing. Not only did they identify fluoride ions in the Fenton's solution water but also identified a fluorinated species with similar characteristics as the side chains of Nafion™. It was suggested that as the fluorinated backbone of Nafion™ degraded it would release

the side chain components. Tang and coworkers [39] also found that fluoride containing polymer fragments entered into the degradation solution.

In addition to the analysis of chemical products that are released during degradation, some authors have also examined the changes to the polymer membrane structure. Inaba and Kinumoto [14,30] performed work with a Fenton's reagent consisting of 30% H_2O_2. Instead of adding iron and peroxide together and exposing Nafion^{TM} to the mixture, they first exchanged iron and other metallic cations into samples of Nafion^{TM} and then added peroxide (Exchange method). They also measured fluoride and sulphate release with ion chromatography and estimated that almost 70% of the initial number of C-F bonds were broken and almost 35% of SO_3^- groups had degraded. Furthermore, a small amount of S=O bonds were identified in the polymer film after degradation using FTIR. On the other hand, Tang and coworkers [39] found no significant new peaks in the FTIR spectra of the degraded membranes. Other common measurements are changes in membrane morphology such as those by Wayne [40] and Tang and coworkers [39]. Other measurements reported in the literature include a reduction in relaxation temperatures, Young's modulus, and weight [1,30,39].

In the first of three preliminary experimental works performed by the author, the difference between two different ex-situ tests was examined. Ex-situ degradation of Nafion^{TM} 112 membranes was studied using a Fenton's reagent with 16 ppm Fe^{2+}, as well as Nafion^{TM} in the exchanged Fe^{2+} form, over several days to investigate the chemical, morphological and mechanical changes in the membrane. The goal was to examine any differences between the two methods of degradation as well as develop a set of features for each degradation method which could be compared against membranes degraded in-situ. The study found no changes in oxygen-to-fluorine atomic ratio and the ion exchange capacity after degradation by both methods indicating no change in backbone to side chain ratio of the remaining polymer.

Despite there being no significant chemical differences between the two degradation methods, differences in morphology of the degraded samples were observed. The

membranes degraded by the solution method had many holes and tears. Large bubbles on the surface and cross-sections revealed that they originated at the centre of the membrane, splitting it in two as shown in Figure 2-5. Membranes degraded by the exchange method did not split into two but instead areas close to the surface appeared 'foamy'. The thickness of the membranes did not change appreciably in both cases although upon degradation, the swollen width increased while the membrane shrank slightly in length.

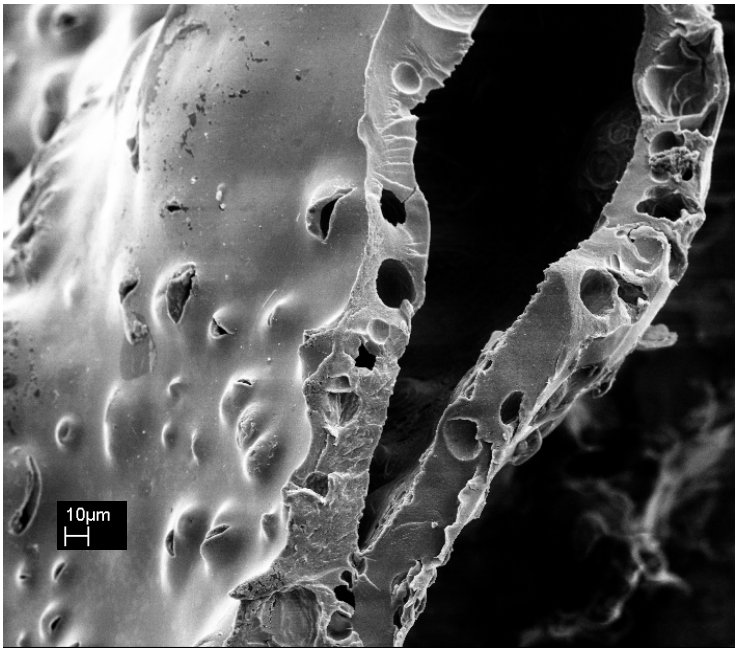

Figure 2-5: Nafion^{TM} 112 degraded by Fenton's testing (solution method) [1].

Mechanical and gas barrier properties were also examined for the degraded membranes. In both degradation methods the modulus decreased with exposure time which was attributed to the reduction in molecular weight of the polymer chains. This was also observed in dynamic mechanical results of the storage modulus. The peak height of the loss tangent curve in dynamic mechanical experiments was lower with increased degradation. This may indicate that ionic clusters in the membrane made up of sulfonic acid groups, shrank as the polymer was degraded. The transition temperature however increased with exposure to the Fenton's reagent which may indicate that the smaller ionic clusters were also more stable. In general, cumulative fluoride release correlated with

weight loss of the electrolyte as shown in Figure 2-6 a) and b). This work was published in the Journal of Power Sources [1].

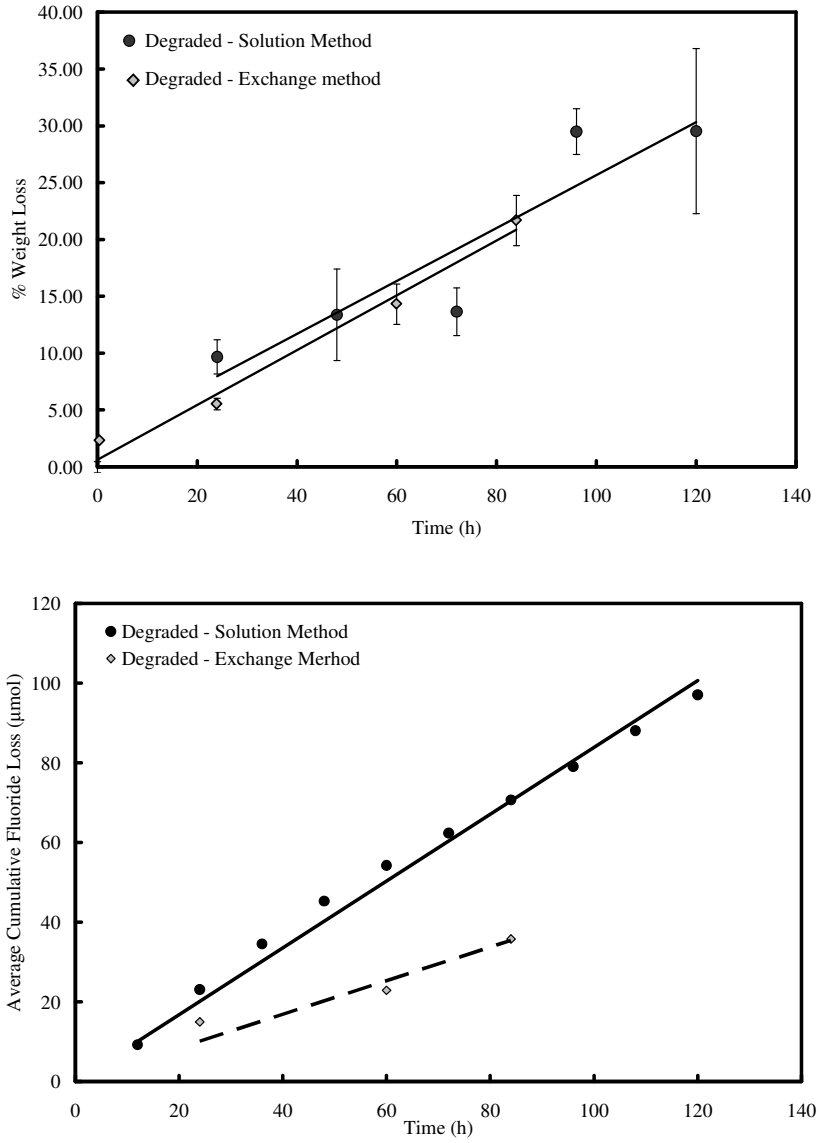

Figure 2-6 : a) Weight loss and b) cumulative fluoride release trends for an ex-situ electrolyte membrane degradation study using Fenton's testing [1].

The advantage of the above ex-situ tests is that it allows easy comparison of the chemical stability of the different membrane materials. However, a Fenton's test does not completely describe the complex environment of a fuel cell and thus has limited applicability to fuel cell electrolytes degraded in-situ. Ex-situ experiments using a system

that more closely resembles a fuel cell have been used to study the production of peroxide within the fuel cell. One technique that has been reported is the use of an anode-only and a cathode-only fuel cell, as illustrated in **Figure 2-7**. In such cells, only the anode or cathode catalyst layer is present. When hydrogen and air are introduced to the system, gas crossover occurs. Peroxide generated at the catalyst site then diffuses across the membrane where it is measured.

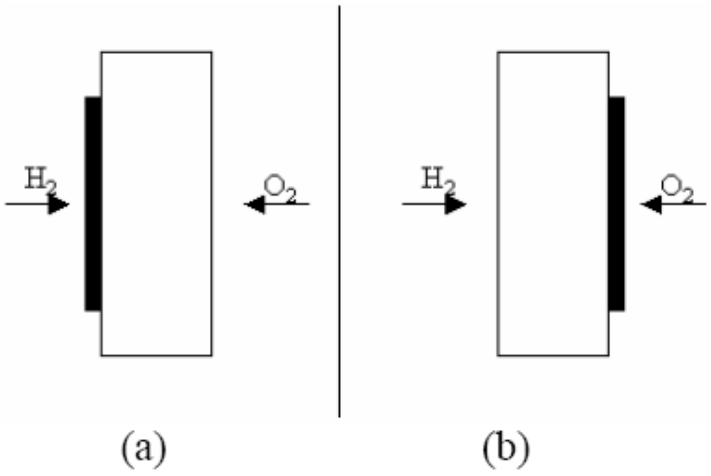

Figure 2-7: Novel ex-situ degradation membrane set up, a) Anode only mode, b) cathode only [41].

Chen and Fuller [42] used this technique to study the effect of changing the partial pressure of air to influence the crossover of oxygen. They found that there was an increase in peroxide formation with increasing partial pressure. Chen also used a completely in-situ degradation method to measure peroxide concentrations. In-situ accelerated tests are also important when studying degradation. These experiments use a working fuel cell under specific operating conditions to promote failure by a certain degradation mechanism.

Chen and Fuller [42] used a full catalyst-coated membrane in a fuel cell under open circuit voltage conditions to promote peroxide generation. They studied the effect of

hydrogen and oxygen partial pressure on the concentration of peroxide found in the membrane. Peroxide concentration was measured by quickly disassembling the fuel cell periodically, removing the catalyst layers, and finally stabilizing the peroxide within the membrane in a form that could be detected. They found that both hydrogen and oxygen partial pressure had an impact on the peroxide concentration though they found that the oxygen partial pressure effect would plateau at moderately high pressures.

In a separate study by Liu and coworkers [43], peroxide was measured in-situ by placing micro electrodes within the electrolyte membrane at locations near the anode and cathode catalyst layer. This work examined the influence of membrane thickness on the concentration of peroxide species. They found that an increase in membrane thickness reduced the peroxide concentration. This is presumably because gas crossover decreases with increasing thickness.

The production of radical species has also been measured by Panchenko *et al* [29] using a electron paramagnetic resonator and chemical species added during fuel cell operation to trap and stabilize radical species so that they can be detected. The study was able to measure radical species at both the anode and the cathode. In a separate study, Kardirov [44] used the same technique and concluded that cation contaminants played important roles in the degradation process.

Despite the measurement of peroxide with anode and cathode-only cells and in-situ measurements, there is still some ambiguity as to the main source of peroxide leading to polymer degradation. It is not clear if anode peroxide generation, cathode peroxide generation, or both are the source of reactant for the degradation reactions.

2.3.3 Thinning, crossover, fluoride ion release, and voltage degradation

As discussed in the previous section, the in-situ measurement of peroxide concentration is difficult. The few examples where it has been done showed that peroxide is generated, but not necessarily where it is generated. It is therefore still a question as to whether anode or cathode peroxide generation is the primary source of peroxide for membrane

degradation. An alternative method for examining this is to observe where degradation takes place in the membrane and measuring variables related to the chemical degradation. The assumption of many of these studies is that the location of degradation is likely close to the point of peroxide generation.

There are four main observations commonly used to identify chemical degradation of the electrolyte membrane. First is membrane thinning which occurs as the membrane is consumed. This has been observed by Healy and coworkers [31] and others [45,46]. Membrane thinning is an excellent method for observing degradation, although this measure provides little insight into where degradation is occurring since there is no way to distinguish degradation close to the anode versus the cathode side. Another difficulty with membrane thinning is that it can only be measured once the fuel cell has been dismantled.

For this reason, a second observation, hydrogen crossover rates, are also used as a measure of membrane integrity. Inspection of Fick's law, Equation (2-6), shows that a decrease in membrane thickness would result in an increase in hydrogen crossover. Unfortunately, mechanical failures in the membrane would also be observed as increased crossover and therefore there is no guarantee that all crossover increases are related to thinning.

In a second set of preliminary experimental work, it was shown that it is possible to determine when a mechanical integrity failure has occurred and when membrane thinning is dominant using gas selectivity measurements. It was proposed by the author that in an operating fuel cell, gas crossover would be limited by the electrolyte membrane and therefore gas selectivity of the membrane electrode assembly would resemble selectivity of the membrane. However, with a large integrity failure, the membrane would cease to be the limiting component and instead the catalyst layer or gas diffusion layer would be the limiting material. Since these materials are porous, it was proposed that gas selectivity would begin to have Knudsen diffusion characteristics. With Knudsen

diffusion, the rate of diffusion is related to the inverse root of the molecular weight and thus gas selectivity is given by

$$\alpha_{AB} = \frac{N_A}{N_B} = \frac{\sqrt{M_B}}{\sqrt{M_A}} \qquad \textbf{(2-8)}$$

With the use of selectivity measurements, Equation (2-8), of different gases, it would be possible to distinguish between membrane thinning and the onset of integrity failures in a membrane electrode assembly. Thinning is considered to have no impact on gas selectivity of the electrolyte membrane while still allowing gas crossover and apparent permeability to increase. The presence of holes and defects however will shift the permeability characteristics from solution diffusion behaviour through the electrolyte to Knudsen behaviour.

Through the use of gas crossover measurements of five gases (H_2, N_2, He, O_2, Ar) across a fuel cell membrane electrode assembly subjected to an open circuit voltage (OCV) durability experiment and subsequent calculation of permeability and selectivity, it was shown that the onset of a mechanical failure could be identified. Overall, with degradation the apparent permeability of gases through the MEA increased exponentially. The results showed that with extended operation at OCV gas permeation behaviour changed from one characterized by solution diffusion behaviour (indicating that the polymer electrolyte membrane was defect-free and therefore controlling the permeation rate) to one that followed Knudsen behaviour (indicating that defects had formed in the membrane and the catalyst/gas diffusion layer was controlling permeation rates). Plots of selectivity versus time, as shown in Figure 2-8, showed that immediately from the start of the durability experiment the selectivity decreased indicating that most of the increased apparent permeability was due to integrity failures though thinning would also be expected to occur simultaneously.

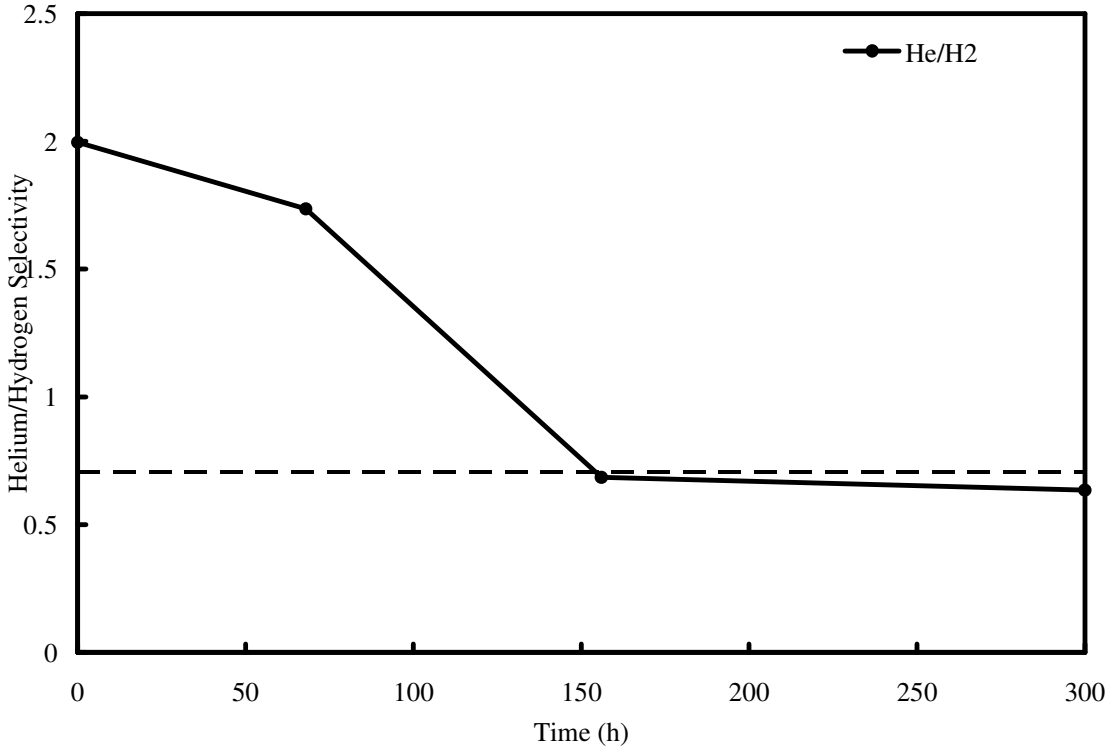

Figure 2-8: Gas selectivity as a function of testing time during an OCV test. The dashed line represents the theoretical value from Equation (2-8) [47].

The change from solution diffusion behaviour to Knudsen behaviour i.e. defect-free to that due to integrity failures, coincided with an increase in the voltage degradation rate and a significant drop in performance as shown by polarization curve measurements. Furthermore, the rate of fluoride ion release increased after the onset of integrity defects, which is consistent with observations of increasing crossover rates. Examination of the decatalyzed membrane with scanning electron microscopy revealed rips and tears in the membrane confirming the interpretation based on the selectivity data. This work was published in the Journal of Power Sources [47].

The third observation is the release of fluoride ions into the effluent water streams. Due to the link between reactant gas crossover and degradation as discussed, measurements of increased gas crossover are generally seen with increases in fluoride release rates as seen by Inaba and coworkers [30]. The most common method for identifying the side of

degradation is to observe the fluoride release rates from the anode and cathode. An alternative observation is the measurement of fluoride emission rate (FER). As suggested by the degradation mechanism, as the PFSA membranes degrade they will release HF as a degradation product. In-situ open circuit voltage (OCV) experiments [48-51] typically observe an increase in fluoride emission rate with time. Many papers have related the side where most of the fluoride is released to the side where degradation is predominant. However, there is no consensus in the literature of where the most fluoride comes from.

In a third preliminary study, the effect of current density and fuel cell material selection on degradation was examined. Under baseline conditions (anode/cathode stoichiometry of 1.4/3 and anode/cathode RH of 100%/60%) and only one GDL with micro porous layer (MPL) on the anode the total fluoride release rate was observed to decrease with increasing current density. This was attributed to changes in hydrogen crossover at higher currents. Cathode fluoride release was higher than anode release which is thought to be due to degradation being close to the cathode catalyst/ionomer interface as well as convective transport of fluoride ions as shown in Figure 2-9. Changes in water drag characteristics were responsible for decreasing cathode fluoride release and increasing anode fluoride release with increasing current density.

Analysis of the morphology of the membranes revealed that the MEA with only one MPL had a thinner membrane than that with MPLs on both electrodes. The membrane in the baseline construction showed thinning of approximately 7.8 μm and a total cumulative fluoride release of 10.1 μmol cm^{-2} while the MEA with two MPLs had a 0.8 μm decrease in thickness and a fluoride loss of 0.5 μmol cm^{-2}. Calculations indicated that both thickness changes would result in a voltage drop that was within experimental variability as a result of the increased hydrogen crossover. This was consistent with polarization curve measurements throughout the cell life. Changes in cathode stoichiometry and relative humidity did not correlate well with fluoride release measurements. This work was published in the Journal of Power Sources [46].

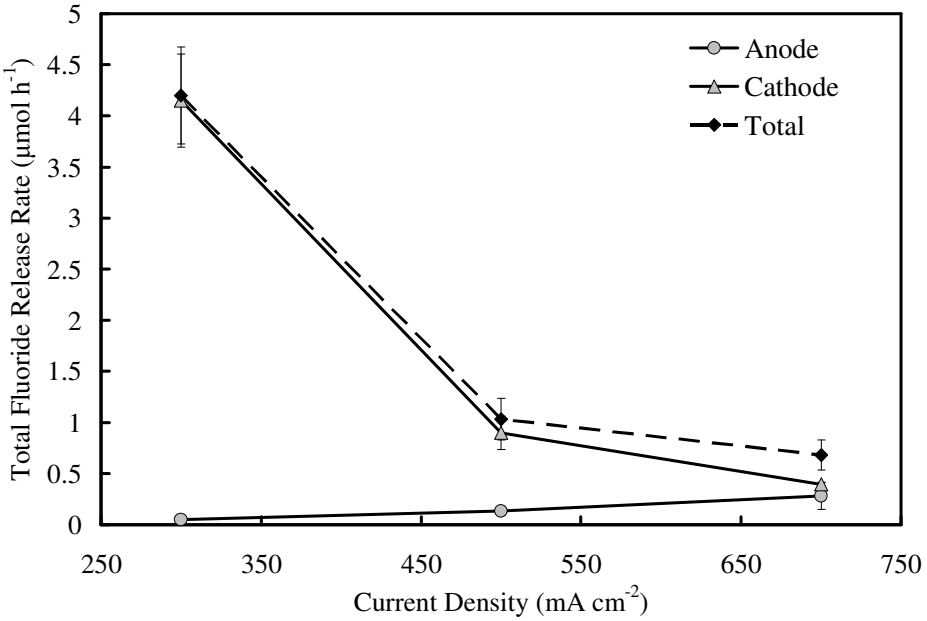

Figure 2-9: The effect of current density on fluoride release rate [46].

Mittal and coworkers [41,52,53] used anode and cathode-only cells to compare fluoride ion emission rates when hydrogen was a crossover gas and when oxygen was the crossover gas. They found that FER increased with increasing partial pressure and decreased with increasing membrane thickness which indicated that crossover was an important factor in degradation.

Finally, the fourth observation of OCV experiments is voltage degradation. Unlike fluoride release rates, voltage degradation is not as direct of a measurement of chemical degradation because both electrolyte degradation and catalyst layer degradation, among other sources, may cause the voltage to drop.

Membrane thinning, gas crossover, fluoride release, and open circuit voltage degradation rates are inter-related and constitute a cycle of degradation illustrated in **Figure 2-10.** Gas crossover due to the natural permeability of the electrolyte membrane instigates the degradation process. As the polymeric structure of the membrane degrades, it will thin due to the loss of material and simultaneously release fluoride ions. The membrane thinning increases hydrogen crossover. The increased hydrogen crossover will cause the

deviation of measured OCV and theoretical OCV due to the mixed potential effect described by Equation (2-4) [3,4,54]. As such, as hydrogen crossover increases through a membrane the open circuit voltage will become lower. Furthermore, the increased hydrogen crossover will cause an increase in the degradation rate as measured by fluoride ion release.

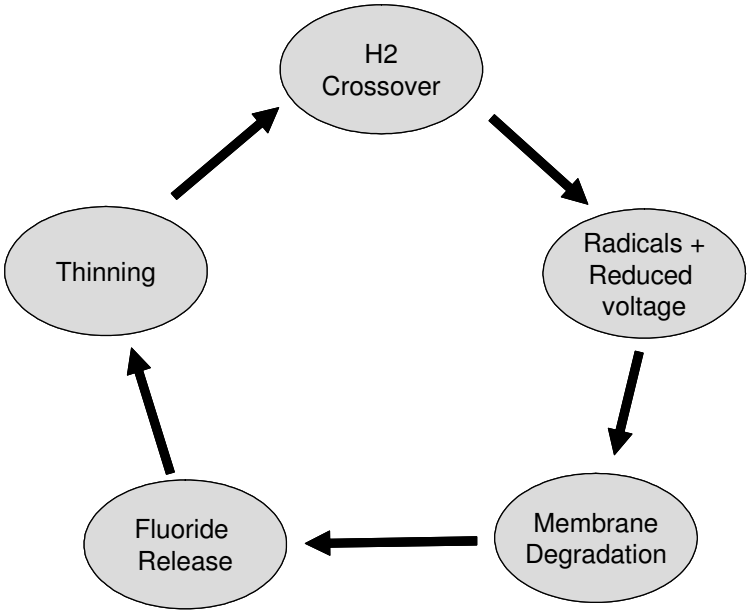

Figure 2-10: Schematic view of the chemical degradation mode cycle.

2.3.4 Platinum Band Theory

An alternative theory to the mechanism of degradation has recently been presented in the literature. Some research groups assert that the production of peroxide, and the location of degradation can be linked to the formation of a platinum band within the electrolyte membrane as shown in **Figure 2-11**.

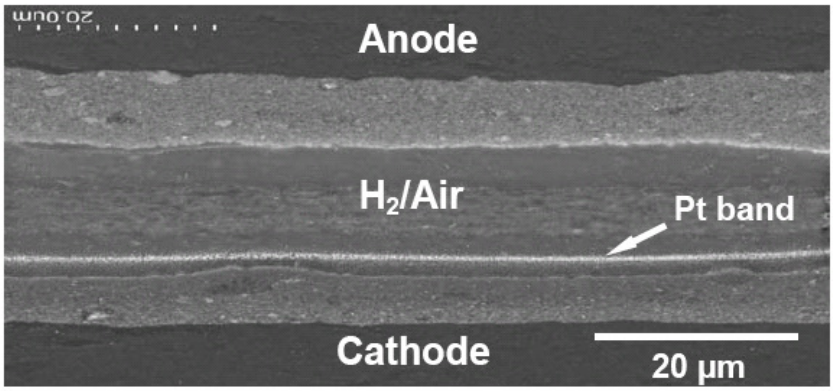

Figure 2-11: Image of the platinum band within the electrolyte layer of a CCM [55].

Work by Bi *et al* [56] and Ohma *et al* [50,57] have observed the platinum band within the electrolyte membrane. Further, they found that increasing the partial pressure of oxygen tended to shift the band location closer to the anode catalyst layer while the opposite was true when hydrogen partial pressure was increased. The shifts in the platinum band location also corresponded to the side with the most fluoride release, though water balance calculations were not done. When the band was close to the cathode, cathode side fluoride release tended to dominate over anode fluoride release. However, Endoh *et al* [58] showed that the degraded portion of an electrolyte cross section does not necessarily correspond to the Pt band location. Using FTIR they found membrane degradation products close to the anode catalyst despite the presence of a platinum band close to the cathode catalyst layer.

2.4 Review of Fuel Cell Degradation Models

The main focus of this work is the development of a degradation model which adequately links the causes of a chemical degradation mode to material changes and consequently changes in performance. There are many different degradation models available in the literature which focus on different modes and it is useful to review these models in order to understand their function and utility.

Generally, fuel cell degradation models can be characterized as being highly detailed mechanistic models or more simple statistical relations. In between these two extremes are semi-mechanistic models. Each type of model has its own strengths and weaknesses and can find use in different applications.

2.4.1 Mechanistic Models

A number of mechanistic degradation models have been reported in the literature. However, these are primarily steady state models and therefore do not attempt to predict how degradation will evolve with time. In general terms, they link the causes of degradation, such as material properties and fuel cell assembly, to degradation modes in order to show that they are possible. The best examples of these types of models are those that predict mechanical stresses on the membrane from fuel cell compression.

Lee *et al.* [59], Cleghorn *et al* [25], and Huang *et al* [26] used a 3-D stress model of a single cell to determine the location of the greatest stresses on the electrolyte membrane and hence where mechanical degradation may be likely to occur. These models combined parameters such as cell assembly variables, number of cells, and operational parameters such as the temperature, with material properties such as tensile modulus and Poisson ratio to predict where membranes would tear. In all cases, the detrimental impact of a mechanical failure was implied in these models although no experimental data were presented to support the claims. Similar models of catalyst support degradation by carbon corrosion have also been proposed. The mechanism of carbon corrosion purports that oxygen existing on the anode side during start-up is involved in reactions which consume the carbon in the cathode catalyst [60,61]. Carbon corrosion models in the literature typically concentrate on a cross-section, as shown in **Figure 2-12**, and are typically steady state.

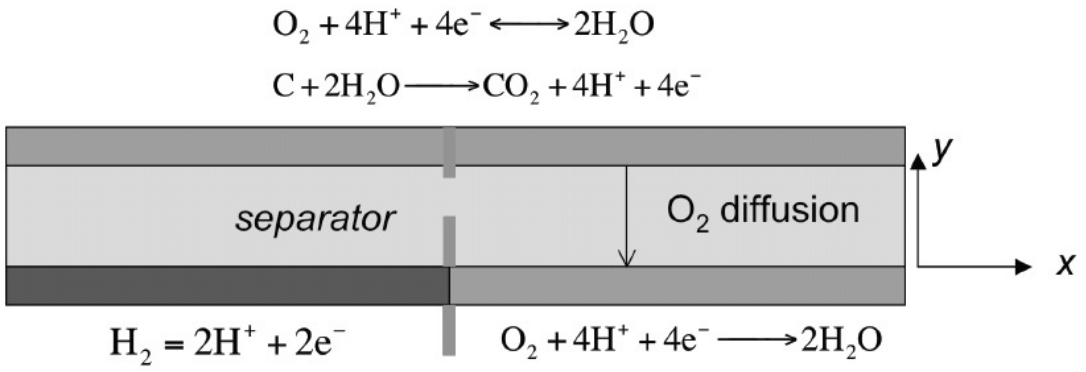

Figure 2-12: Carbon corrosion model domain and processes [62].

From the point of view of chemical degradation, the main mechanistic models that have been developed are those that attempt to predict where the platinum band may form in the membrane [55]. Other than this, no other attempts to model the effects of the proposed degradation mechanisms have been presented thus far and compared to experimental data. A separate model dealing with chemical membrane degradation has been proposed by Liu *et al*. [18] who used data such as crossover and surface area measurements over the testing time, as the basis for a steady state 0-D fuel cell voltage model similar to the discussed 0-D model above. In this work, material property changes were measured with time and the effect on voltage was estimated. No mechanistic model that predicted the change in material properties as a result of operating conditions has been reported.

The strengths of the mechanistic models that have been pursued are that they allow a deep understanding of the influence of different causes on the severity of degradation. As such, they are useful when attempting to compare the results of different materials. However, since these models are typically steady state, they do not provide dynamic information such as the effect on performance when degradation exceeds failure limits. Exception are mechanistic models of carbon monoxide poisoning [17]. Such questions are crucial to improved operation of full-scale cells.

2.4.2 Statistical Relationships

At the other end of the modeling spectrum are models (which are better described as relationships) that examine the effects of causes on degradation from a statistical standpoint. Though typically used to identify operating parameters for optimum beginning of life performance [63], recent studies have examined their effect on the durability of fuel cells.

Statistical methods are often used to examine fuel cell system reliability. Such published studies as the work by Feitelburg *et al* [64] and Astrom *et al* [65] provide information on the statistical probability of failure of a fuel cell system through failure of the balance of plant components. Both studies propose statistical models based on a design of experiment, that predict the mean time to failure (MTTF).

On a smaller scale, Pierpoint and coworkers [66] attempted to create predictive models for single cell lifetime. Two methods were used. First, voltage degradation curves were fitted to models using regression analysis. This regression was to a simple linear fit with parameters that did not reflect actual material properties or chemical processes. The second method attempted to correlate the initial fluoride release to the lifetime of a fuel cell. In the first case, the effect of different operating conditions, such as relative humidity, on the fitting parameters of the model was studied in order to predict voltage degradation over all reasonable conditions. Similarly, in the second case, the effect of RH on the initial fluoride release rate was also studied. A similar screening test was proposed by Fowler *et al* [2] whereby design of experiment principles could be used to determine how key variables in fuel cell models would change with time. Variables such as membrane conductivity and active surface area were examined and empirically fit to data.

The main strengths of the above statistical models are that they are easy to derive and use. The experiments can be organized quickly and the results are useful when attempting to understand fuel cell products. Since these models typically need a large number of cells to ensure statistical significance, they are often employed by industrial researchers.

However, these models have certain weaknesses as well. These models typically link fuel cell performance degradation to operating conditions without consideration of the degradation mechanism that may be involved. As such the usefulness of the models is limited by the data used to create them, and they are specific to the cell under a limited number of operating conditions. Further, when attempting to design new materials or when selecting the best materials, these models offer no insight into what is taking place within the fuel cell.

2.4.3 Semi-mechanistic models

There have been some attempts to describe fuel cell performance degradation dynamically by attempting to model mechanistic processes. Jiang *et al* [67] attempted to model degradation by an empirical function for internal stack temperature. The temperature function was then linked to two parameters that describe fuel cell performance, the ionic conductivity of the electrolyte membrane and the mass transfer losses in the gas diffusion layer. They argued that temperature within the cell is a major factor which determines ionic conductivity (though drying out of the electrolyte membrane) as well as mass transfer losses (by controlling condensation in the GDL). As such, the model was able to connect causes of degradation, such as current density and stack temperature, to the observed voltage degradation over time. This model focused on reversible performance degradation linked to membrane and GDL water content.

Currently there are no models in the literature that attempt to link causes of irreversible degradation to a chemical degradation mode and further attempt to describe the effect on performance. The strength of such a model is that it would offer insight into how the material properties and operational regimens impact the material properties and how that impacts performance. In this sense, a semi-mechanistic model would also be useful to design new materials and develop control strategies that protect the fuel cell. These types of model can also be used to predict effects of degradation due to their connection to material property degradation. As such, these models could also be used by industry for material selection and the development of more detailed reliability models.

There are currently few models in the literature and in use in industry that adequately combine mechanisms based on conditions found with fuel cell use while at the same time creating output that can be linked to degradation effects in a manner useful to the operator. Such models should use the current knowledge of mechanisms to create more widely applicable models. This gap in the current literature will be addressed by the work presented here with respect to chemical degradation of the electrolyte membrane.

2.5 SUMMARY

Fuel cell material durability is an important topic of fuel cell research today. There is a clear link between material properties and fuel cell performance. Consequently, there is also a link between the mechanism of fuel cell material degradation, which will change material properties, and performance degradation. Ultimately, these are linked with the operating conditions of the cell.

Chemical degradation of the electrolyte membrane is an important degradation mechanism that has been studied. It is currently believed that crossover gases react to form peroxide species which then also continue to react to form hydroxyl or peroxyl radical species. These radicals then attack vulnerable groups on the electrolyte polymeric structure. The result is that fluoride ions are released and the membrane thins. Further, degradation causes crossover to increase which promotes more degradation as well as degradation in voltage.

Although there is considerable experimental research on chemical degradation of the electrolyte membrane, currently no degradation models are available in the literature that link causes such as material properties and operational conditions to the degradation mechanism and performance decay in a dynamic manner. Such a model would serve as a useful tool for fuel cell manufacturers and as a complement to experimental research.

This work proposes the study of one such degradation mechanism, chemical degradation by radical attack, in an effort to model the degradation processes with a semi-mechanistic

model. The model presented in this work is new to the field and can be used as a guide for future models on other types of materials.

CHAPTER 3 : EXPERIMENTAL

3.1 FUEL CELL MATERIALS AND TESTING APPARATUS

In experiments for this work, single-cell fuel cells made by Hydrogenics Corporation each, with a geometric active area of 80.1 cm^2 on each electrode, were used. The cells were assembled using Gore™ PRIMEA® series 5510 catalyst coated membranes (CCM) and proprietary gas diffusion layers (GDL) with a microporous layers (MPL). An MPL is a composite of carbon particles and a hydrophobic agent that is coated on one side of the conventional gas diffusion media and can be used on one or both of the anode or cathode electrodes. The electrolyte membranes contained ePTFE reinforcement layers, as shown in Figure 2-3, which increases mechanical stability of the membrane. The single-cell hardware is shown in Figure 3-1. The three ports at the top of the fuel cell are the inlets for the fuel stream (hydrogen), oxidant stream (air), and water. The design of this particular fuel cell uses water flowing on the outside of the anode and cathode graphite plates to control temperature. In the case of the single cells tested, hot water from an external water bath was used to heat the cell. Extra insulation was used around the cell to help maintain temperature. All streams flow through parallel flow channels which run straight from the inlets to the outlets.

Three sets of single cell equipment were used in rotation for all testing. Once a test was completed, the cell would be dismantled and the hardware reused in subsequent tests. The

only materials that were replaced were the gas diffusion layers and the catalyst-coated membrane. Cells were assembled and disassembled in the labs at Hydrogenics Corporation under the supervision of Natasha Beydokhti and Rami Abouatallah. Leak tests described below were performed to establish if there were any major defects in the membrane or cell assembly. If leak tests were failed, the cell would be re-assembled, possibly with new gasket material or plates, until leak tests were passed.

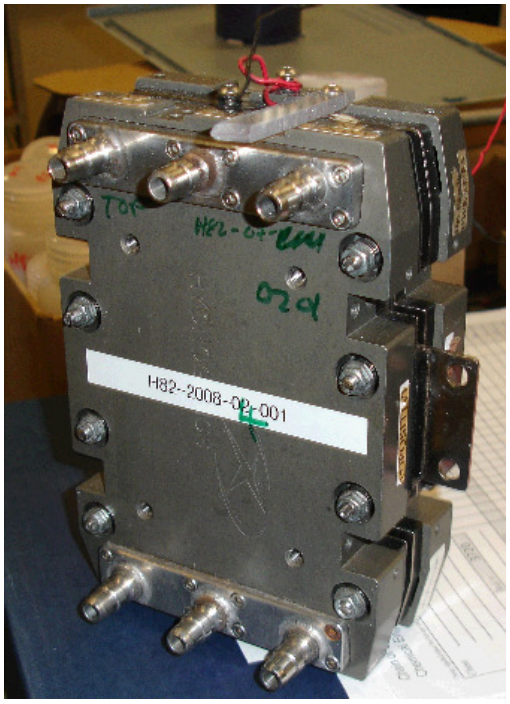

Figure 3-1: Hydrogenics Series 82 single-cell fuel cell hardware.

The cells were tested on a Hydrogenics FCATS™ test station (Figure 3-2) which controlled temperature, humidity, and gas flows. Hydrogen from compressed gas tanks and house air were used. Mass flow controllers were used to maintain the inlet gas flow rates as set by the user. Gas then flowed through two humidifiers. The dew point temperature of the humidifiers was set by the user. As the gases exited the humidifiers, they entered a length of tubing connecting to the fuel cell inlet ports. This stainless steel tubing was heated using heating tape wrapped around the exterior of the tube and was controlled by the test station software. Over this length of tube, the temperature of the gas stream was raised to achieve a desired relative humidity.

Prior to entering the cell, gas temperature and pressure were measured. As discussed, cell temperature was controlled using an external water bath. Hot water flowed to an external pump and then through a filter to eliminate any particulates in the water, and then to the cell water inlet port. Large particulates can block water channels within the fuel cell and cause poor temperature distribution. Deionised water (DI) was used to further eliminate the possibility of particulates and mineral deposits. For all the experiments in the following studies, cell temperature was maintained at 90°C. This required the water bath temperature to be kept between 92°C and 95°C. Due to the high temperatures, evaporation from the water bath was inevitable although rubber gaskets were used to seal the water bath.

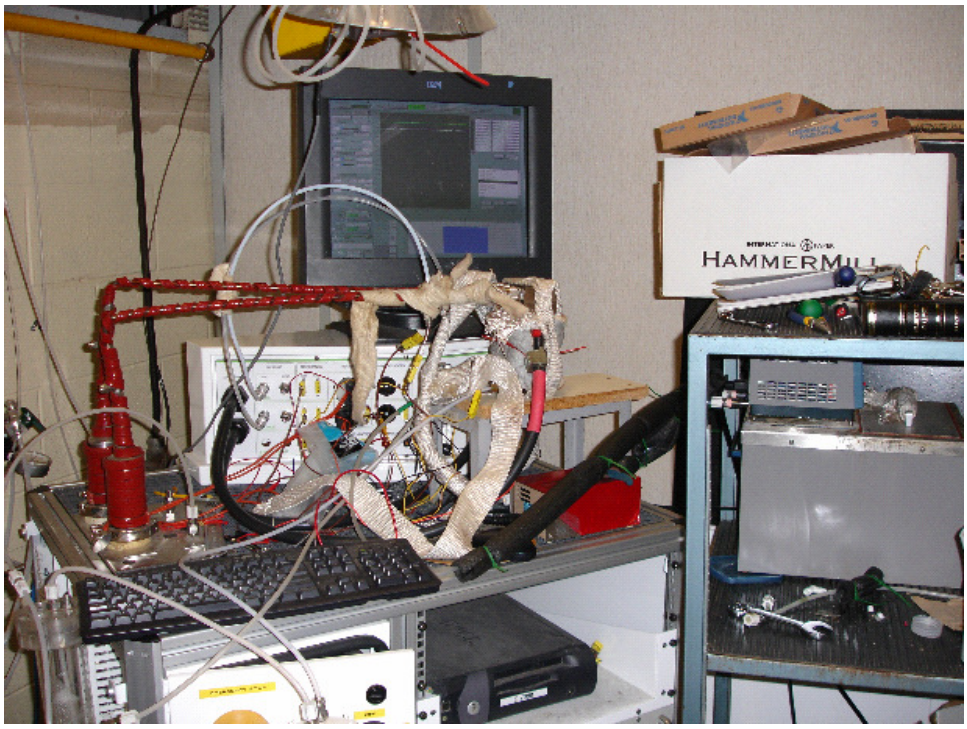

Figure 3-2: FCAT fuel cell test station.

When refilling the water bath, it was necessary to use hot water to minimize cell temperature excursions. This was especially important with experiments operating at or near 100% RH since cell cooling phenomena would result in condensation within the cell.

There were no internal thermocouples to monitor cell temperature. Instead the outlet water temperature was treated as the cell temperature. Outlet gases from the fuel cell were allowed to flow into knockout drums. The purpose of these drums was to capture effluent water from the fuel cell. This water was then analyzed for material degradation products. During a typical experiment, knockout drums were emptied daily. Gases exiting the knockout drums then flowed to the exhaust vents and to the fume hood system. Finally, a Dynaload loadbox was used to control the cell current.

3.2 FUEL CELL COMMISSIONING

Prior to accelerated durability testing, all cells underwent a commissioning procedure which included initial leak testing and break-in of the cell. Leak testing consisted of three different tests designed to evaluate three types of failures. First an external leak test was performed with the cell set-up as illustrated in Figure 3-3a. By blocking the cell outlets and pressurizing the cell to 30 PSIG the integrity of the seals between the cell interior and the surroundings was tested. The second test checked if there was any leak between the coolant channels and the internal gas channels. The cell was set up as shown in Figure 3-3b. The coolant channels were pressurized to 15 PSIG and gas flow out of the anode and cathode ports is measured. The final leak test was a simple crossover test which determines if there were any large failures between the anode and cathode gas channels which could allow gas crossover. In this test the cell was set up as shown in Figure 3-3c and the cathode pressurized to 5 PSIG. Crossover gas flow was measured out of the anode. The two sides are were reversed to determine any crossover occurred in the reverse direction.

For the tests in this study, all leak rate measurements showed no problems. The above crossover measurements were only considered to be rough and not sensitive to very small flow rates that would be expected from a well sealed membrane with no integrity failures. Crossover current measurements were a better method for determining the rate of hydrogen crossover through the membrane. Measurement of the crossover current is described below.

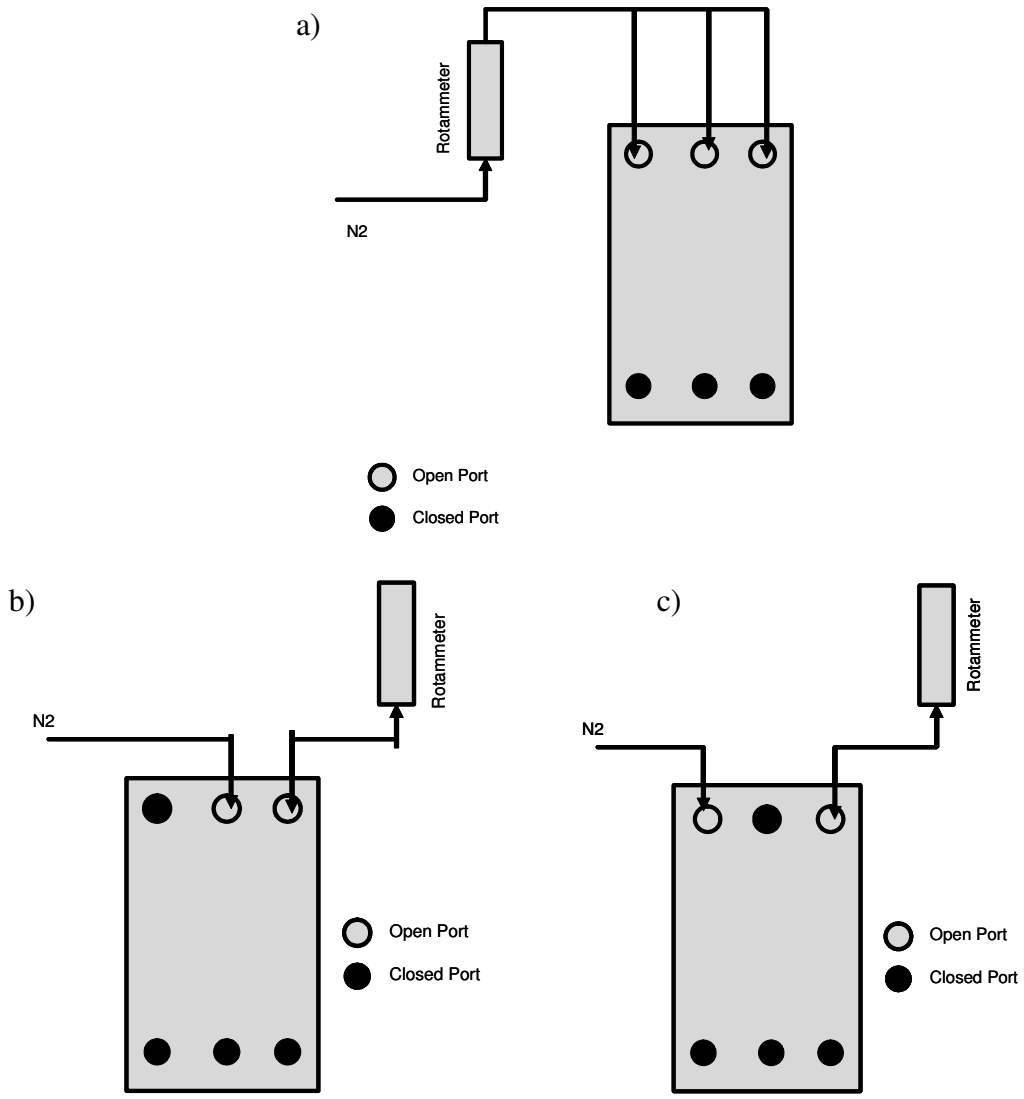

Figure 3-3: Single cell leak testing set-up. a) External leak test, b) coolant leak test, c) crossover leak test.

Fuel cells were operated after break-in for a period of 8 - 12 hours. Breaking-in the fuel cell allowed the fuel cell membrane and catalyst layer to become fully hydrated and for all catalyst sites to become activated. During break-in, cell voltage was kept at approximately 0.6 V until performance stabilized. The anode and cathode stoichiometries, which is analogous to the amount of excess gas delivered to the fuel cell, were maintained at 2.0 and 2.5 (100% and 150% excess), respectively, and the cell temperature was maintained at 80°C. The anode and cathode dew points were also 80°C,

i.e. 100% RH. The inlet pressure was also maintained at 100 kPag. Once break-in was completed, initial performance curves, "polarization curves" were measured. A full description of the procedure is available in Appendix B.

3.3 POLARIZATION CURVES

Polarization curves were obtained at two different conditions. The first was at a cell temperature of 80°C, 100 kPag, and anode and cathode relative humidites of 65% and 50%, respectively. This first polarization curve is referred to as the "high pressure high temperature" or HPHT polarization curve. The second polarization curve was obtained at a cell temperature of 65°C, 20 kPag, and anode and cathode relative humidity of 65% and 50%, respectively. The second polarization curve is referred to as the "low pressure low temperature" or LPLT polarization curve. Procedures are available in Appendix B.

3.4 ELECTROCHEMICAL CHARACTERIZATION

Two types of electrochemical tests were employed in this study. The first test was a cyclic voltammetry test and the second was a crossover current test. Electrochemical measurements were performed using an EG&G Princeton Applied Research potentiostat/galvanostat model 273 and Coreware software. For both tests, humidified hydrogen was passed to the anode and humidified nitrogen (or any other inert gas) was supplied to the cathode.

Cyclic voltammetry measurements allow the electrochemically active surface area (EAS) of the fuel cell cathode catalyst layer to be determined. In this measurement the voltage was scanned from 0.1 to 1V and back to 0.1V for several cycles with a sweep rate of 20 mVs^{-1}. A typical curve has several main features such as hydrogen adsorption and desorption and platinum oxidation. The area under the hydrogen adsorption portion of the curve allows calculation of the EAS as shown in Figure 3-4 using Equation (3-1).

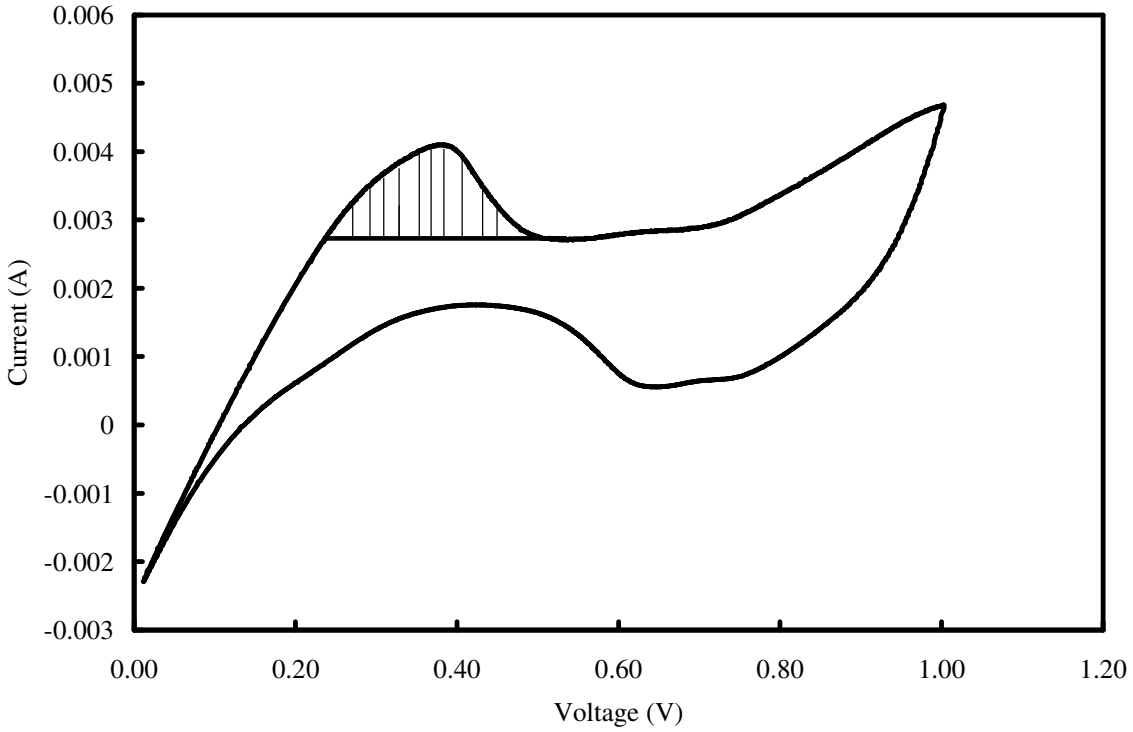

Figure 3-4: Typical CV curve for a Hydrogenics single cell. Shaded area is used to calculate electrochemically active surface area (EAS).

$$A_{Pt,el} = \frac{Q}{210\mu C cm^{-2} L_{ca} A_{geo}} 10^5 \tag{3-1}$$

where the L_{ca} is the loading of the electrode in question (mg_{pt} cm^{-2}) and A_{geo} is the geometric area of the electrode (cm^{-2}). Q is given by the area under the hydrogen desorption region and has units of Coulombs. $A_{Pt,el}$ is in units of m^2_{Pt} g^{-1}_{Pt}. Alternatively the electrochemically active surface (EAS) area can be given in units of m^2_{Pt} cm^{-2}_{geo} using Equation (3-2).

$$EAS = A_{Pt,el} L_{ca} \cdot 10^{-3} \tag{3-2}$$

Since the exact catalyst loading and surface area are proprietary information, EAS values will be typically given as relative quantities.

In a crossover current measurement, also known as a hydrogen pump experiment, molecular hydrogen which permeates across the fuel cell electrolyte membrane is split into hydrogen ions and electrons at the anodes. The hydrogen ions then travel back to the anode electrolyte where they recombine with the electrons back into hydrogen gas. The measured current from this test is known as the crossover current. Crossover current measurements were conducted by scanning voltage from 0.1 to 0.6 V with a sweep rate of 2 mVs^{-1}. A typical measurement is shown in Figure 3-5. The crossover current, i_{H_2}, is related to the actual molar flux of hydrogen permeating through the membrane, N_{H_2}, with Faraday's law, Equation (3-3).

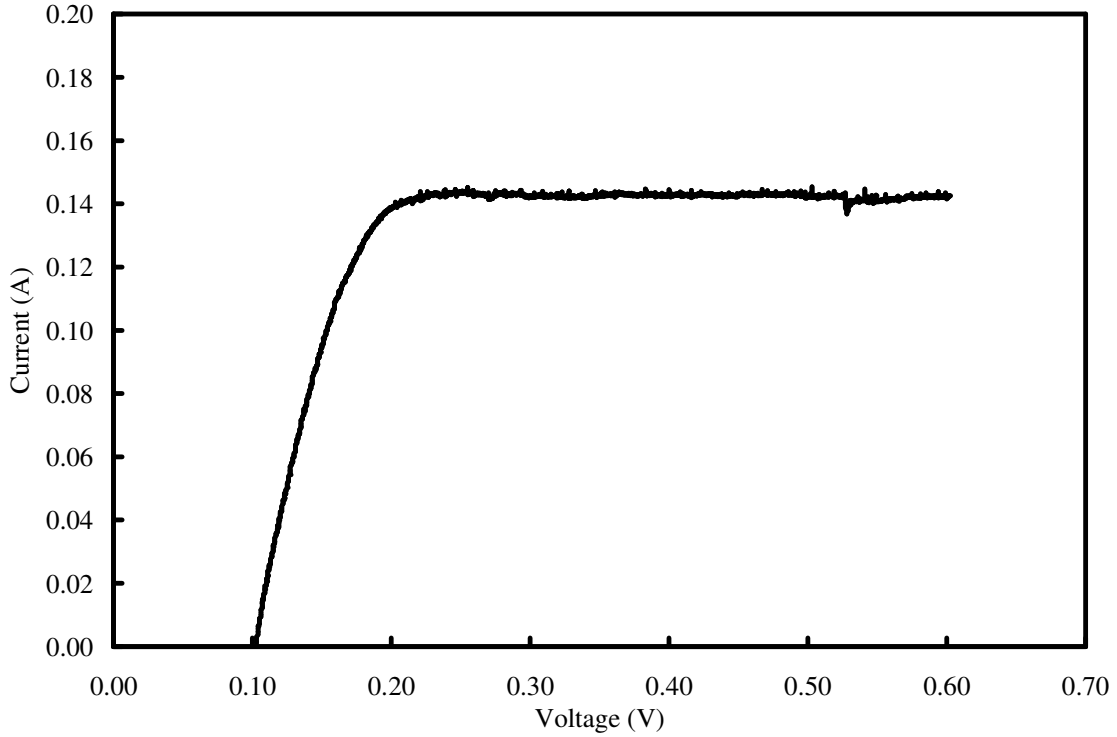

Figure 3-5 : Typical crossover current measurement from a Hydrogenics single cell.

$$N_{H_2} = \frac{i_{H_2}}{2F} \tag{3-3}$$

3.5 OPEN CIRCUIT VOLTAGE TESTING

The open circuit voltage (OCV) durability test was conducted at a cell temperature of 90°C, and no backpressure. Knockout drums were used on the fuel cell outlets to condense and collect water during fuel cell operation. Water samples were collected daily and were kept in polyethylene bottles prior to analysis. A total of 6 cells were run under open circuit voltage conditions summarized in Table 3-1. Pure hydrogen was used on the anode and air on the cathode. Anode flow rate was 0.2 standard litres per minute (SLPM – 0°C, 1 atm) and cathode flow rate was 0.8 SLPM. Cell 3, operated at 75% RH was used as a baseline case for the development of a chemical degradation model and thus will be termed as "baseline". Cell 5, operated at 100% RH was chronologically one of the first cells tested. During the testing of this cell, fluoride emission was not measured and so Cell 5 will not be used in discussions regarding fluoride emission rates. Cell 4 and Cell 6 were two repeat experiments that were performed. Since each experiment could last between 1 – 2 months, it was not possible to repeat all experiments. Cell 4 was a repeat of Cell 3 at 75% RH though it was allowed to operate only up to 380 h rather than 860 hours. Its purpose was to obtain data on how membrane thickness changed with time. Cell 6 was a repeat of Cell 5 which was used to properly gather fluoride emission data at 100% RH.

Table 3-1: Relative humidity and cell temperature conditions for cells operated at open circuit voltage (OCV).

Cell	Anode/Cathode RH (%)	Cell Temperature (°C)
1	20	90
2	50	90
3 (Baseline)	75	90
4	75	90
5	100	90
6	100	90

The above cells were used to study the effects of RH on durability and chemical degradation. The length of durability tests ranged from 500 to 900 hours for each experiment. The total time for completion of each experiment including assembly of the cell ranged from 1 – 2 months.

One problem with any long-term durability study is the possible influence of intentional and unintentional cell stoppages for diagnostic tests (polarization curves), shutdowns, safety issues, and maintenance. For these reasons, it is not always possible to run a cell for 1000 hours without some shutdowns. The effect of shutdowns or other breaks in testing on voltage and fluoride release data will be discussed in the following chapters. Table 3-2 lists the total testing duration of the above cells as well as times where shutdowns or other significant interruption occurred.

Table 3-2: Total testing time and points in testing hours where shutdowns or other significant interruption.

Cell	Total Testing Time (h)	Shutdown/interruption at: (h)
1	478	None
2	756	136
3 (Baseline)	860	436, 519, 734, 744 and 809
4	360	35, 85 and 126
5	380	100, 200 and 325
6	918	191

Cells were allowed to run as long as possible to acquire the necessary data. A minimal number of measurements were taken throughout the experiments to reduce the effects of stoppages on the degradation data. As such, it was not possible to use any particular measurement, such as crossover, as a failure criterion. Voltage was not considered as a failure criteria due to ambiguity as to the cause of the actual irreversible voltage degradation when examining the trends over short periods of time (which will be discussed in Chapter 4).

3.6 Durability testing at multiple Current Densities

An additional 3 cells were run to determine the effect of current density on the chemical degradation and voltage degradation rates as shown in Table 3-3. These cells were run at low, medium, and high current densities of 300, 500, and 700 mA cm^{-2}. Gas flow rates were kept at 1.2/2 anode/cathode stoichiometry and the cell temperature was maintained

at 90°C with anode and cathode relative humidity of 50%. A 50% RH was selected in order to accelerate the degradation of the cells. Water collection procedures and analysis were the same as the OCV experiments and the run time of each experiment was also similar. Cell 7 operated for 380 hours without interruption while Cells 7 and 8 ran without interruption.

Table 3-3: Conditions used to study the effect of current density on degradation.

Cell	Anode/Cathode RH (%)	Current Density ($mA\ cm^{-2}$)
2	50	0
7	50	300
8	50	500
9	50	700

3.7 FLUORIDE ION CHROMATOGRAPHY

Fluoride ion analysis was carried out with a Dionex ED40 electrochemical detector working with a Dionex GP40 gradient pump. The minimum detectable fluoride ion concentration was 0.011 ppm F^- .

All effluent water during a fuel cell test was collected using knockout drums between the anode and cathode exits and the test station exhaust. Water was collected daily and stored in PE bottles. Bottles of water were weighed to determine the amount of water deposited during a collection period. Effluent water was then analysed for fluoride ions using ion chromatography described below. In this way, the fluoride release rates and cumulative fluoride release from the anode and cathode sides could be determined. Sample data and calculations for cumulative fluoride release are shown in Appendix C.

3.8 SCANNING ELECTRON MICROSCOPY

Scanning electron microscopy (SEM) analysis was carried out using a LEO SEM with field emission Gemini Column. The gas diffusion layers were first removed from the membrane electrode assemblies. This was done by repeatedly heating, humidifying and then cooling the MEA until the GDL could be removed easily. Cross sections were made by freeze fracture from a strip of sample submerged in liquid nitrogen. Once frozen, the

sample was broken in half while still submerged. Cross-sections were mounted on the sides of stainless steel nuts so that the fractured side was vertical as shown in Figure 3-6.

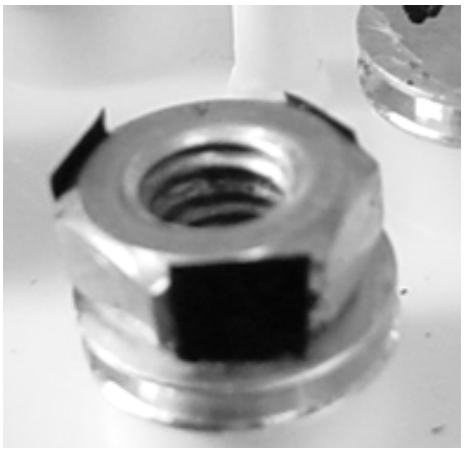

Figure 3-6: Preparation of upright catalyst coated membrane samples for SEM analysis using stainless steel nuts.

Samples were also sputter-coated with gold to improve conductivity. SEM images were later analyzed with Scion Image Analysis software to obtain estimates of layer thicknesses.

3.9 GAS CROSSOVER

Crossover measurement of oxygen and hydrogen were manually measured by pressurizing the anode side of the fuel cell to 5 PSI of the test gas and measuring the crossover rate. From this information, an estimate of the permeability was obtained. Measurements were conducted at room temperature with fully humidified gases. The permeability k_i was determined from the differential pressure Δp_i, membrane thickness δ, and the molar flux across the membrane N_i, as shown in Equation (3-4) below.

$$N_i = P_{M,i} \frac{\Delta p_i}{\delta} \qquad \textbf{(3-4)}$$

3.10 WATER BALANCE

Water balance calculations were performed to identify if there was a net flow of water from one side of the fuel cell to the other. Known parameters were the hydrogen and air flow rates on a dry basis as well as the relative humidity. Calculations are shown in Appendix C.

The rate of water entering can then be compared to the moles of water exiting though collection in a knockout drum. It was assumed that exhaust gas was at 100% RH and room temperature.

CHAPTER 4 : EFFECT OF CROSSOVER AND EAS ON OPEN CIRCUIT VOLTAGE

The goal of this chapter is to present the results of voltage degradation plots obtained from open circuit voltage (OCV) experiments including the identification of reversible and irreversible voltage degradation. Reversible degradation is often a result of transient processes where the loss in voltage may be reversed by changing the operating conditions (or with the aid of an 'in-situ' recovery procedure while the fuel cell remains in service) and consequently the cell performance may return to pre-degraded levels if allowed to completely recover. An example of reversible degradation includes water flooding, which can reduce cell performance, although performance may be recovered by removing the excess water (through a temperature change, change in flow rate, or change RH of the reactant stream) as illustrated in Figure 4-1.

Irreversible degradation includes irreversible changes to the fuel cell materials such as membrane thinning or loss of catalytic surface area from platinum migration or carbon corrosion. This type of degradation permanently changes the performance that could be achieved from an cell, and will eventually lead to considering the cell to have failed when performance degrades below an acceptable value. The type of mitigation strategy employed to minimize voltage degradation will be influenced by the cause and mode of degradation, specifically if the degradation is reversible or irreversible. Therefore, it is

important to understanding when observed voltage decay is due to reversible processes and when it is due to irreversible materials degradation. The effect of irreversible changes in materials, as measured by changes in crossover current (CC) and changes electrochemically active surface area (EAS), on performance will be investigated in this chapter. Another aim is to demonstrate how crossover current and EAS measurements can be used in performance models to predict irreversible degradation as measured by the degradation of the voltage observed at 'steady state' operation points.

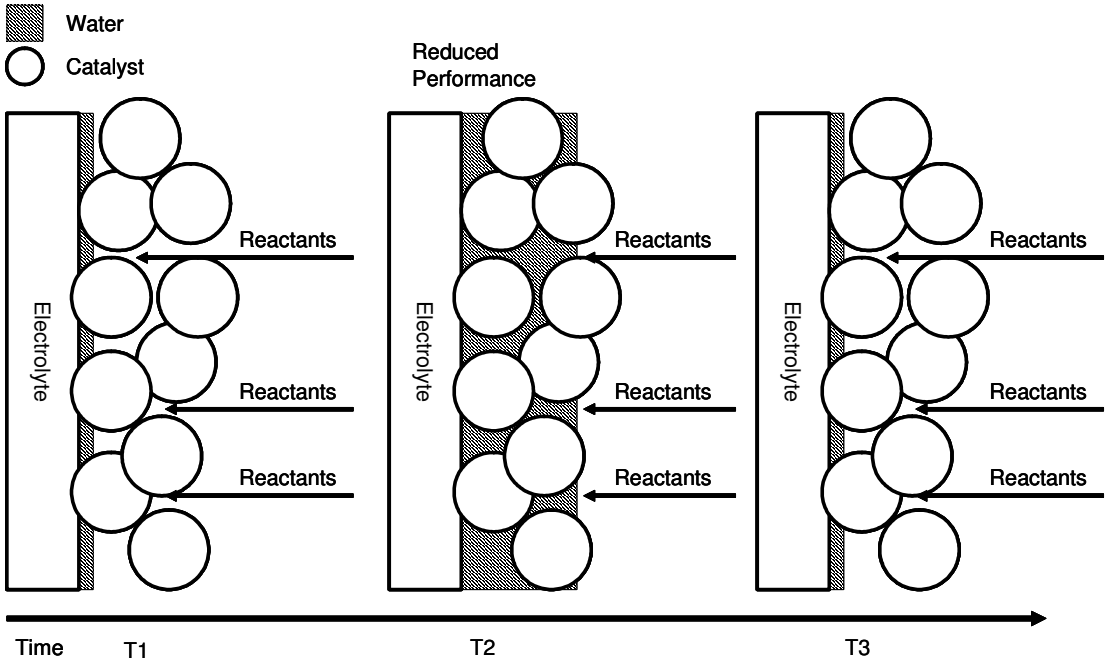

Figure 4-1: Water flooding as reversible degradation. At time T1 flooding begins to block pores until time T2, where blocked pores cause a reduction in performance. Once a mitigation strategy adopted, performance can be recovered by removing water in T3.

The main results can be summarized as follows:

- Voltage degradation is caused by reversible and irreversible voltage losses.
- Irreversible losses are related to irreversible changes in fuel cell materials.
- Irreversible voltage loss can be predicted by measuring irreversible changes in crossover (from membrane thinning) and surface area.

Two cells were tested under OCV conditions - Cell 5 and Cell 6. Cell 5 was exposed to regular interruptions for CC and EAS measurements while Cell 6 was operated without interruptions for comparison. This work has been published in the Journal of Power Sources [68].

4.1 OPEN CIRCUIT VOLTAGE DEGRADATION EXPERIMENT

Initial OCV degradation experiments involving testing Cell 5 continuously at 100% RH for a total of 380 hours. Cell 6 was also operated at 100% RH for its entire 900 h testing period. Figure 4-2 depicts OCV curves of both cells over the testing period. Though data was taken every minute, for clarity of presentation, the OCV curves only display data from every 5 hours. Cell 5 was subjected to multiple breaks in OCV operation for maintenance and scheduled stoppages where polarization curves and other electrochemical tests were conducted. Cell 6 was stopped very infrequently for diagnostics and maintenance. From Figure 4-2, it can be seen that both OCV durability experiments produced a similar voltage trend between 0 and 380 hours of operation.

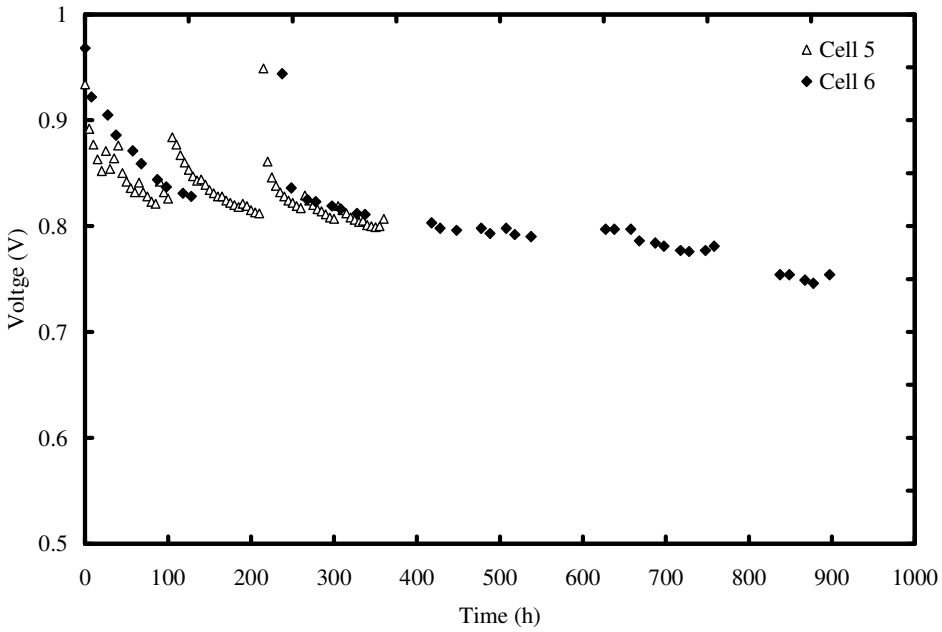

Figure 4-2: Variation of open circuit voltage for Cell 5 and Cell 6 with time during durability test.

At the beginning of testing or after an interruption, such as polarization curve measurement, the open circuit voltage rises to a relatively high value. For example, at 0 hours the potential of both cells range between 0.93V and 0.97 V which is a typical open circuit potential for a fuel cell of this configuration. These initial voltages seem stable for periods on the order of minutes, as shown in Figure 4-3, varying by less than 2 mV between 15 and 30 minutes of operation. However, as shown in Figure 4-4, when examined on larger time scales the voltage decays relatively rapidly until it eventually approaches a more steady decay trend which may take many hours to establish. The steady decay was identified with the voltage data from Cell 6 which was not interrupted as frequently as Cell 5 and hence is considered to have a fully stable degradation trend free of transient effects. The initial decay region will be termed the transient decay period while the latter period will be referred to as the steady decay period. This is an important observation because it demonstrates that error may be introduced when voltage degradation values are reported if they fall in the transient period since they will contain a contribution from reversible and irreversible effects.

Figure 4-4 also clearly shows voltage recovery phenomena caused by three types of interruptions: polarization curve measurement, maintenance, and temperature excursions. These periods when polarization curves were measured are marked with dotted lines while interruptions for maintenance can be seen encircled in the data segment from 0 to 100 h as sharp voltage spikes. Finally, cell temperature excursions, which are short periods where cell temperature deviates significantly from the setpoint, can be seen in the data after 100 h as smaller jumps in voltage followed by a relatively smooth decay as marked within the ‘square’. In all cases interruptions resulted in a temporary voltage recovery which returned to the overall steady decay trend with time. The recovery phenomenon also raises an important issue of what it means to report a voltage degradation rate. Ideally voltage degradation rates would represent irreversible changes to fuel cell materials. However, if part of the voltage loss is recoverable or transient, then this specific measurement misses some of its meaning. From Figure 4-2 and Figure 4-4, it would seem reasonable to estimate an irreversible voltage degradation rate from the steady decay period although some justification is needed.

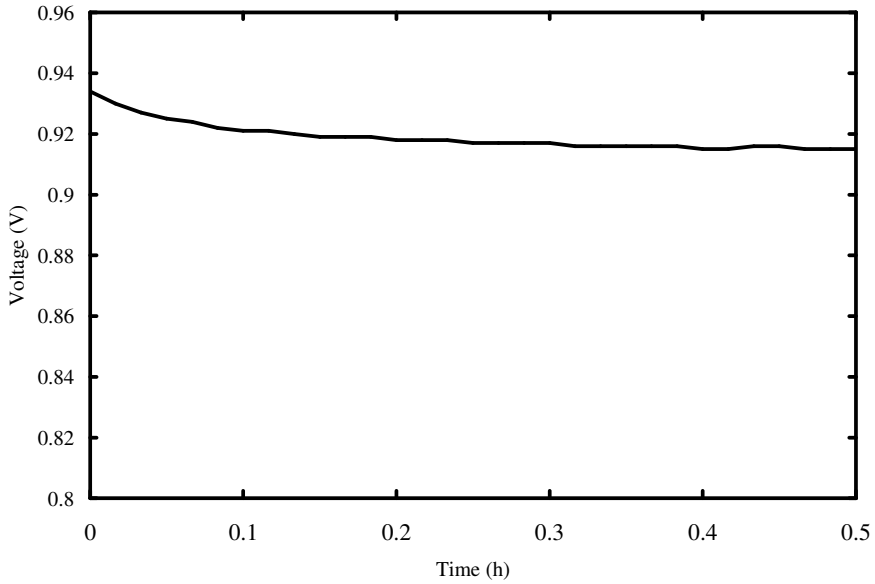

Figure 4-3: Stability of OCV for Cell 5 on small time scales.

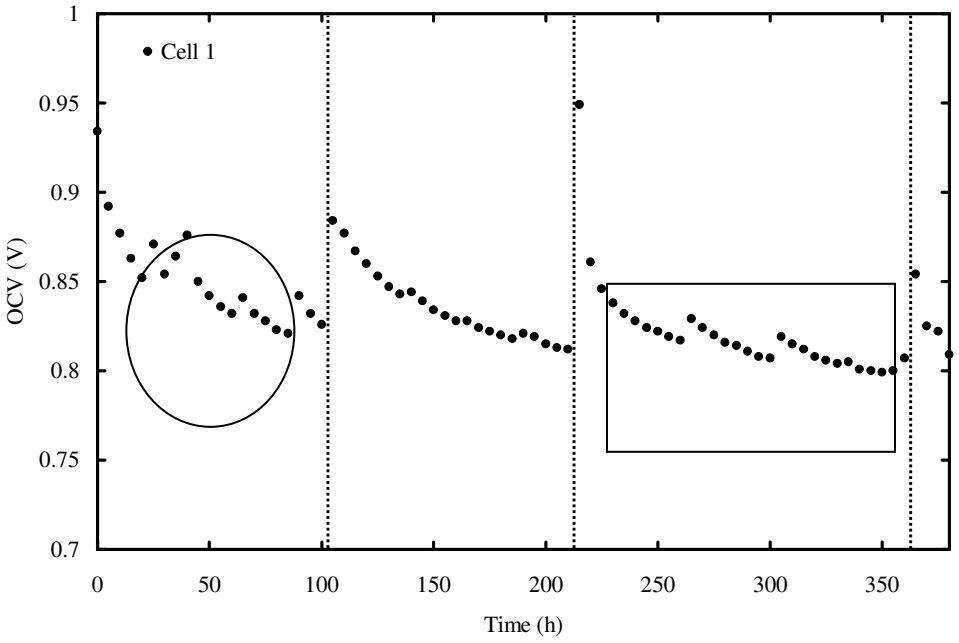

Figure 4-4: OCV durability of Cell 5 over the first 380 hours. Dotted lines represent times at which polarization curve measurements were made. Interruptions for maintenance are shown within the circle, and voltage recovery due to temperature excursions are shown within the box.

Equation (4-1) suggests that irreversible changes to the membrane, leading to increased crossover, as well as the catalyst layer, leading to reduced electrochemically active surface area (EAS), will result in an irreversible change in OCV.

$$\eta_{act} = \frac{RT}{F} \ln\left[\frac{i + i_{H_2}}{10 \cdot \left(L_{ca} A_{Pt,el}\right) \cdot i_o}\right] \tag{4-1}$$

During the testing of Cell 5, diagnostic tests such as crossover current (CC), electrochemically active surface area (EAS), and polarization curves were carried out at 0, 100, 200, and 360 hours of operation. CC and EAS results are given in Table 4-1. Cell 6 was not tested in this way in order to limit the number of .interruptions. The results show that over time the CC generally increased, which is consistent with the literature [30,47], and this is likely caused by irreversible material degradation processes such as membrane thinning or pin-hole formation. The EAS decreased with operational life, possibly as a result of irreversible contact loss between the electrolyte membrane and the catalyst layer, carbon corrosion, or from platinum migration as suggested in the literature [50,55,69]. Some platinum migration was observed in the membranes after degradation during this study. The effect of the irreversible decrease in EAS and increase in CC can be seen in the polarization curves as shown in Figure 4-5 which show an overall downward translation of the curve with testing time.

Table 4-1: Crossover currents and electrochemical surface areas for Cell 5.

Time (h)	EAS Normalized to 0h	CC (mA/cm^2)
0	1.00	2.40
100	0.77	2.31
200	0.86	2.58
361	0.23	3.17

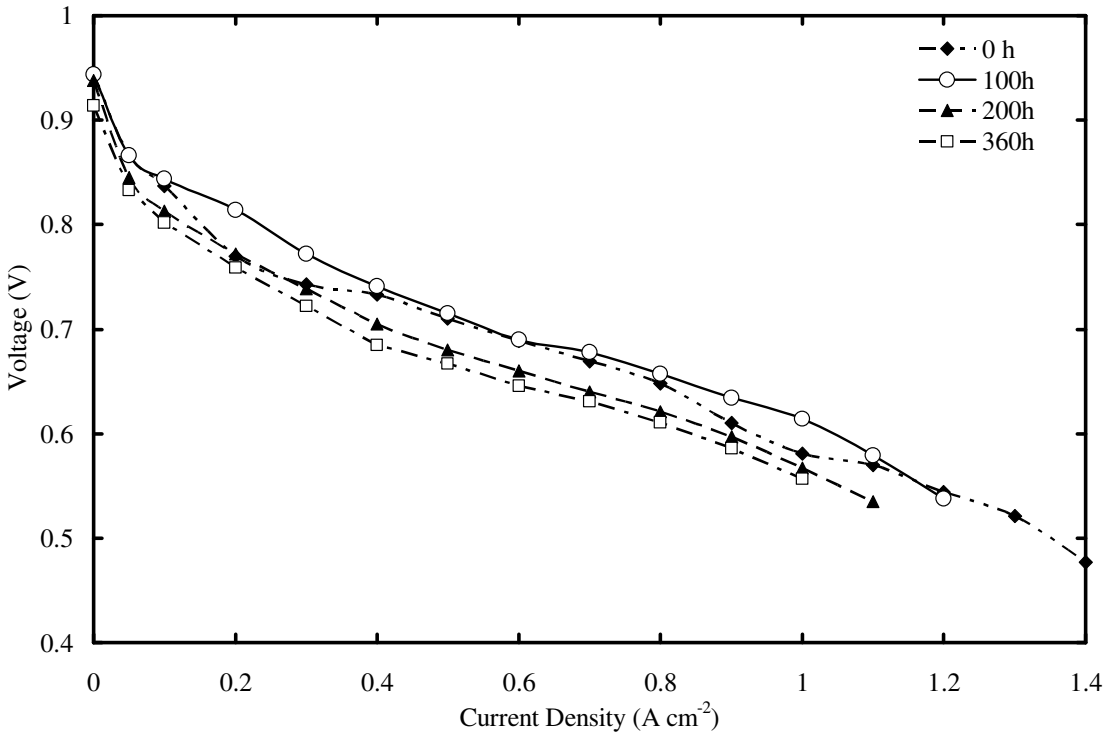

Figure 4-5: 'High pressure high temperature' polarization curves for Cell 5.

The rate of irreversible degradation was estimated using different diagnostic tests:

1) HTHP polarization curves,

2) LTLP polarization curves, and

3) through application of Equation (4-1), which can be simplified to Equation (4-2) to isolate the voltage loss from crossover.

The voltage loss from hydrogen crossover can be modeled using a Tafel-like expression as shown in Equation (4-2)[3]

$$\eta_{ix} = \frac{RT}{F} \ln\left[\frac{i_{H_2}}{EAS \cdot i_o}\right] \tag{4-2}$$

$$V_{Cell,OCV} = E^{\circ} - \eta_{ix} \tag{4-3}$$

where EAS is the electrochemically active surface area per geometric surface area (m^2_{pt} cm^{-2}_{geo}), i_o is the exchange current density per cm^2 of platinum (A cm^{-2}_{pt}) of the ORR and $i_{crossover}$ is the crossover current considered on a geometric area basis (A cm^{-2}_{geo}). Equation (4-3) assumes that under conditions where no current is drawn, i.e. OCV, the open circuit cell voltage will be the difference between the Nernst potential and the hydrogen crossover overpotential. Inspection of Equations (4-2) and (4-3) reveals that an increase in hydrogen crossover or a reduction in active surface area should result in higher voltage loss and consequently lower open circuit potential.

Since the measurement of polarization curves causes temporary voltage recovery and requires only the short measurement times, it is believed that the OCV measurements obtained for the curves will only be affected by irreversible changes in the materials and be free of reversible effects. The predicted rate of voltage degradation from CC and EAS data was estimated by rearrangement of Equation (4-3) for two data points at times t_1 and t_2. Thus the amount of voltage degradation, ΔE_{OCV}, can be calculated from by Equation (4-4).

$$\Delta V_{Cell,OCV} = V_{Cell,OCV\,t2} - V_{Cell,OCV\,t1} = (E^{\circ} - \eta_{ix})_{t2} - (E^{\circ} - \eta_{ix})_{t1} = \eta_{ix,t1} - \eta_{ix,t2} \tag{4-4}$$

Substituting Equation (4-2) into Equation (4-4) gives

$$\Delta V_{Cell,OCV} = \frac{RT}{F}\ln\left[\frac{i_{H_2,t1}}{EAS_{t1}\cdot i_o}\right] - \frac{RT}{F}\ln\left[\frac{i_{H_2,t2}}{EAS_{t2}\cdot i_o}\right] \tag{4-5}$$

Assuming that the exchange current density remains constant and simplifying:

$$\Delta V_{Cell,OCV} = \frac{RT}{F} \ln\left[\frac{i_{H_2,t1}(EAS_{t2})}{(EAS_{t1})i_{H_2,t2}}\right] \quad (4\text{-}6)$$

The estimated voltage degradation rates from polarization curves and from application of Equation (4-6) are summarized in Table 4-2. The average rate of irreversible voltage degradation calculated from OCV points of the polarization curves are 0.083 mVh^{-1} for the HPHT and 0.141 mVh^{-1} LPLT polarization curves. The estimated rate of voltage decay from the Equation (4-6) was an average decay rate of 0.146 mVh^{-1}. The estimated irreversible decay rates are similar and within the same order of magnitude. The voltage degradation rates reported for this study are higher than those typically reported in the literature which range from 0.09 to 0.001 mVh^{-1} for cells degraded by various mechanisms [2]. Cleghorn *et al.* [45] report a degradation rate between 0.004 and 0.006 mVh^{-1} at operational conditions of 800 $mAcm^{-2}$ and a similar type of membrane used in this study. The data by Paik *et al.* [12] shows a degradation rate of approximately 0.016 mVh^{-1} using a similar membrane and test conditions found in this study (although this number is low due to recovery phenomena in the presented data).

The reason for the differences in the results obtained in this thesis and the values reported in the literature are likely associated with the conditions used for testing and specific membrane electrode assemblies used. The conditions used in this study represent accelerated ageing test conditions so a relatively high rate of degradation is expected, and was observed. The average decay rate during the steady decay portions of the voltage degradation curves for Cell 1, estimated by taking the final data points at the end of each segment, was calculated to be 0.089 mVh^{-1} which shows good agreement with the polarization and modeled data. In comparison, voltage decay rates calculated over the first 20 hours after a recovery phenomenon, during the transient decay period, can be as high as 5.8 mV h^{-1}.

Table 4-2: Comparison of irreversible degradation rates from polarization curves, durability data, and calculations.

Open Circuit Irreversible Voltage Degradation Rate (mV h^{-1})

High Pressure/Temperature Polarization Curve (HPHT)	Low Pressure/Temperature Polarization Curve (LPLT)	Proposed Model	OCV Durability Data
0.083	0.141	0.146	0.089

These results emphasize that the rate of voltage change during the transient period, which is higher than the degradation rate in the steady decay period, should not be mistaken for voltage degradation caused by irreversible changes in the materials.

The cell used in this study was able to recover most of the voltage loss after drawing current confirming that the loss was unrelated to material degradation. Had the transient voltage degradation been permanent it would have been evident in the polarization curves given the magnitude of the transient voltage loss. The identification of the reversible and irreversible voltage loss as well as the irreversible voltage decay rate is illustrated in Figure 4-6. Though the exact mechanism for reversible voltage loss was not studied, it is proposed that it is related to platinum oxidation or water content in the fuel cell.

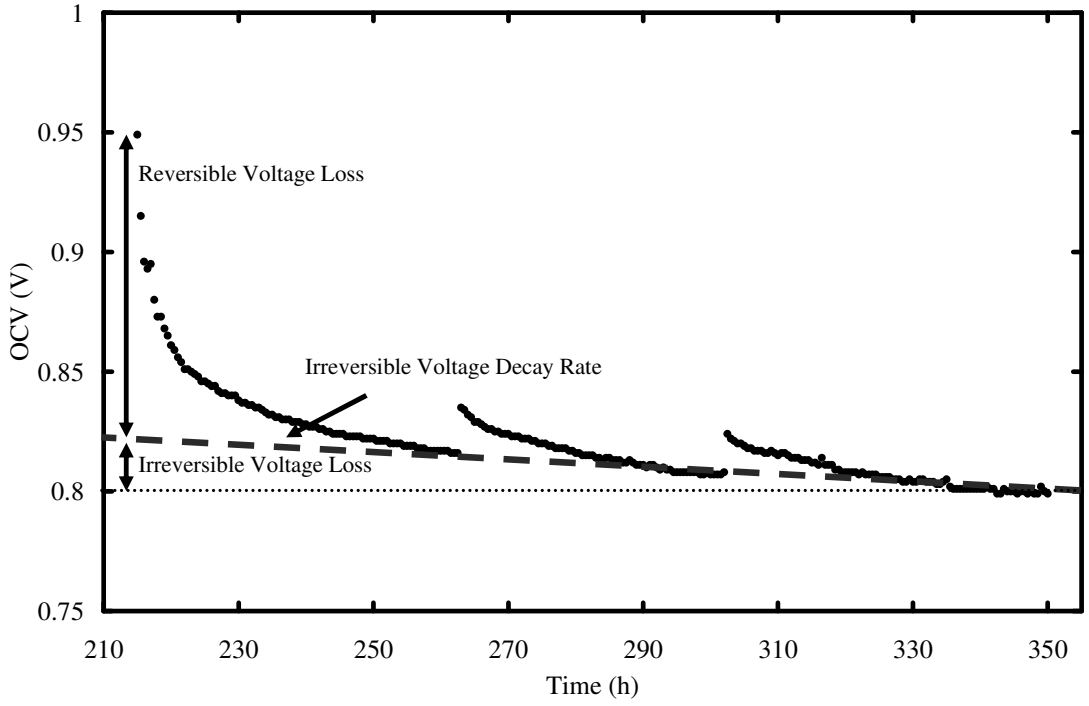

Figure 4-6: Reversible and irreversible degradation as well as irreversible degradation

rate for Cell 5.

4.2 CHAPTER SUMMARY

The above work demonstrates how some of the voltage loss observed during an open circuit voltage durability experiment can be considered reversible, and some of the loss is irreversible. This irreversible loss, primarily identified through changes in polarization curves, can also be predicted using measurements of degradation such as changes in crossover current and changes in electrochemically active surface area. In terms of degradation modeling then, it is reasonable that if crossover and changes in electrochemical active area could be predicted using a model that is linked to degradation causes such as material properties and operational conditions. By doing that the irreversible performance degradation could also be predicted. The development of such a model is the subject of the next chapter.

CHAPTER 5 : INITIAL DEVELOPMENT OF A CHEMICAL DEGRADATION MODEL

In order to model performance degradation, it is necessary to understand the irreversible changes in the materials. Chemical degradation of the electrolyte membrane can lead to membrane thinning and consequently increased hydrogen crossover which further leads to performance degradation. In order to model this process it is necessary to first understand how the materials change with time and how material properties and operational conditions may influence the process.

This chapter presents the result of an open circuit voltage degradation experiment on Cell 5. This experiment will be used to understand aspects of the chemical degradation mechanism of a fuel cell electrolyte membrane. This understanding will then be used as the basis for a semi-mechanistic degradation model. The intent is to create a model that links material properties and operating conditions to the irreversible degradation of the membrane. Further, the model will propose how these material changes can be used to estimate changes in performance.

The key results of this chapter are:

- Open circuit voltage testing causes chemical degradation of the electrolyte membrane.
- The rate of degradation, as measured by fluoride ion release and voltage degradation, begins rapidly and then slows with time
- Based on SEM and fluoride release data, the electrolyte degradation starts on the cathode sie and then slows when the cathode electrolyte has been consumed.
- A model of the chemical and physical transport processes is proposed and successfully simulates the experimental data.
- The semi-mechanistic model is also able to describe fluoride release behaviour in experiments with multiple interruptions in testing.
- The results show that such interruption in testing, especially early during testing, can have a significant effect on cumulative fluoride release trends.

The initial OCV test examines a Hydrogenics single cell with a Gore PRIMEA 5510 reinforced catalyst coated membrane. This membrane is reinforced which allows the side of degradation to be identified. The OCV experiment was conducted at 90°C and 75% anode/cathode relative humidity. The effluent water was collected over the testing time for fluoride ion measurement. SEM analysis was used to determine the extent of degradation on the membrane.

Some of the contents of this chapter have been accepted for publication in the Journal of Power Sources and is expected to be published in August 2008 [70].

5.1 EXPERIMENTAL RESULTS

Initial Gore™ Membranes – Terminology and Crossover

The reinforced catalyst coated membrane used in this study consists of several layers. Figure-5-1 is a scanning electron microscope (SEM) image identifying the 5 main layers of a Gore™ PRIMEA® series 5510 catalyst-coated membrane (CCM). The most distinguishing feature of these membranes is the expanded polytetrafluroethylene

(ePTFE) reinforcement layer at the centre of the membrane. The reinforcement layer is a porous ePTFE membrane and is discussed in the literature [8]. Since this layer bisects the electrolyte membrane, the electrolyte closest to the anode will be referred to as the anode electrolyte and the electrolyte closest to the cathode will be referred to as the cathode electrolyte. Initially, anode and cathode electrolyte layers have similar thicknesses measuring between 4 – 6 μm. The reinforcement layer thickness ranges between 6 – 7 μm. The total thickness of CCM is approximately 50 μm.

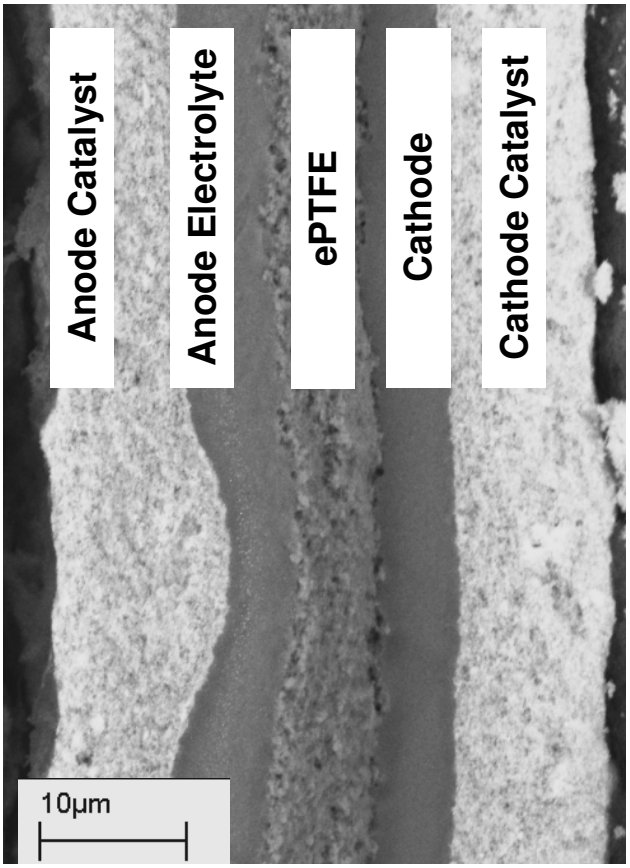

Figure-5-1: SEM cross-section of a fresh GoreTM PRIMEA 5510 reinforced catalyst coated membrane.

Hydrogen permeation across the CCM was measured by crossover current (CC) as described in Chapter 3. Since hydrogen permeability is a function of the hydration and temperature of the membrane [10,32,71], measurements were taken at the same conditions of the experiment (in this case 90°C, 75% RH). A typical crossover current curve is shown in Figure 5-2, the current stabilized at 0.143A or 1.8 mA cm^{-2}. Hydrogen

and oxygen permeability was also measured in a separate test using conventional flow measurements. Those results showed that hydrogen was 2.6 times more permeable than oxygen which is consistent with literature [32,33].

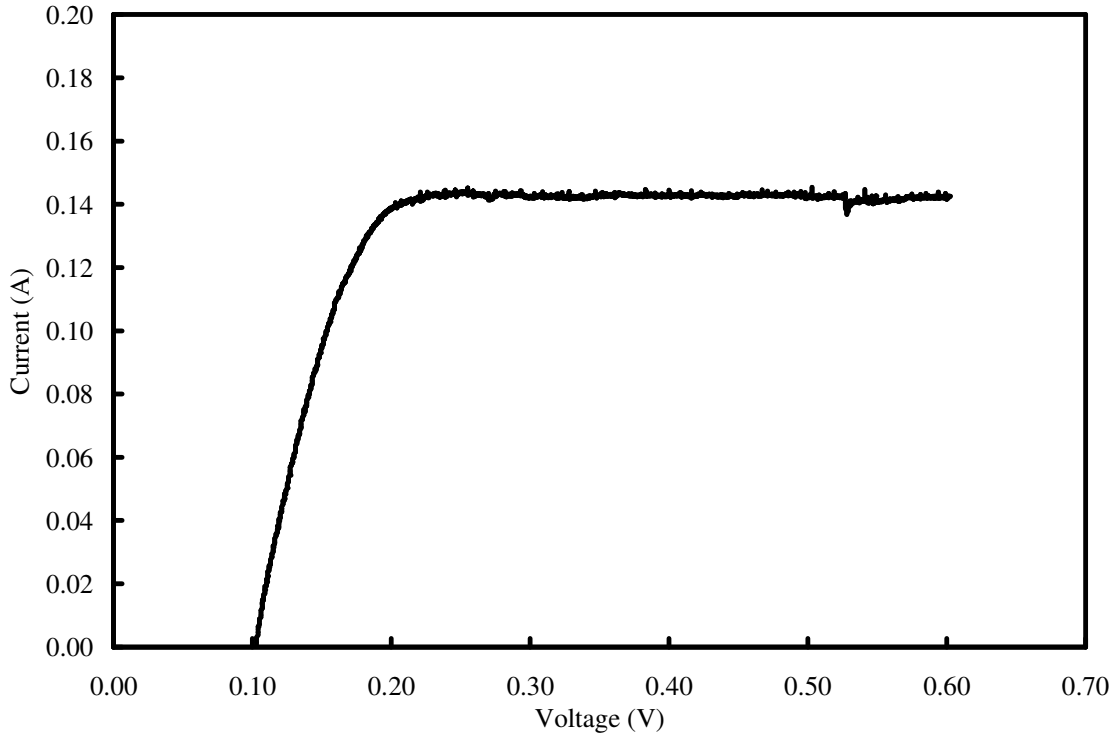

Figure 5-2 : Crossover current curve for Cell 3 using a GoreTM CCM at 90°C,75% RH, and no backpressure using 2 mV/s scan rate.

Diagnostic Tests: Open Circuit Voltage Performance

The variation of the cell open circuit voltage for Cell 3 with time is shown in Figure 5-3. The voltage degradation curve displays several characteristics typical of Gore™ membrane degradation under OCV conditions [12,68]. First, there is an initial rapid drop in voltage followed by stabilization. Interruption of the testing for polarization curve measurement causes voltage recovery, as discussed in the previous chapter.

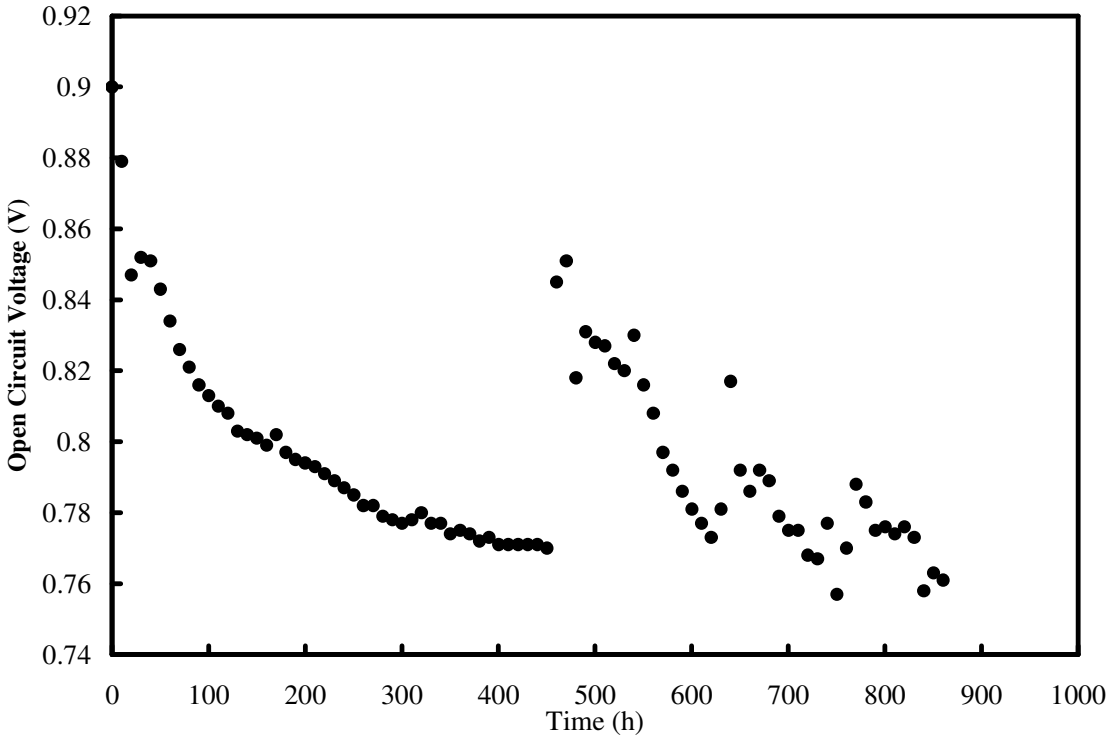

Figure 5-3: OCV durability data for Cell 3 at 90ºC, 75% RH, and no backpressure for Cell 3.

The cell was operated for the first 460 h without interruption. From 460 to 860 hours, the experiment was stopped several times. The initial voltage drop during the first 100 hours is mostly attributed to recoverable processes as described in the previous chapter. Overall the voltage dropped from 0.9 V to approximately 0.77 V. There was little observed voltage degradation between 380 h and 460 h. Further, between 460 h and 860 h, despite the high degree of scatter caused by the more frequent stoppages, the voltage was observed to remain around 0.77 V, also indicating that no significant voltage degradation was occuring.

Diagnostic Tests: Fluoride Release

Effluent water was collected from both anode and cathode sides of the fuel cell and fluoride ion concentration was measured using ion chromatography. Using measurements of the total amount of water collected, the cumulative mass of fluoride released as well as the fluoride release rates could be determined (Figure 5-4a and b). There are several

sections of the cumulative fluoride release curve (Figure 5-4a) of note. Both anode and cathode curves begin with a slow rise before increasing linearly and finally reaching an upper limit. This is also reflected in the release rate data (Figure 5-4b) which shows that fluoride release rates peak at approximately 150 hours. This is consistent with data reported by Liu and coworkers [72] using similar Gore^{TM} membranes. Finally, cathode cumulative release was higher than anode cumulative release. A discussion of uncertainty in fluoride release results is available in Appendix D.

Water balance calculations were conducted to determine if there was any net water flow from the anode to the cathode which could be involved in transporting ions across the membrane. Over the course of the experiment, measured cathode and anode effluent water flow rates ranged between 15-40 mL/h and 9-13 mL/h, respectively. Calculated rates based on inlet RH and gas flow rate were determined to be 32.9 mL/h and 12.1 mL/h for the cathode and the anode sides, respectively. The bulk of the measurements were similar to the theoretical values (Figure 5-5) and deviations are attributed to ambient temperature fluctuations or water balance collection error and variability. Sample calculations for theoretical values can be found in Appendix C. From this data, there is no evidence of 'net water transport' from the anode to cathode indicating that it was not a factor in fluoride ion transport.

a)

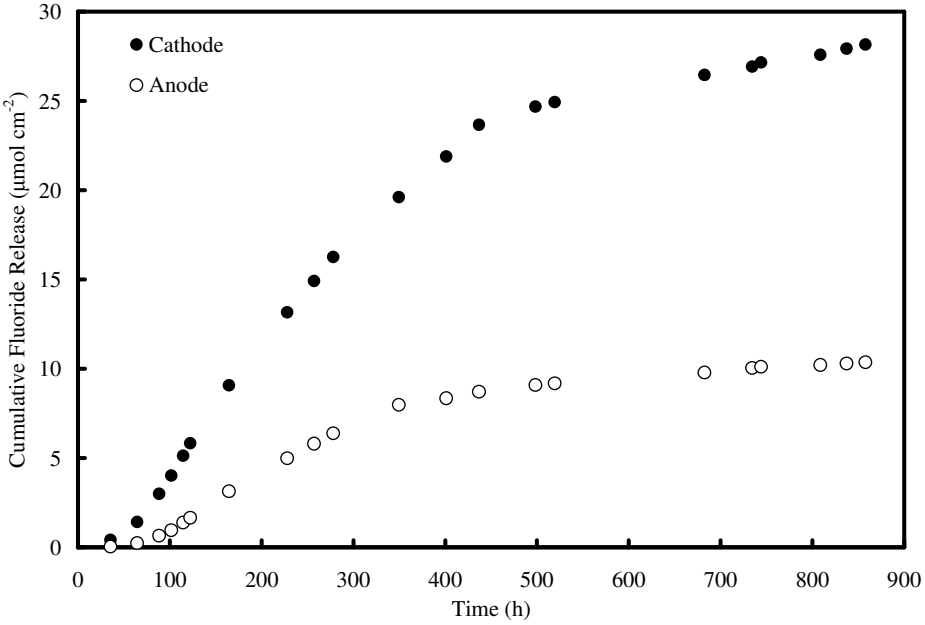

b)

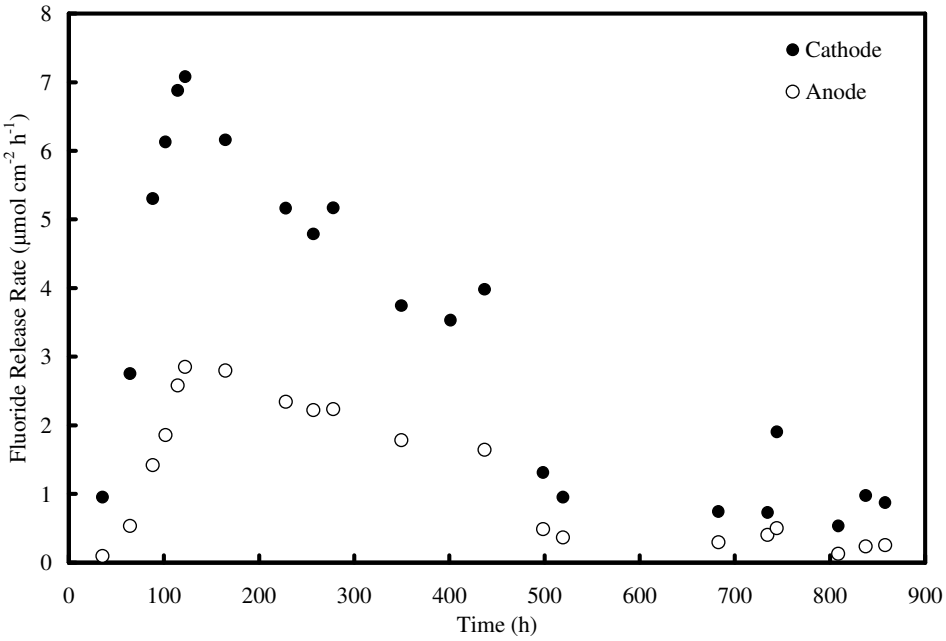

Figure 5-4: Anode and cathode a) cumulative fluoride release and b) fluoride release rates during the duration of testing for Cell 3.

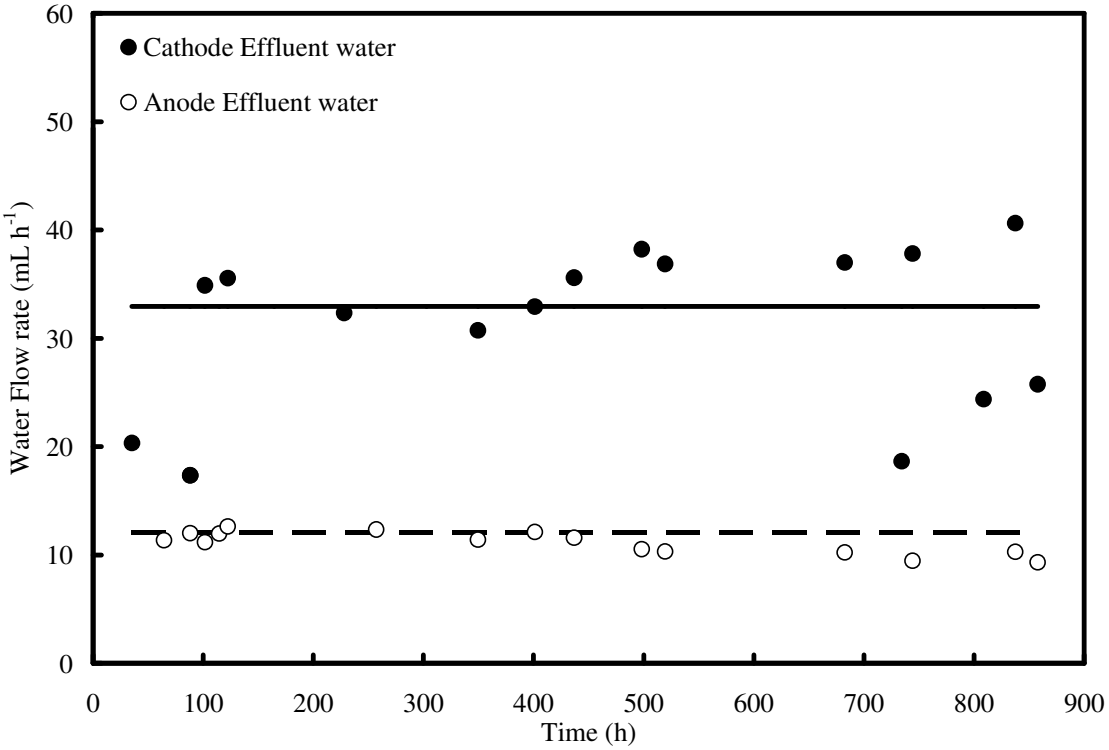

Figure 5-5: Effluent water flow rates. Solid and dotted lines represent theoretical values.

Diagnostic Tests: Crossover Current Measurements

Due to the voltage recovery phenomenon, which occurs when cell operation is interrupted in these particular cells, crossover measurements were only done at the beginning of life (BOL) and after 460 h. Between these times, the crossover current increased from 1.8 mA cm^{-2} to 3.5 mA cm^{-2}.

Forensic Tests: Scanning Electron Microscopy Results

Forensic analysis of the CCM, consisting mainly of SEM imaging, allowed visualization of the effects of degradation. These forensic results will be used to understand the trends in diagnostic testing results which were described in the previous section.

Images of cross-sections from nine evenly distributed locations over the membrane area of the cell were taken. Figure 5-6 shows a typical cross-sectional image of the CCM after 860 hours of operation. A total of 9 evenly distributed sections of the CCM were

analyzed. The cathode catalyst layers, anode catalyst layer, reinforcement layer and the anode electrolyte layer are clearly visible and well defined. However, the cathode electrolyte layer shows significant thinning which is considered to be a sign of chemical degradation. Measurements with Scion Image Analysis software revealed that the anode electrolyte had an estimated average thickness of 3.6 μm and the cathode electrolyte had an average thickness of <1 μm after 860 hours. This result indicates that the cathode electrolyte degrades much more rapidly and extensively than the anode electrolyte. It was also observed that areas where the anode electrolyte had thinned appreciably were only in areas where the cathode electrolyte had degraded extensively. This suggests that the anode electrolyte degrades only after the cathode electrolyte has degraded significantly

One explanation for the severity of cathode electrolyte degradation is that the membrane is more permeable to hydrogen than oxygen. It should be noted that the partial pressure of hydrogen is higher than oxygen under the experimental conditions. Under the test conditions, 75% RH and a total pressure of 760 mmHg, the partial pressure of hydrogen is 364 mmHg, while the partial pressure of oxygen in air at 75% RH and 760 mmHg is only 77 mmHg. From initial permeability experiments, it was also found that hydrogen permeability was 2.6 times greater than oxygen permeability. As discussed in Chapter 1, using Fick's law, the overall crossover rate of hydrogen to the cathode side can be expected to be 12 times greater than the crossover of oxygen to the anode side.

Analysis of the images also revealed platinum deposits in the cathode electrolyte. It is not yet clear if the platinum deposits were a product of the degradation process or if they facilitated degradation. Recent work [50,55,57] has suggested that the platinum deposits are responsible for catalyzing the production of radical species in the membrane. Furthermore, it was postulated that higher hydrogen crossover causes the platinum band to appear close to the cathode. This is consistent with the observed cathode electrolyte degradation since the Pt band was only observed in the cathode electrolyte.

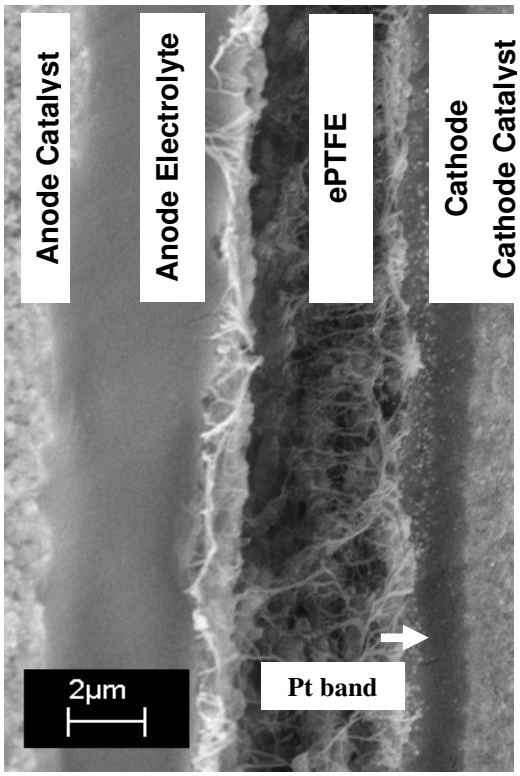

Figure 5-6: Typical cross-section of the aged CCM for Cell 3 after 860 h, 5000X magnification. A platinum band can be seen as white specks within the cathode electrolyte layer.

5.2 THE DEGRADATION PROCESS

Several observations from the SEM analysis and fluoride release data have not been adequately explained in the literature to the author's knowledge. First, degradation reflected in membrane thinning has occurred severely on the cathode electrolyte. Second, fluoride ions are detected in both the anode and cathode effluent water. Although it may be suggested that separate degradation processes are occurring on the anode and cathode sides, a third observation that both fluoride release curves begin to plateau at the same time suggests that all the fluoride is generated at a common reaction location. This is also mirrored in the observation that the OCV stabilized after a period of degradation.

To rationalize the image analysis and the cumulative fluoride release data, it is proposed that degradation, and hence the generation of fluoride ions, occurs on the cathode side,

where hydrogen crossing over from the anode promotes the production of peroxide and hence OH radicals. It is further proposed that a “degradation front” will move through the cathode electrolyte, slow at the inert reinforcement layer, and then begin degrading the anode electrolyte layer.

The reinforcement layer itself does not degrade however the electrolyte embedded within the reinforcement will degrade if radicals are able to reach those locations from the generation point. The fluoride produced on the cathode side may be transported out of the cell by two paths as depicted in Figure 5-7. The first path (Path 1) considers fluoride diffusing from the generation point, through the cathode GDL/MPL and to the cathode channels. The second path (Path 2) requires that the fluoride ions diffuse through the electrolyte membrane as well as the anode GDL/MPL to reach the anode channels.

This mechanism is supported by the SEM observations which suggests that the cathode electrolyte degrades before the anode electrolyte. It also explains why the cumulative cathode fluoride release is much higher than the cumulative anode fluoride release since there would be less diffusion resistance, because of the shorter path length, following Path 1 rather than Path 2.

Finally this mechanism also explains why anode and cathode fluoride release curves plateau at the same time. Since all fluoride is being produced by a reaction between radicals and the cathode side electrolyte the fluoride production rate would be expected to slow or stop when the electrolyte has been depleted. It is possible that once the cathode electrolyte is severely degraded anode degradation may become significant as the degradation front moves. The reason why the cathode degradation is dominant is attributed to the higher driving force for hydrogen permeation over oxygen permeation as previously discussed.

A final feature of the cumulative fluoride release curves is the initial lag time. This is attributed to the time delay between the production of fluoride ions within the electrolyte and movement into the channel caused by the resistance to diffusion in both paths. The

path to the anode channel (Path 2) has higher resistance because of the extra layers of material to diffuse through and hence would have a longer lag time. This is consistent with the cumulative fluoride release observations.

The OCV data can also be similarly interpreted. Open circuit voltage has been shown to be related to hydrogen crossover. As degradation of the electrolyte proceeds, it becomes thinner and allows hydrogen permeation to increase, and the OCV to decrease. Once the cathode electrolyte has been substantially degraded, the degradation slows. Since the degradation slows, the membrane ceases to thin, or the rate of thinning decreases substantially and crossover rates can be expected to stabilize. As such, the open circuit potential will also stabilize.

5.3 Formulation of a Semi-Mechanistic degradation model

To understand the mechanisms involved in the degradation process, a semi-mechanistic 1-dimensional transient model is proposed. The overall purpose of this model is to provide a simple tool to investigate the effects of membrane permeability and relative humidity on cathode electrolyte degradation, fluoride release, and open circuit voltage degradation, as well as identify parameters which help explain the experimental results. Further uses of this model include incorporation into fuel cell system reliability models since it predicts membrane degradation with time as well as offering a framework to evaluate other proposed degradation mechanisms.

The model incorporates degradation processes caused by hydrogen crossover and the transport of fluoride ions in an attempt to simulate the experimental data. The system studied experimentally is highly complex, consisting of many different layers. In order to simplify the system four main regions will be considered, as shown in Figure 5-7. The anode and cathode GDL/MPL/catalyst layers constitute two such blocks while the electrolyte membrane will split into anode and cathode blocks. Degradation is considered to occur at the cathode electrolyte/catalyst interface where oxygen transport to the reaction sites is fast. It is also assumed that the electrolyte and ePTFE layers within the membrane controls permeation of hydrogen from the anode to the cathode. Under

OCV conditions the reactant pressures are assumed to be uniform from the channels to the electrolyte membranes.

The main processes modeled here are: a) the permeation of hydrogen to the cathode catalyst/electrolyte interface; and b) the degradation of the cathode electrolyte. This degradation process is modeled as a reduction in membrane thickness (reduction of mass) accompanied by the release of fluoride ions. Anode electrolyte degradation is not considered at this time. Fluoride ions are considered to diffuse through the various layers to either the cathode or anode channels (Path 1 and Path 2 as indicated in Figure 5-7) where they are swept away. The impact of increased crossover with time due to the reduction of thickness and changes in the electrochemically active surface area on open circuit potential are also modeled.

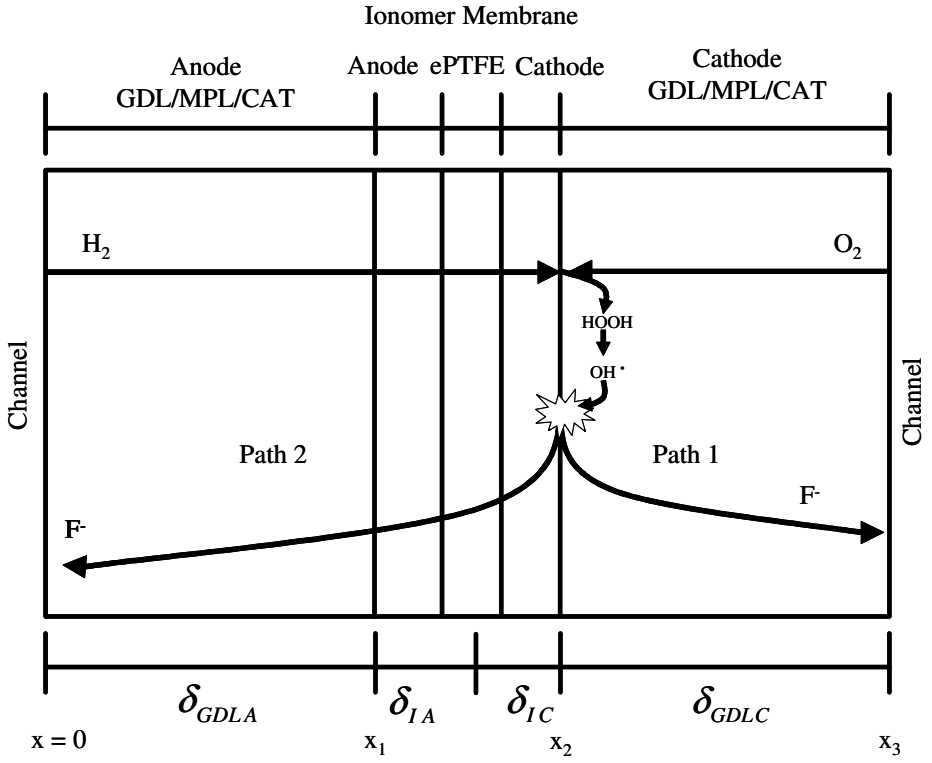

Figure 5-7: Model domain and processes highlighting fluoride ion transport pathways.

Membrane Degradation and Fluoride Ion Production

The rate of hydrogen crossover is determined by the permeability of the membrane, the partial pressure difference across the membrane and the thickness of the electrolyte membrane layers. The hydrogen flux N_{H_2} can be calculated from Equation (5-1) and is related to the crossover current measured during linear sweep voltammetry tests by (5-2).

$$N_{H_2} = P_{M,H_2} \frac{\Delta p_{H_2}}{\delta_m} \tag{5-1}$$

$$i_{H_2} = P_{M,H_2}(2F)\frac{\Delta p_{H_2}}{\delta_m} = P'_{M,H_2}\frac{\Delta p_{H_2}}{\delta_m} \tag{5-2}$$

Once at the reaction site, the hydrogen will react with oxygen to form peroxide species which will then form radicals. These radicals are responsible for the chemical degradation of the electrolyte. Oxygen is presumed to be abundant and thus the radical generation reaction will be controlled by hydrogen permeation. The rate N_{OH} at which radicals are produced is therefore proportional to the flux of hydrogen permeating through the membrane and can be described by Equation (5-3).

$$N_{OH} \ \alpha \ N_{H_2} \tag{5-3}$$

Once created, OH radicals will degrade the polymer electrolyte membrane producing fluoride ions as a product. Consumption of the electrolyte therefore depends on the rate of OH radical production as well as the amount of electrolyte available for reaction. In this case the accessible polymer is the cathode electrolyte since radicals are short lived will react near where they are created. The rate of electrolyte consumption will therefore be related to the rate of radical production and the fraction of remaining cathode electrolyte, f_1, as shown in equation (5-4).

$$-\frac{df_I}{dt}\alpha(N_{OH})(f_I) \quad \textbf{(5-4)}$$

Substituting the hydrogen flux and a proportionality constant yields Equation (5-5):

$$-\frac{df_I}{dt} = K_1(N_{H_2})(f_I) \quad \textbf{(5-5)}$$

where K_1 is a proportionality constant relating the hydrogen flux and electrolyte fraction to the electrolyte degradation rate. This degradation rate determines the rate of fluoride production as well as the rate of thickness change. It has been suggested in the literature that the dependence of degradation on the hydrogen flux may be of a higher order [55]. For the purposes of the initial model development based on the above data set, a first order relationship has been assumed. This assumption will adequately serve the purpose of demonstrating how the model was developed and its uses until more data are presented in later chapters. This model will be referred to as the first-order model. A second relationship that will be explored is a second order dependence on hydrogen flux, a second-order model as shown in Equation (5-6).

$$-\frac{df_I}{dt} = K_1(N_{H_2})^2(f_I) \quad \textbf{(5-6)}$$

The release of fluoride ions is related to the rate of electrolyte degradation through the polymer chain structure. Equation (5-7) relates the rate at which fluoride is produced to the rate of loss of electrolyte by a proportionality constant. Physically this constant is related to the number of fluorine atoms in the electrolyte chain structure.

$$\frac{dn_{F^-}}{dt} = -K_2\frac{df_I}{dt} \quad \textbf{(5-7)}$$

Fluoride Ion Transport

Once generated fluoride ions may be transported to the channels of the bipolar plates by Path 1 and Path 2, as previously discussed. Path 1 considers fluoride ion diffusion from the cathode electrolyte/catalyst interface through the cathode GDL layer and ultimately to the cathode channels. Path 2 involves diffusion of fluoride ions from the cathode electrolyte/catalyst interface, through the electrolyte layer, the electrolyte-filled ePTFE layer and the anode GDL layer to the anode channels. The rate at which these processes occur depends on the concentration gradients in the different layers. These gradients are time-dependent and are modeled according to Fick's law as shown in Equation (5-8).

$$\frac{\partial C_{F-}}{\partial t} = D_i \frac{\partial^2 C_{F-}}{\partial x^2} \quad \text{where } D_i = \begin{cases} D_{GDL}, 0 < x < x_1 \\ D_1, x_1 < x < x_2 \\ D_{GDL}, x_2 < x < x_3 \end{cases} \tag{5-8}$$

At the generation site, x_2, the flux of fluoride is considered to be balanced by the flux of fluoride away from the site by the two transport paths (1 and 2) as shown in Equation (5-9):

$$N_{F-}\big|_{x_2} = \left[N_{F-}\right]_{Path\,1} + \left[N_{F-}\right]_{Path\,2} \tag{5-9}$$

Further, the flux of fluoride out of the GDL and into the channel is described by Equation (5-10).

$$N_{F-} = D_{GDL} \frac{dC_{F-}}{dx} \tag{5-10}$$

Finally, the cumulative fluoride release into the cathode or anode channels is given by (5-11).

$$F_C = \int_0^t N_{F-} dt \tag{5-11}$$

Electrolyte Thickness Change

Degradation of electrolyte material is considered to result only in a change in thickness, therefore the percentage loss of thickness will be equivalent to the percentage change in mass from the initial mass as in (5-12). As the thickness changes with time, permeability can be calculated by Equation (5-2).

$$\delta_m = \delta_{IA} + \delta_{IC}^o f_I \tag{5-12}$$

For the reinforcement layer, it is only considered a barrier to gas crossover when filled with electrolyte. This model considers that radical species may reach the electrolyte within half of the reinforcement layer, eventually reducing its barrier properties. This half of the reinforcement layer is included in δ_{IC}^o.

Open Circuit Voltage

The measured voltage of an OCV durability experiment is influenced by reversible and irreversible processes as previously discussed. Reversible processes may be affected by platinum oxidation or water content of the fuel cell while irreversible processes are affected by membrane thinning and degradation. The open circuit potential during an OCV durability test can be written as:

$$V_{Cell,OCV} = E^\circ - \eta_{reversible} - \eta_{irreversible} \tag{5-13}$$

The irreversible loss dominated by hydrogen crossover can be described as:

$$\eta_{ix} = \frac{RT}{F} \ln\left[\frac{i_{H_2}}{EAS \cdot i_o}\right] \tag{5-14}$$

which was developed in the previous chapter. Furthermore the total change in OCV from initial crossover and EAS conditions can be described by:

$$\Delta V_{Cell,OCV} = \frac{RT}{F} \ln\left[\frac{i^{o}_{H_2}(EAS_{t2})}{(EAS^{o}) i_{H_2,t2}} \right] \tag{5-15}$$

This $\Delta V_{Cell,OCV}$ is due to irreversible losses and does not account for reversible voltage losses. Finally, the electrochemically active surface area will also decrease as the electrolyte degrades as reflected by the "Pt band" (in Figure 5-6) causing a loss of surface platinum. A specific mechanism for this process cannot be proposed at this time. The net effect of a reduction in EAS is an increase in the crossover current on an active platinum surface area basis. As a first approximation this effect will be modeled by:

$$\Delta V_{Cell,OCV} = \frac{RT}{F} \ln\left[\frac{i^{o}_{H_2}}{i_{H_2}} \right]^{\gamma} \tag{5-16}$$

where γ is a crossover current modifier which accounts for the degradation of the catalytic surface area. The above equations were solved numerically using the 'method of lines'. The Matlab code used can be found in Appendix E. Initial concentrations were zero at all locations. Fluoride concentrations at the GDL/channel boundary were assumed to be zero. The initial cathode electrolyte fraction, f_I, was unity. Parameters were determined by fitting the model to fluoride release data. Model parameters using a first order dependence on N_{H_2} are given in Table 1. The initial hydrogen permeability, $k^{o}_{H_2}$, was measured experimentally.

Table 5-1: Model parameters for first order degradation model.

Variable	Value	Obtained by:
Δp	364.4 mmHg	Measured
δ_{IA}	7.5 x10^{-4} cm	Constant
δ_{IC}^{o}	7.5 x10^{-4} cm	Constant
$P_{M,H_2}^{'}$	1.9 x 10^{-8} A cm cm^{-2} mmHg^{-1}	Measured
K_1	1.8 x 10^{-4} mol^{-1}	Fitted
K_2	4.0 x 10^{-7} mol cm^{-2}	Fitted
D_{GDL}	4.2 x 10^{-9} cm^2 s^{-1}	Fitted
D_I	7.4 x 10^{-11} cm^2 s^{-1}	Fitted
R	8.314 J mol^{-1} K^{-1}	Constant
T	363.15 K	Constant
F	96485 C mol^{-1}	Constant
$E^{\circ} - \eta_{reversible}$	0.814V	Fitted
γ	2.6	Fitted

5.4 MODEL RESULTS

The proposed degradation model was able to adequately describe the observed fluoride release trends shown in comparison to the experimental results. The model fit resulted in a fluoride ion diffusion coefficient of 7.4 x 10^{-11} cm^2 s^{-1} which shows good agreement to ion diffusion coefficients in Nafion™ 117 which are on the order of 2 x 10^{-10} as calculated from Unnikrishnan and coworkers [73]. This provides evidence that the modeled parameters are reasonable. The differences in diffusion resistances in the two fluoride transport paths resulted in differences in anode and cathode fluoride release lag times as shown in Figure 5-8. The slight differences in the experimental and modeled lag times are caused by some of the model simplifications. Degradation was considered to primarily occur at the catalyst-electrolyte interface, though it may actually happen within the cathode electrolyte layer. As such the resistance to ion diffusion was slightly underestimated for Path 1 in the model, resulting in a shorter lag time than experimental results. The differences in diffusion resistance also effectively captured the differences in cumulative fluoride levels after long degradation times. Due to the increased diffusion length from the degradation location in the cathode electrolyte to the anode channels (Path 2) anode cumulative release was smaller than the cathode release. Finally, use of

the cathode electrolyte fraction in the calculation for degradation and fluoride generation rate was able to model the plateau that the cumulative fluoride release curves reach.

It should be noted that the effect of interruptions after 436 hours of operation on fluoride release behaviour have not been discussed. It is not clear from the experimental cumulative fluoride release data shown below if interruptions had any significant effect. Further, since fluoride release rates were low approaching the first interruptions, it is possible that they had minimal effect on the overall trends.

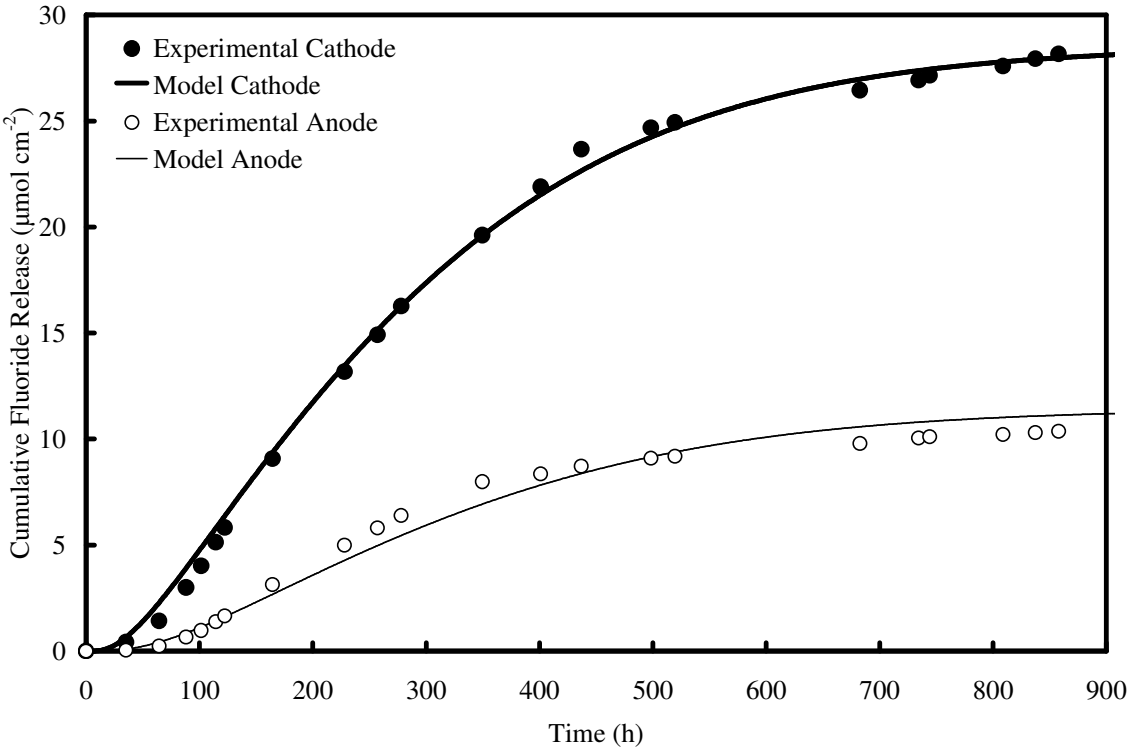

Figure 5-8: Model and experimental fluoride release results for Cell 3.

The model also explains hydrogen crossover. Figure 5-9 is a plot of the two crossover current measurements taken during testing and the predicted crossover curves from the model. The trend cannot be confirmed due to the small number of experimental points, however, the crossover results show good agreement with the point after 460 hours of operation. Note that the number of crossover current measurements was intentionally limited in order not to interfere with the OCV degradation behaviour of the cell.

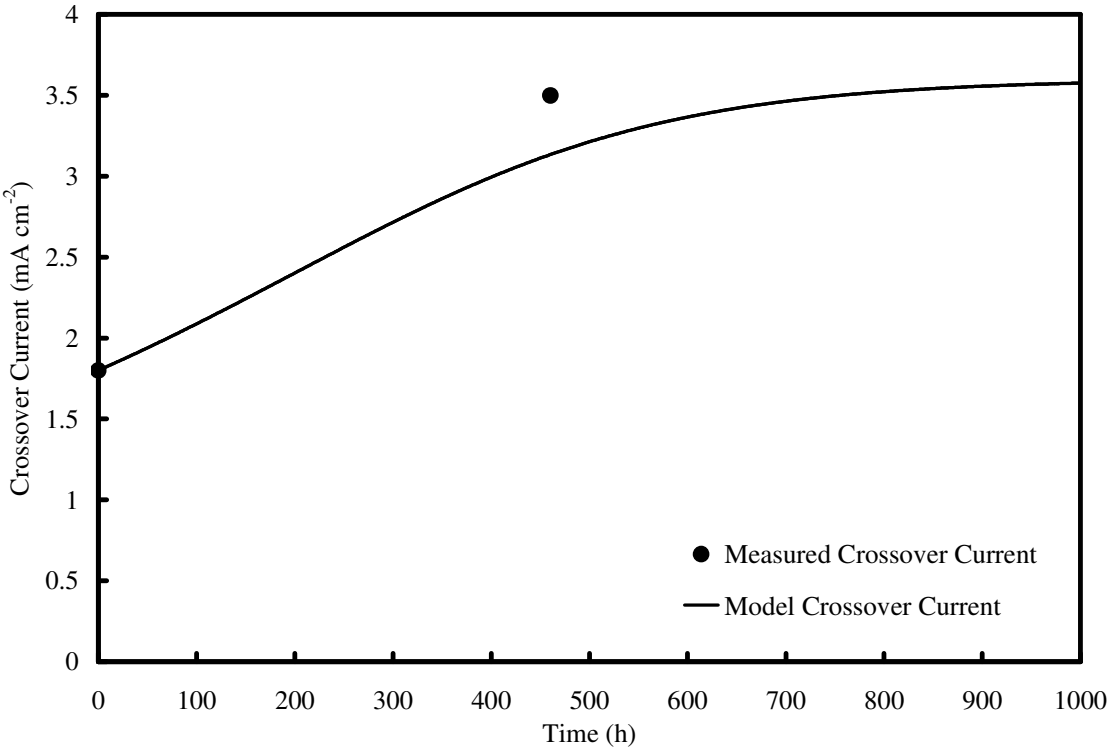

Figure 5-9: Model and experimental hydrogen crossover results for Cell 3.

It was shown in Chapter 4 that under open circuit conditions there are reversible voltage degradation processes which impact the open circuit voltage. At the same time voltage degradation was also shown to be linked to the crossover current as well as the electrochemically active surface area. This model only considers irreversible voltage loss and attributes this loss to hydrogen crossover and loss of active surface area. Figure 5-10 shows model results together with open circuit voltage data.

The difference in simulated and actual voltage between 0 and 200 h is attributed to the reversible voltage loss and is on the same order of the reversible losses shown in Chapter 4. This reversible voltage loss is not considered in the present model. After 200 h the experimental data reaches a steady degradation rate which is where the modeled voltage begins to match experimental data, except for the interruption at 460 h.

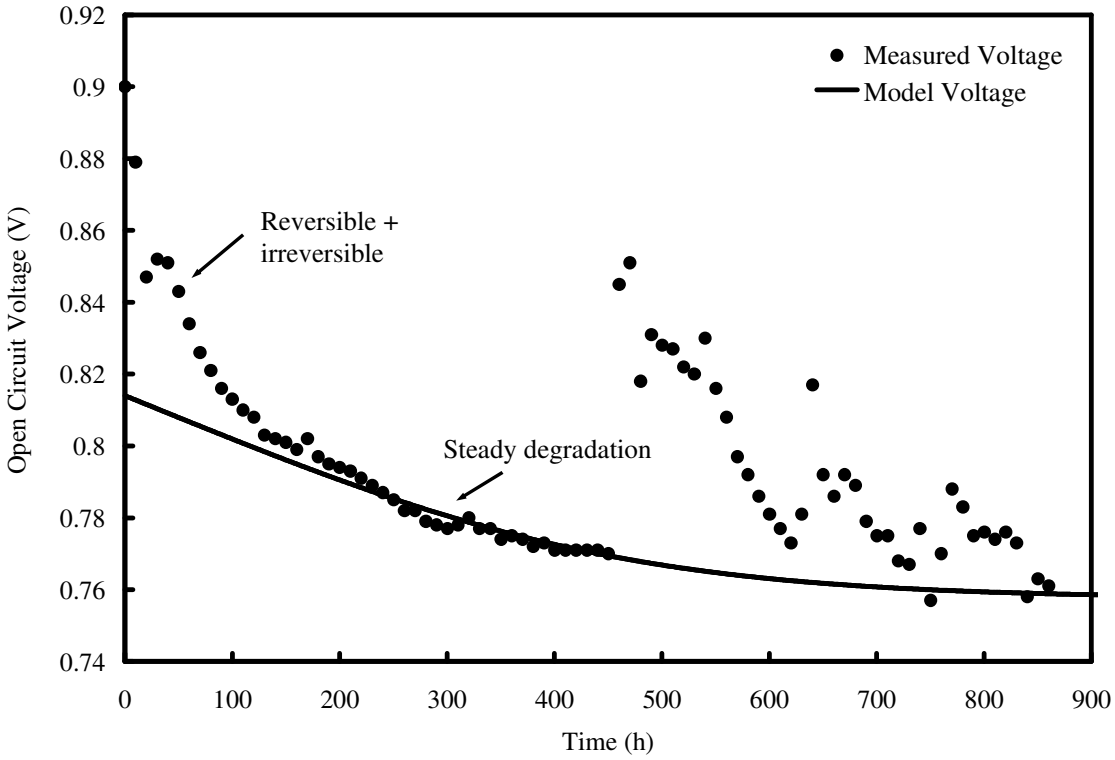

Figure 5-10: Experimental and modeled open circuit voltage results.

The above results show that the proposed degradation model is able to explain the various degradation features seen in the experimental work.

5.5 FLUORIDE RELEASE RESULTS WITH INTERRUPTIONS

A second OCV experiment at 75% relative humidity (Cell 4) was conducted as a repetition of the baseline experiment (Cell 3). Unlike the baseline cell, this experiement had two main differences. First, the cell was only operated for 360 and the second difference was that over the first 436 hours of operation, Cell 4 was interrupted at 35, 85, and 126 hours of operation.

Comparison of Total Cumulative Fluoride Release

Total cumulative fluoride release curves, which combine the contribution from the anode and cathode sides, are shown in Figure 5-11 for the baseline experiment (Cell 3) and for

Cell 4. It is clear from Figure 5-11 that the fluoride curves from the two cells do not match. Cell 3 had a higher total cumulative fluoride release than Cell 4. Inspection of the fluoride curve of Cell 4 shows that initial parts of the curve increase in steps followed by plateaus. Further, it is only after 150 hours of operation that the fluoride release curve increases steadily.

Upon closer analysis it was found that the beginning of each plateau coincided with a break in testing. It is a test station safety measure to purge gas lines with nitrogen and to shut down all heaters when stopping unexpectedly. It was hypothesised that with each stoppage the fluoride concentration profiles within the membrane and GDL were disrupted and cleared. Thus each time the cell was restarted there was an initial lag in the fluoride release as concentration profiles were re-established giving the appearance of a plateau.

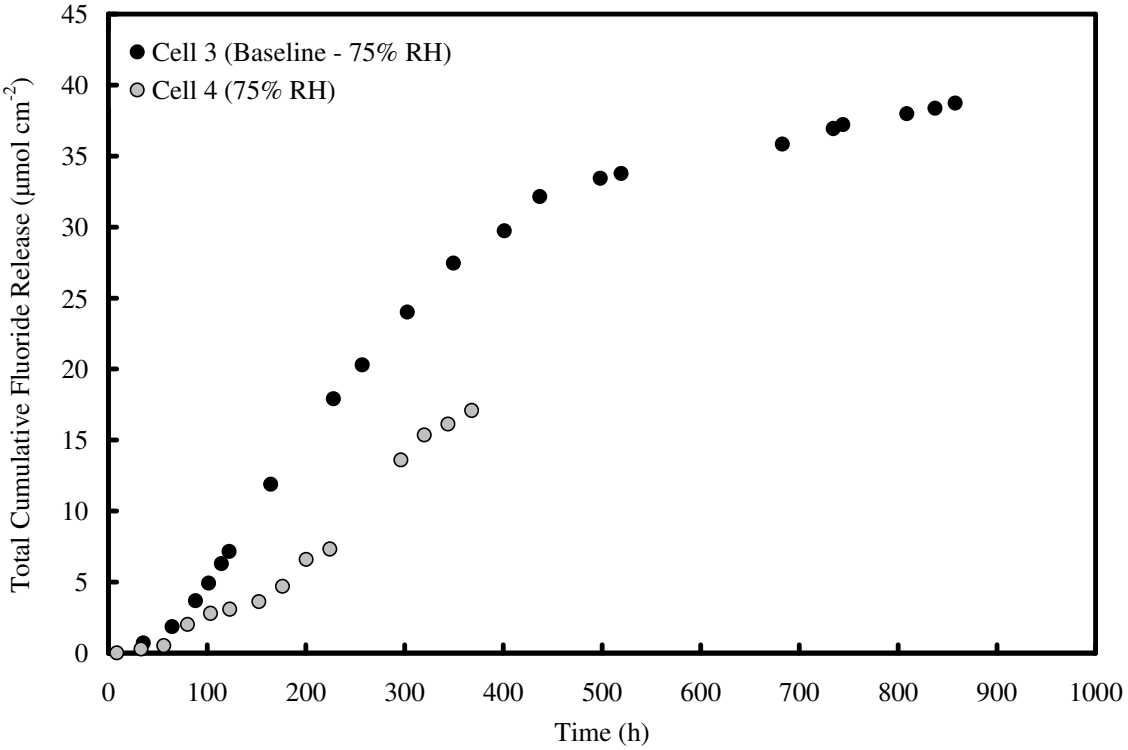

Figure 5-11: Comparison of total (anode + cathode) cumulative fluoride release for Cell 3 and Cell 4 (75% RH).

SEM Analysis

SEM images of the catalyst coated of Cell 4 and Cell 3 are shown in Figure 5-12. Overall, Cell 4, which operated for 360 hours, showed significantly less degradation than Cell 3 which was operated for over 890 hours. Both images show cathode side thinning. Furthermore, in Cell 4 there was no anode thinning. This further reinforces the assertion that the observed degradation and fluoride ion release originates in the cathode electrolyte layer. There was also a platinum band visible in the cathode electrolyte of Cell 4, similar to the baseline case.

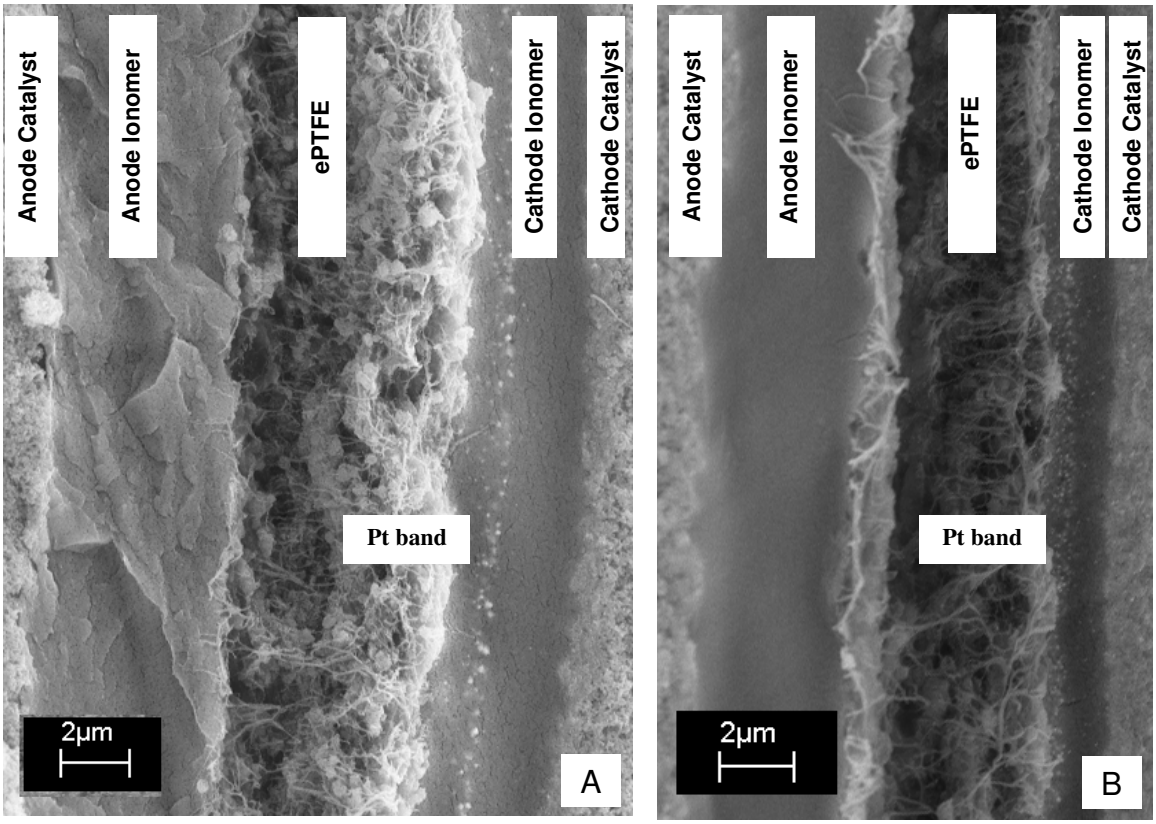

Figure 5-12: Comparison of SEM cross-sections of two degraded Gore CCMs from A) Cell 4 after 360h, 75% RH, and B) Cell 3, Baseline cell after 860h, 75% RH.

Application of Semi-mechanistic Model

The semi-mechanistic model developed in the previous section was applied to the conditions of Cell 4 in order to examine if cell purging was responsible for the discrepancy in fluoride release behaviour with Cell 3. The model formulation and constants used were unchanged from those presented previously.

To simulate stoppages and purging, the model was first allowed to run until a stoppage time. At 35, 85, and 126 hours all fluoride concentrations were reset to 0 and the simulation was restarted. Variables such as the fraction of cathode electrolyte remaining were not reset. Anode and cathode cumulative fluoride release curves and simulation are shown in Figure 5-13. The results show good agreement with the general trends of the experimental data, although the amounts predicted on the cathode side are slightly higher than the experimental data while the model tends to underestimate the fluoride released on the anode side.

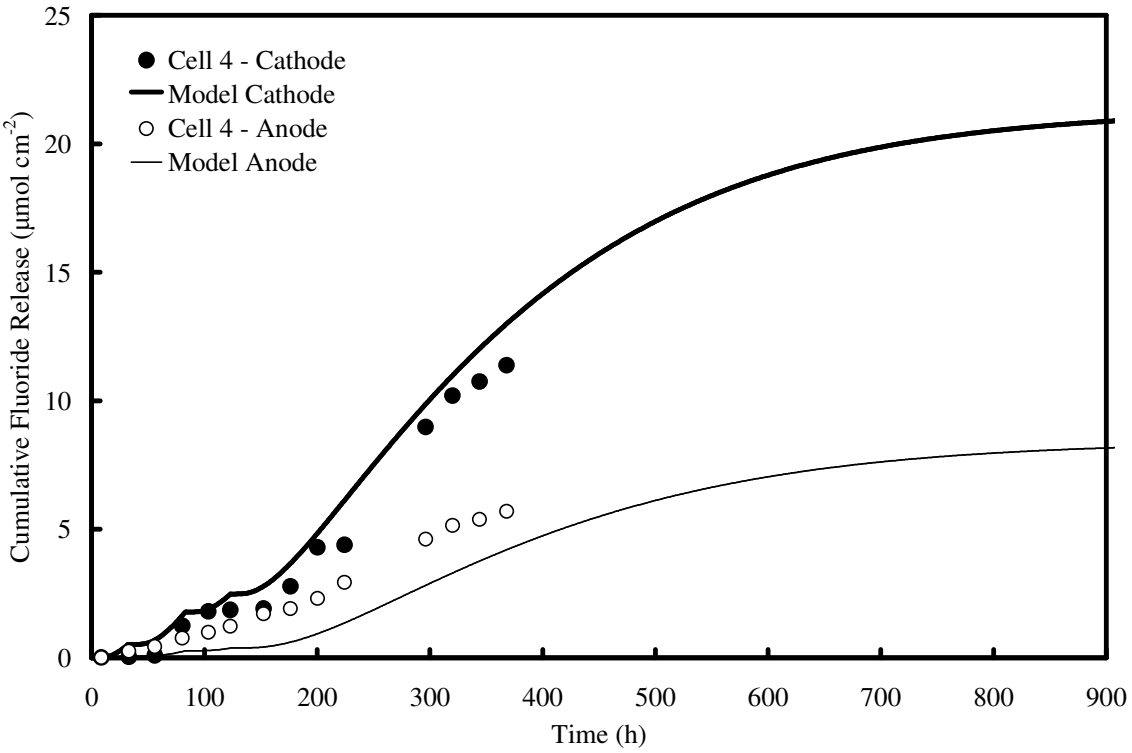

Figure 5-13: Cumulative fluoride release results from Cell 4 for the anode and cathode sides. Solid lines represent simulation with consideration of interruptions.

Total (anode + cathode) cumulative fluoride release experimental results and simulation predictions are shown in Figure 5-14. The model was able to effectively match the total release data with no extra fitting of the parameters. This indicates that the discrepancy between the fluoride release behaviour of Cell 3 and Cell 4 is due to the stoppages which

changed the fluoride release trends. Furthermore, as will be shown in Chapter 7, the differences in the simulated results and experimental data can be explained by differences in the fluoride diffusion coefficients through the electrolyte layer.

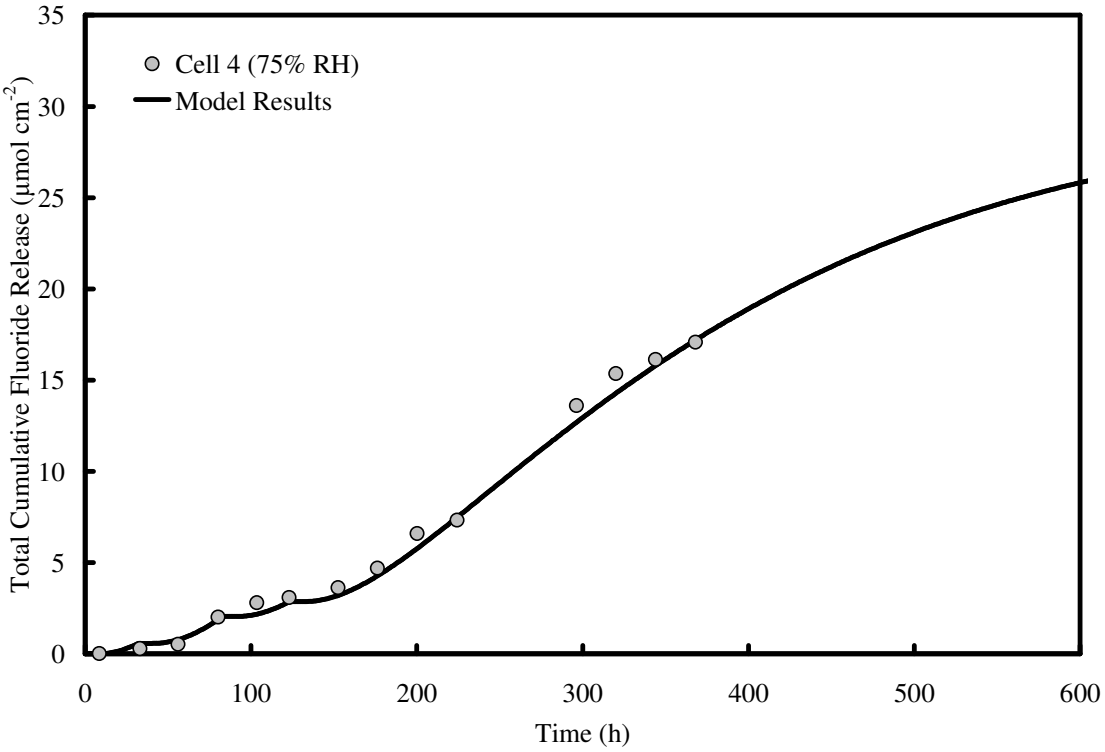

Figure 5-14: Total (anode + cathode) cumulative fluoride release results for Cell 4. Solid lines represent model predictions.

The above result also shows that interruptions may have a significant effect on overall cumulative fluoride release curves and therefore should not be ignored. Previously, it was postulated that the effect of interruptions in testing for the baseline cell is insignificant. Using the above technique to account for the effect of interruptions, a new plot of the modeled and experimental baseline data was prepared (Figure 5-15). The simulation result shows that with the above fitted parameters the model underestimates the fluoride release after 436 hours though it still captures the general trends. Since the interruptions occurred late in the testing after fluoride release rate had already reached a peak, the impact of the interruptions appear to be small.

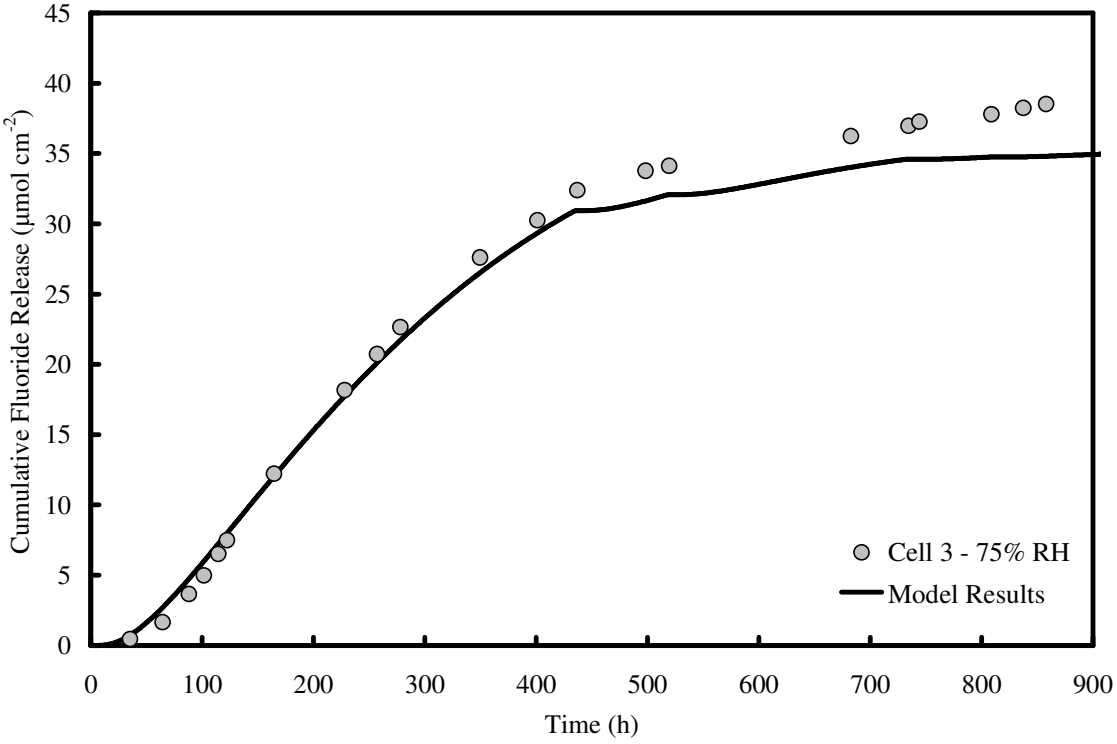

Figure 5-15: Baseline data using the proposed model with consideration of interruptions.

5.6 Chapter Summary

In this chapter a Gore™ PRIMEA® series 5510 catalyst coated membrane was degraded under controlled conditions using an open circuit voltage durability experiment at 90°C, 75% anode and cathode relative humidity and no backpressure. The forensic analysis of the membrane after 860 hours of operation showed that the cathode electrolyte had become severely degraded while the anode electrolyte remained largely intact. A platinum band was also observed within the cathode electrolyte.

Fluoride release results were also consistent with forensic results. Cathode cumulative fluoride release was much higher than anode fluoride release. With time, the anode and cathode cumulative fluoride release began to reach a plateau. The open circuit voltage data was observed to decrease with time. However, as with the cumulative fluoride release results the voltage degradation rate also slowed down.

It is proposed that the majority of the fluoride was generated through the degradation of the cathode electrolyte. It is further proposed that a degradation front starts at the cathode and moves towards the ePTFE reinforcement layer. Once the cathode electrolyte has been consumed, the rate of fluoride generation slows as the degradation front penetrates into the inert reinforcement layer. At this point, it is postulated that the cumulative amount of fluoride released will remain constant until anode electrolyte begins to degrade. Also, the rate of increase in hydrogen crossover, which depends on the rate of thickness reduction of the electrolyte layers, will stabilize. This results in a stabilization of open circuit potential as seen experimentally for the duration of the test.

A semi-mechanistic model was proposed. The model showed that the proposed mechanism can suitably explain the observed trends. The simulation results show that the differences in anode and cathode cumulative fluoride release may be due to the differences in path lengths, and consequently resistance to diffusion, that fluoride ions encounter when moving from the generation point in the cathode to either the anode or cathode channels. These differences in diffusion also explain the lag times seen in the cumulative fluoride data. Further, the model is able to fit the voltage results and it shows good agreement with crossover current data.

On the surface, the data from Cell 4, performed at 75% RH, did not match the baseline fluoride release data from Cell 3. It was postulated that cell stoppages early on in the testing may have retarded the development of the cumulative fluoride release curves. The semi-mechanistic model was used to predict the fluoride release behaviour with these stoppages based on the assumption that stopping the cell would clear out all the fluoride and therefore fluoride concentration gradients would have to restore themselves once the cell is restarted. The model results were able to match the fluoride release behaviour of the repeat cell without any additional fitting of the parameters.

CHAPTER 6 : MODEL VALIDATION AND LIMITATIONS

The focus of this chapter is to apply the semi-mechanistic chemical degradation model developed in the previous chapter to situations of different relative humidity in order to evaluate its predictive capabilities and to propose any necessary modifications to improve these capabilities. This chapter will show:

- Chemical degradation trends at the OCV follow crossover current trends.
- Comparison of first order and second order chemical degradation models show that a second order dependence on hydrogen flux best describes the data.
- Inclusion of interruptions in testing was crucial to fitting fluoride release parameters.
- One limitation of the model is that it does not describe degradation of the anode electrolyte.
- Irreversible voltage degradation rates compare well with initial crossover values.
- It was not possible to model the voltage trends with the proposed model.
- Voltage degradation is likely influenced by other factors beyond chemical degradation.

The study of the effects of relative humidity on chemical degradation of the electrolyte and voltage degradation of the cell was carried out using four different cells. Each cell

was operated at a different relative humidity so that full cumulative fluoride release curves could be gathered. The four cells are listed in Table 6-1 .

Table 6-1: Durability test conditions for Cells 1-3, and 6.

Cell	Anode/Cathode RH %	Cell Temperature °C
1	20	90
2	50	90
3 (Baseline)	75	90
6	100	90

6.1 INITIAL HYDROGEN CROSSOVER

Inspection of the proposed semi-mechanistic model indicates that the initial hydrogen crossover plays an important role in determining how quickly degradation will occur. When measured at the desired temperature and relative humidity, the initial crossover rate essentially summarizes the contribution of thickness, permeability, and pressure through Fick's law (Equation (6-1)) and all of which may be affected by temperature and relative humidity.

$$N_A = \frac{\mathrm{P}_M \Delta p_{H_2}}{\delta} \qquad \textbf{(6-1)}$$

The influence of relative humidity on crossover through a single CCM was measured under constant total gas pressure. The results, shown in Figure 6-1, show a linear decrease of crossover with an increase in relative humidity. An increase in relative humidity has been shown to increase the permeability, P_M, of GORE^{TM} reinforced membranes in the literature [8]. Under the constant pressure conditions used during testing, an increase in relative humidity will also decrease the partial pressure of hydrogen, and hence reduce the driving force for permeation (Δp_{H_2}). Overall, increases in relative humidity have a greater effect on the driving force than the permeability and thus results in a decrease in cross-over current.

The trend in Figure 6-1, which was obtained from a single membrane test at different RH, differs significantly when compared to the crossover results of the four different membranes each tested at a single RH. The initial crossover performance of the membranes was measured at the relative humidity at which each membrane would ultimately be operated during testing. Cells 1 through 3 and 6 were tested at 20%, 50%, 75%, and 100% RH respectively. The results in Table 6-2 show that overall the cells operating at lower relative humidity exhibited a higher crossover rate, which is consistent with Figure 6-1.

An exception to this trend is the higher crossover current through Cell 6, tested at 100% RH, of 2.08 mA cm^{-2}, as compared to Cell 3 which was tested at 75% RH and measured 1.98 $mAcm^{-2}$. Compared to the results in Figure 6-1, Cell 6 is much more permeable than a typical membrane at 100% RH. This behaviour is attributed to membrane-membrane manufacturer variability in permeability and indicates that such variability is more influential to initial gas crossover than humidity conditions alone. Cells 1 – 3 have consistent hydrogen crossover rates with Figure 6-1.

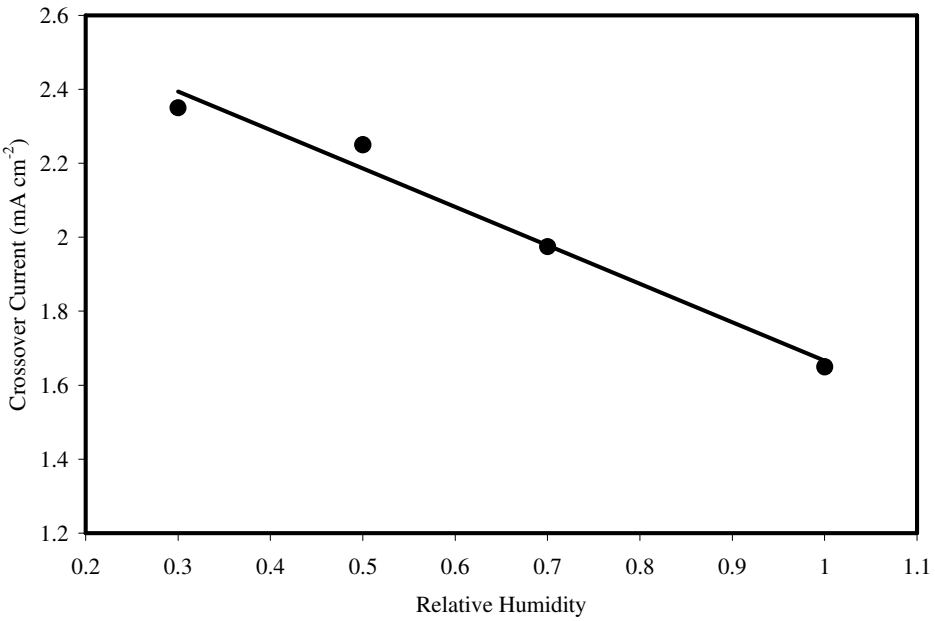

Figure 6-1: Effect of changing RH on hydrogen crossover current at constant total pressure.

Table 6-2: Crossover rates of Cells 1-3, and 6 at their respective test relative humidity.

Cell	Anode/Cathode RH %	Crossover mA cm^{-2}
1	20	2.40
2	50	2.36
3 (Baseline)	75	1.98
6	100	2.08

6.2 Examination of Fluoride Release Behaviour and Membrane Degradation

Total Cumulative Fluoride Release and Microscopy Analysis

An important measure of fuel cell degradation is the extent of fluoride release in the effluent water. In Chapter 5, the fluoride release was linked to degradation of the electrolyte layer. The total (anode + cathode) cumulative fluoride release for the four membranes used in this study are shown in Figure 6-2. The fluoride release curves share many of the same characteristics as reported previously. Though not shown, anode fluoride release was lower than cathode release indicating that cathode side degradation was predominant in all cells.

Overall, the total cumulative fluoride release showed some lag time which is attributed to the time necessary for fluoride ions to be produced within the fuel cell and then diffuse to the channels. It was postulated in Chapter 5 that the cumulative release rates begin to slow when the cathode electrolyte has been completely consumed, and the degradation front has moved into the reinforcement layer towards the anode electrolyte layer.

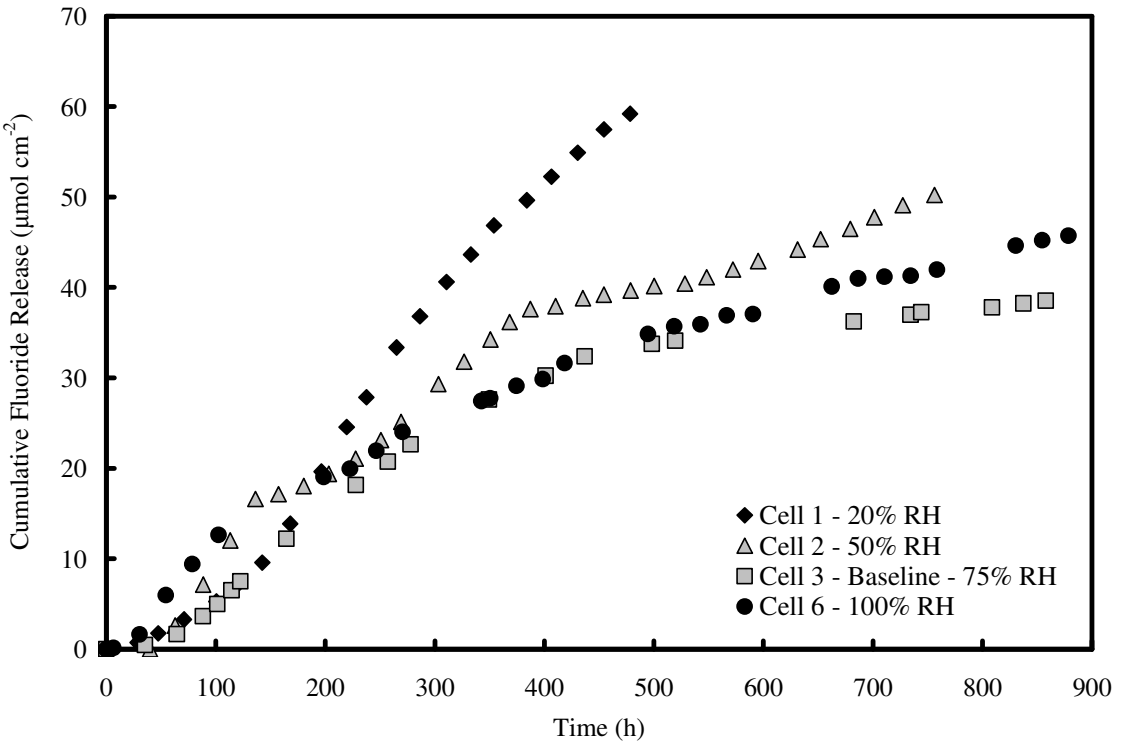

Figure 6-2: Total (anode + cathode) cumulative fluoride release for Cell 1 (20% RH), Cell 2 (50% RH), Cell 3 (75% RH), and Cell 6 (100% RH).

The total (anode + cathode) cumulative fluoride release effectively represents the amount the electrolyte membrane has degraded. From Figure 6-2, it can be seen that after long testing durations the total cumulative fluoride release decreases in the following order: Cell 1(20% RH), Cell 2 (50% RH), Cell 6 (100% RH), and Cell 3 (75% RH). A discussion of uncertainty in fluoride release results is presented in Appendix D.

The relationship between the total cumulative fluoride release and membrane morphology can be seen with scanning electron microscopy. The membranes used in this study contain a reinforcement layer which bisects the membrane. The electrolyte closest to the anode catalyst layer is referred to as the anode electrolyte, and similarly the cathode electrolyte refers to the electrolyte closest to the cathode catalyst layer. The results show that after testing, Cell 3 (75% RH) had significant cathode electrolyte degradation and minimal anode electrolyte degradation (Figure 6-3 b).

Cell 6 (100% RH) exhibited significant cathode electrolyte degradation and some anode electrolyte degradation (Figure 6-3 a). Finally, Cells 1 and 2 (20% and 50% RH respectively) both showed extensive degradation of the anode and cathode electrolytes (Figure 6-3 c and d). Some anode electrolyte could still be observed in Cell 2, although no observable cathode or anode electrolyte remained in Cell 1.

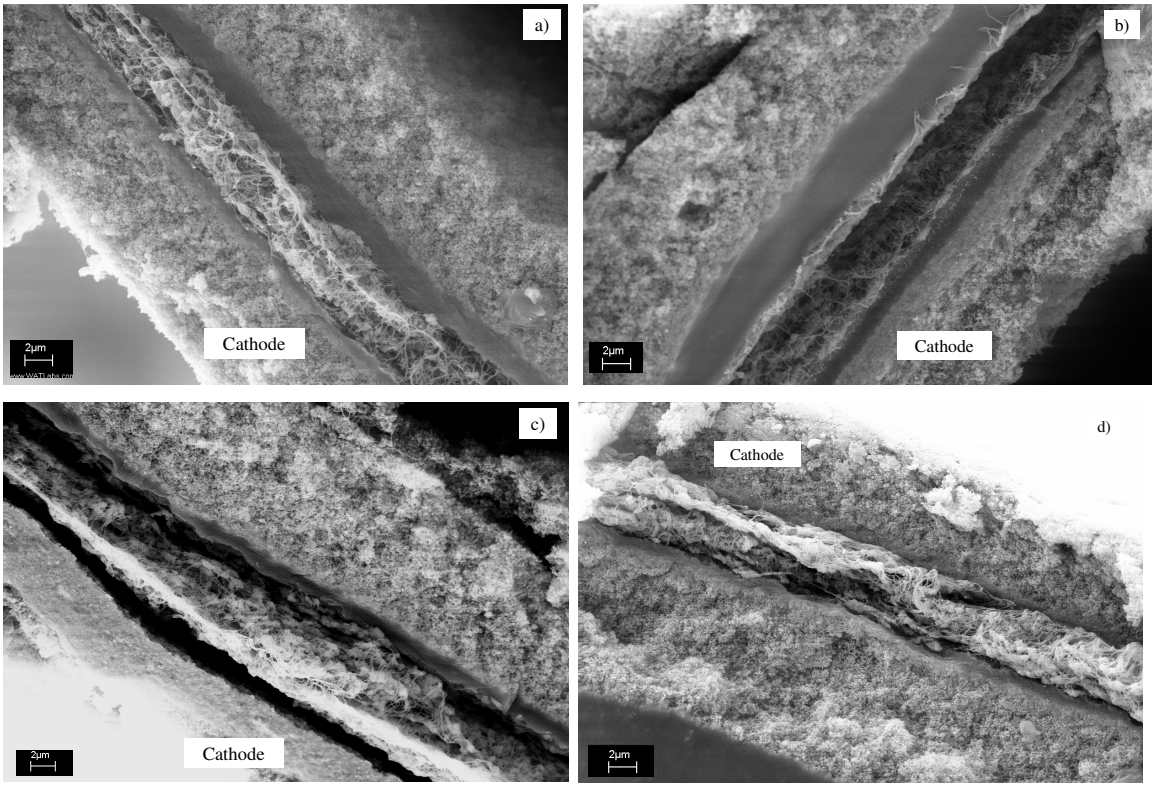

Figure 6-3: SEM images of degraded membranes from a) Cell 6 (100% RH), b) Cell 3 (75% RH), c) Cell 2 (50% RH), and d) Cell 1 (20% RH).

The mechanism of degradation for these membranes that was proposed in Chapter 5 is based on the results of the baseline case shown in Cell 3 (75% RH). It is briefly re-explained here. Hydrogen crossover from the anode to the cathode is considered to be primarily responsible for the observed degradation. It is proposed that at the cathode electrolyte/catalyst layer interface the cross over species promotes the production of hydroxyl radicals. The radicals are then able to penetrate into the electrolyte layer and cause its degradation thus producing fluoride ions, hence creating a degradation front. With degradation, the electrolyte layer begins to thin causing the observed cathode

electrolyte thinning. It is postulated that because of the inert nature of the reinforcement and the small amount of electrolyte in the pore spaces the fluoride release rate slows because of lack of reactants. For example it almost stops in the case of Cell 3.

Degradation of the anode electrolyte will occur if the reaction front penetrates into the anode layer. It is clear from the SEM images that the anode electrolyte layer was significantly degraded in Cells 1 and 2, with some degradation in Cell 6, and minimally degraded in Cell 3.

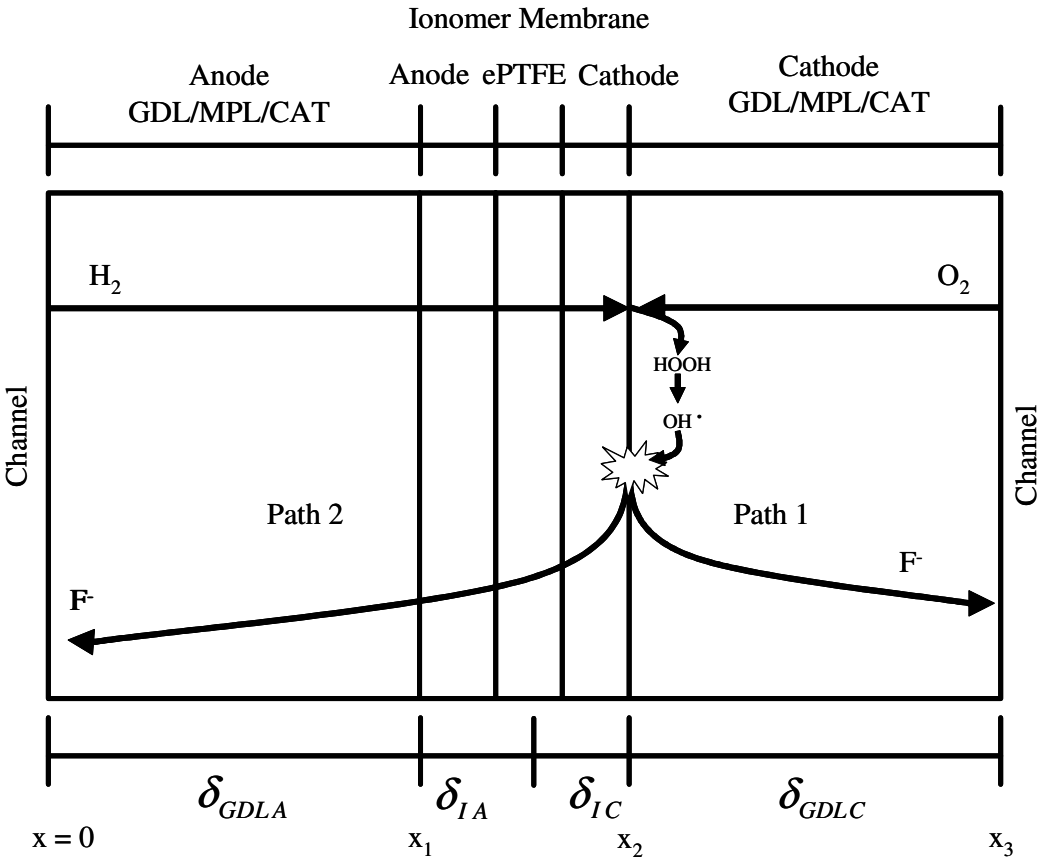

Figure 6-4: Degradation schematic.

To explain the trends seen with relative humidity, the proposed semi-mechanistic model developed in Chaper 5 was employed to simulate the behaviour observed on experimental data presented above. All fitting parameters were held the same as in Chapter 5 and only

the measured membrane permeability and experimental hydrogen partial pressures were inputted for each membrane.

The experimental data and simulation results, using the first-order model, are given in Figure 6-5. The interruptions in testing were considered in simulations and the fluoride concentrations were reset at interruptions. The results show that the model consistently under estimates the experimental data for Cells 1,2, and 6 (20, 50, and 100% RH respectively). Simulation and experimental results are shown in Figure 6-5a,b,and d. Different data fits were attempted using the first order model but none were able to successfully capture the fluoride release trends of all cells.

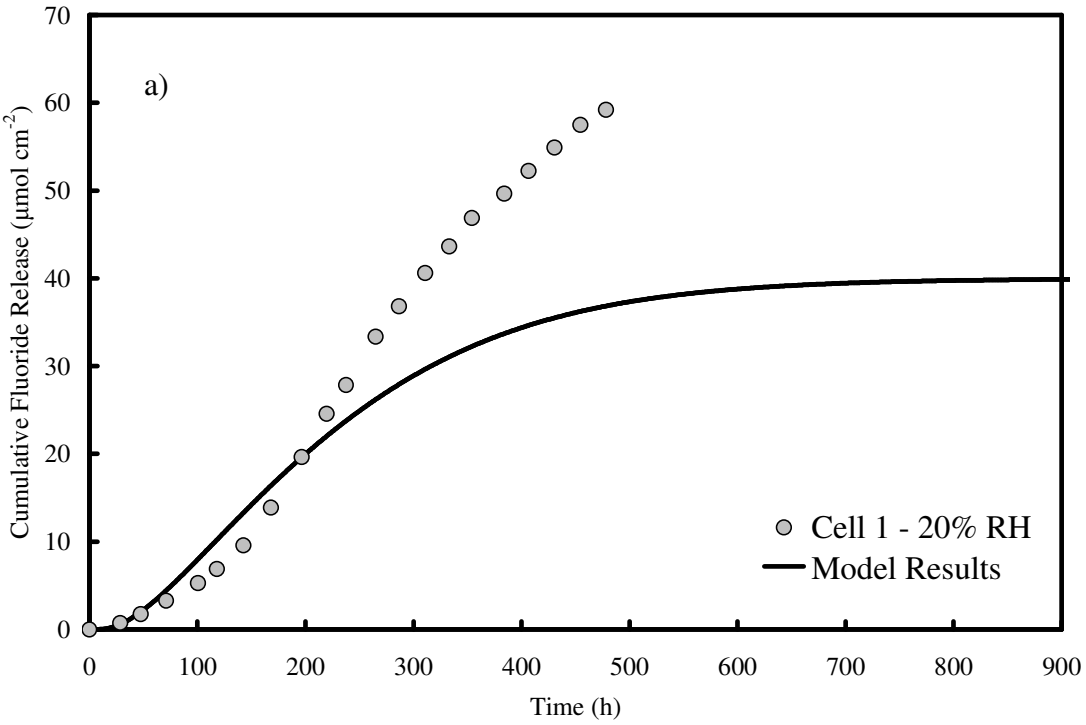

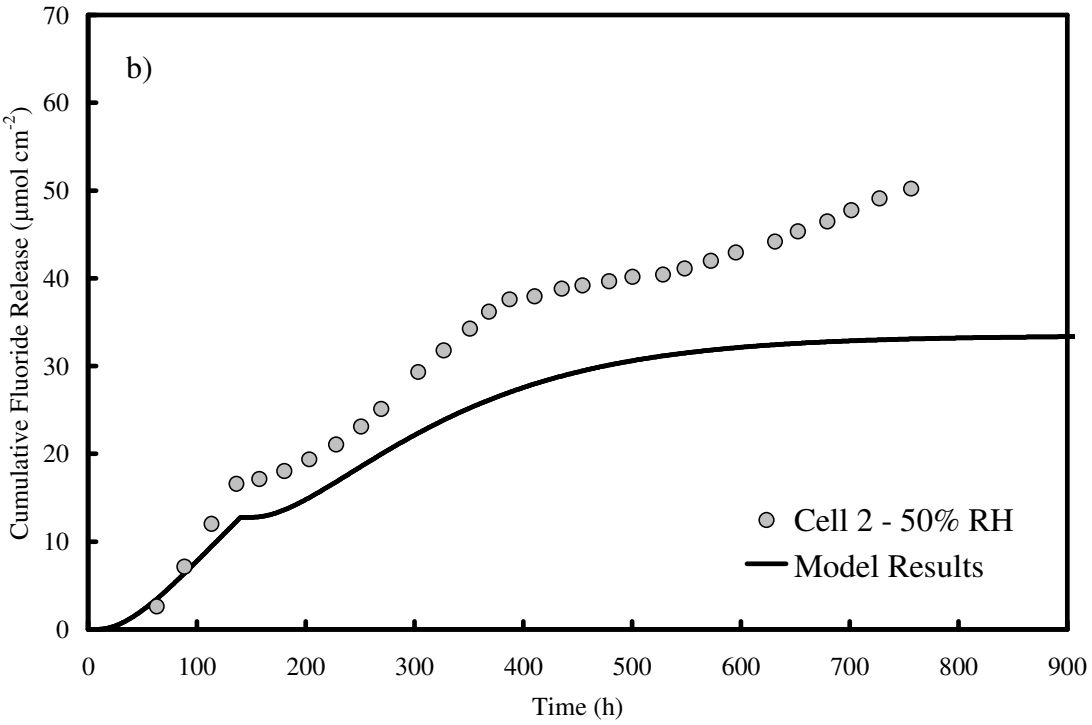
b)
Cumulative Fluoride Release (µmol cm-2)
Time (h)
Cell 2 - 50% RH
Model Results
0
10
20
30
40
50
60
70
0
100
200
300
400
500
600
700
800
900

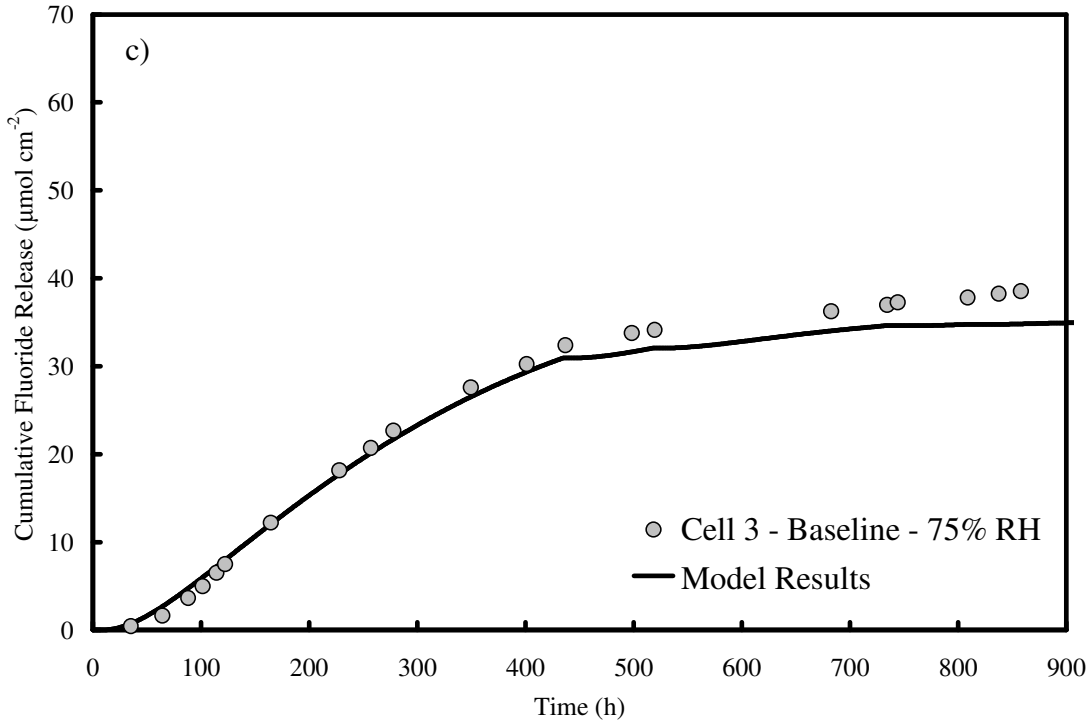
c)
Cumulative Fluoride Release (µmol cm-2)
Time (h)
Cell 3 - Baseline - 75% RH
Model Results
0
10
20
30
40
50
60
70
0
100
200
300
400
500
600
700
800
900

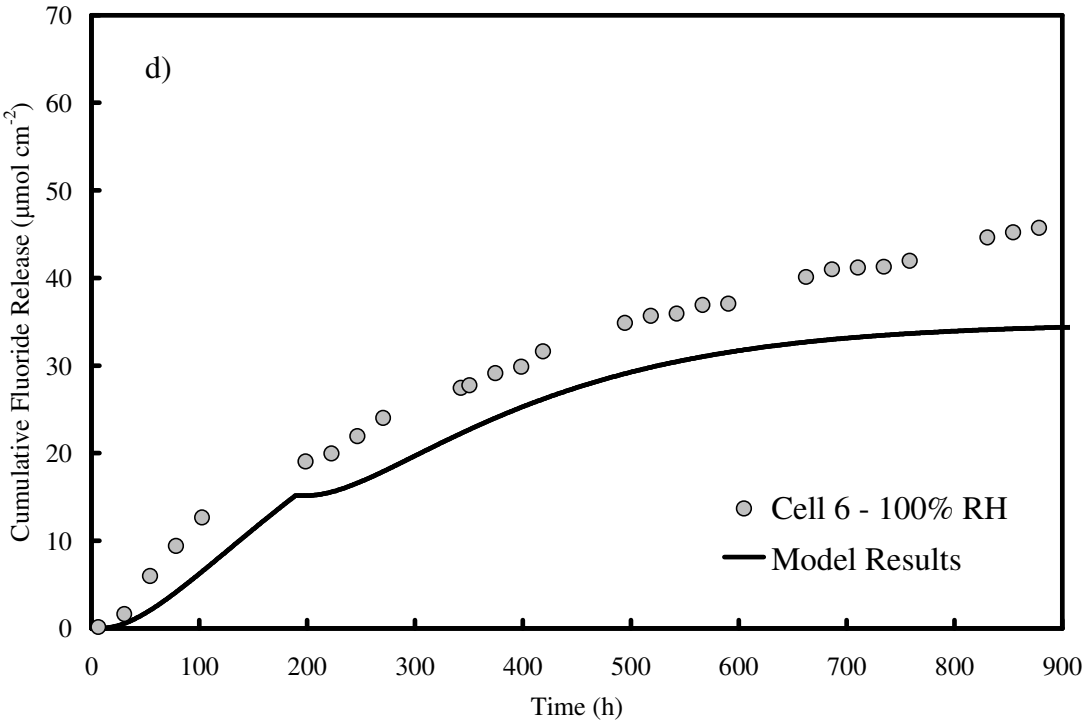

Figure 6-5: Total (anode + cathode) cumulative fluoride release experimental and model results using the first order model for a) Cell 1, b) Cell 2, c) Cell 3, and d) Cell 6. Model was fit to data from Cell 3 and then applied to Cells 1,2 and 6 without further fitting. Cell shutdown phenomena was accounted for in each case.

A second order model where degradation depends on the square of the hydrogen flux was also explored. With the exception of changing Equation (5-5) for Equation (5-6) all other aspects of the model were maintained. As with the first order model, the model was fitted to the baseline data (Cell 3) with consideration of the effect of interruptions and stoppages, and then used to simulate the data from cells 1,2, and 6 (20, 50, and 100% RH respectively) without further modification of the fitting constants. The new parameters are given in Table 6-3, only K_1 , K_2 , and D_I , were changed from the first order model fit.

Table 6-3: Model parameters for second order degradation model.

Variable	Value	Obtained by:
Δp_{H_2}	364.4 mmHg	Measured
δ_{IA}	7.5 x10^{-4} cm	Constant
δ_{IC}^{o}	7.5 x10^{-4} cm	Constant
P'_{M,H_2}	1.9 x 10^{-8} A cm cm^{-2} mmHg^{-1}	Measured
K_1	2.9 x 10^{-2} mol^{-2}	Fitted
K_2	4.7 x 10^{-7} mol cm^{-2}	Fitted
D_{GDL}	4.2 x 10^{-9} cm^2 s^{-1}	Fitted
D_I	1.2 x 10^{-10} cm^2 s^{-1}	Fitted
R	8.314 J mol^{-1} K^{-1}	Constant
T	363.15 K	Constant
F	96485 C mol^{-1}	Constant
$E^{\circ} - \eta_{reversible}$	0.814V	Fitted
γ	2.6	Fitted

The results show good agreement between the simulation results and experimental data. After long degradation times (> 300 hours for Cell 1, 500 hours for Cell 2, and 650 hours for Cell 6) the experimental total cumulative fluoride release rises above model predictions. It is believed that at this time anode electrolyte degradation significantly contributes to the fluoride release which is not covered in the model. This is currently a limitation of the model. The model is also able to capture the higher fluoride release of Cell 6 over Cell 3. This is primarily due to the higher initial hydrogen crossover rate of Cell 6.

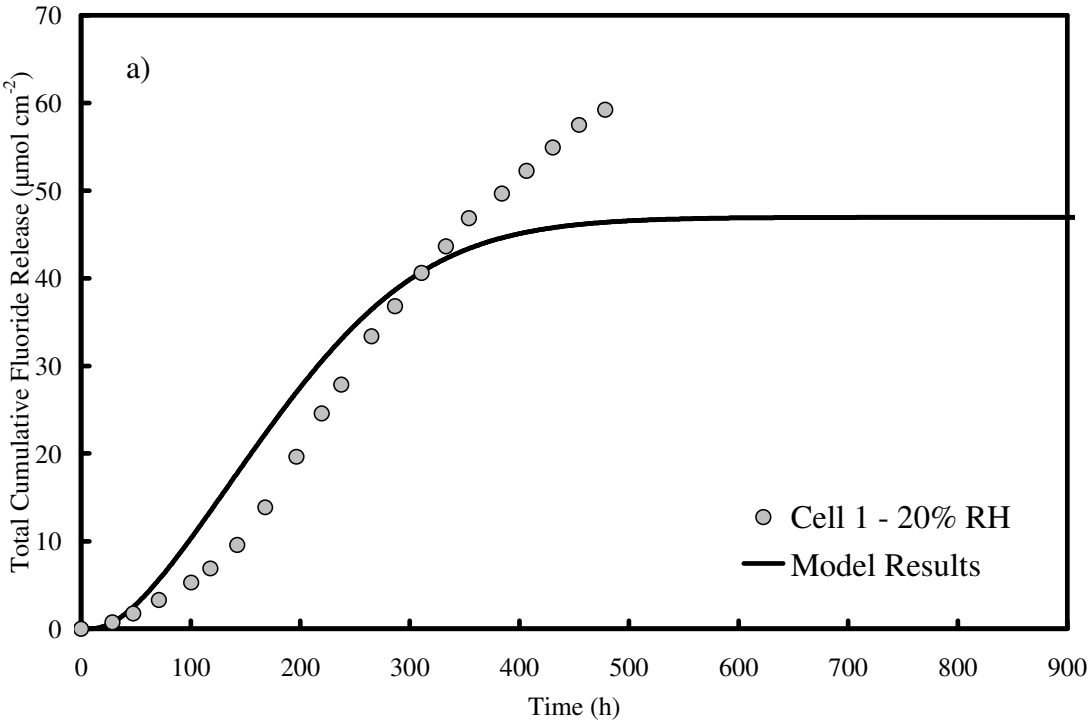
a)
Total Cumulative Fluoride Release (µmol cm-2)
Time (h)
Cell 1 - 20% RH
Model Results
0
10
20
30
40
50
60
70
0
100
200
300
400
500
600
700
800
900

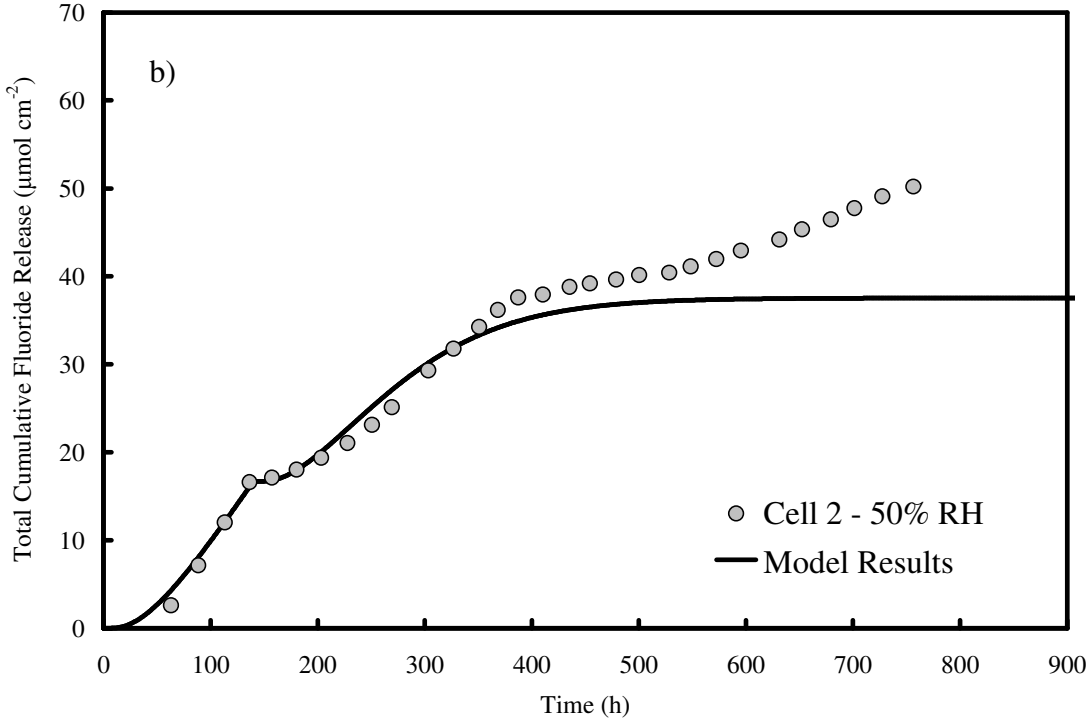
b)
Total Cumulative Fluoride Release (µmol cm-2)
Time (h)
Cell 2 - 50% RH
Model Results
0
10
20
30
40
50
60
70
0
100
200
300
400
500
600
700
800
900

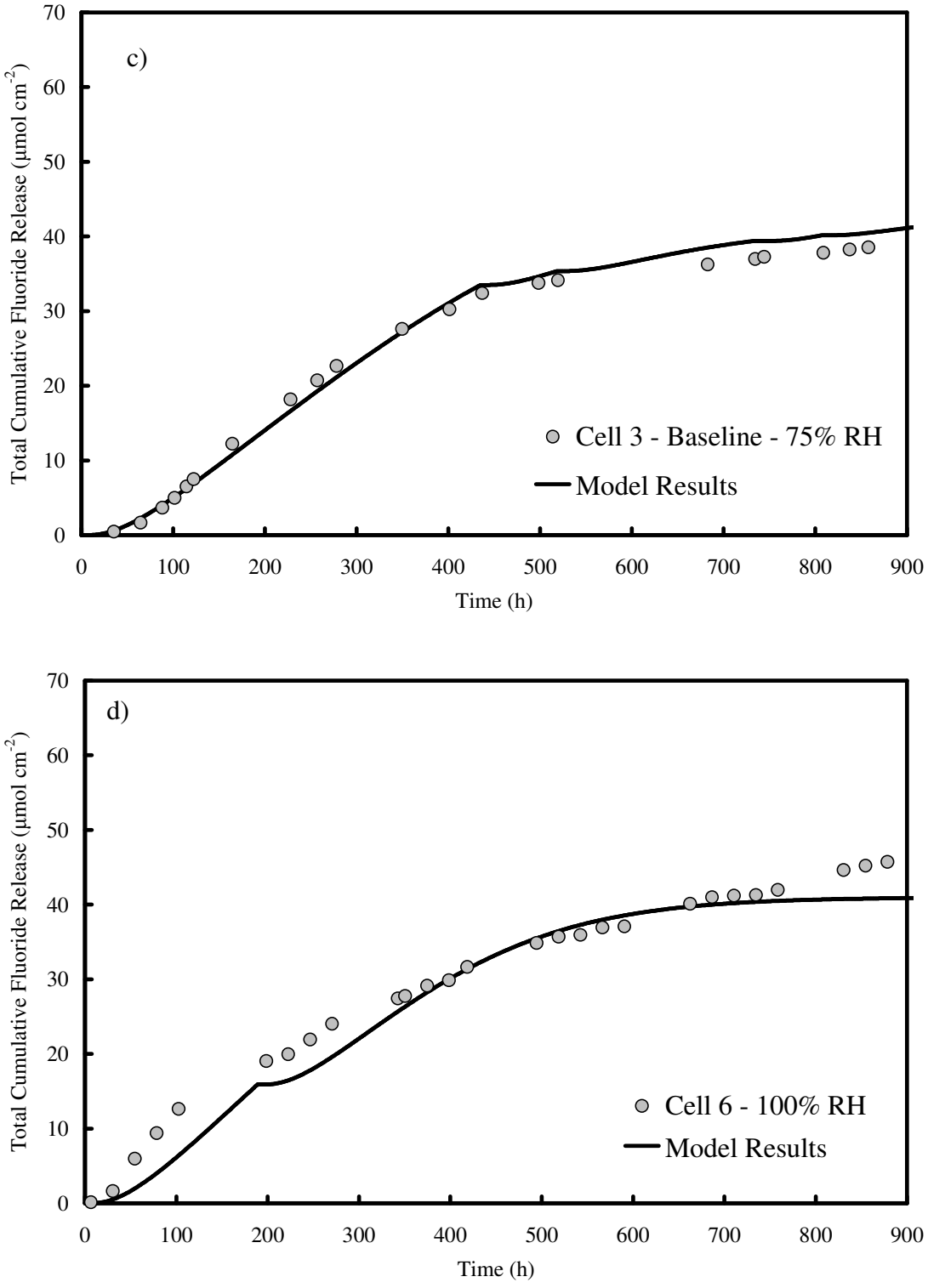

Figure 6-6: Total (anode + cathode) cumulative fluoride release experimental and model results using the second order model for a) Cell 1, b) Cell 2, c) Cell 3, and d) Cell 6. Model was fit to data from Cell 3 and then applied to Cells 1,2 and 6 without further fitting. Cell shutdown phenomena was accounted for in each case.

The above results show that the initial crossover rate is an important factor which influences degradation at moderate to high relative humidity. The effect of relative humidity on permeability and hydrogen partial pressure are important since they contribute to the overall crossover rate. A higher initial hydrogen crossover accelerates the degradation cycle of thinning and crossover resulting in the above results. This is consistent with a study by Pierpoint and coworkers who correlated initial fluoride release rate to cell lifetime [66]. Since there is a relationship between the initial crossover rate and initial fluoride release rate as described in the model formulations, the initial crossover rate should also be a strong indicator of durability. This held true for the cells tested in the above work.

6.3 Examination of Voltage Degradation and Crossover Trends

Open Circuit Voltage Measurements

One of the metrics for evaluation of fuel cell degradation is the OCV durability testing, which measures the rate of voltage changes during the experiment. The curves obtained for each of the four membranes are shown in Figure 6-7. The curves show features consistent with those shown in Chapters 4 and 5.

Initially, voltage values begin above 0.9V and rapidly decrease. This initial transient period has been shown to be primarily the result of reversible voltage losses and to a smaller extent due to irreversible voltage losses promoted by the permanent degradation of the catalyst layer and ionomer. After 150 hours, the voltage degradation rate begins to stabilize and enters a steady degradation period which can be considered irreversible caused by material degradation. The value of the open circuit voltage is given by the Nernst potential minus losses associated with hydrogen crossover and the reversible degradation losses as shown in Equation (6-2).

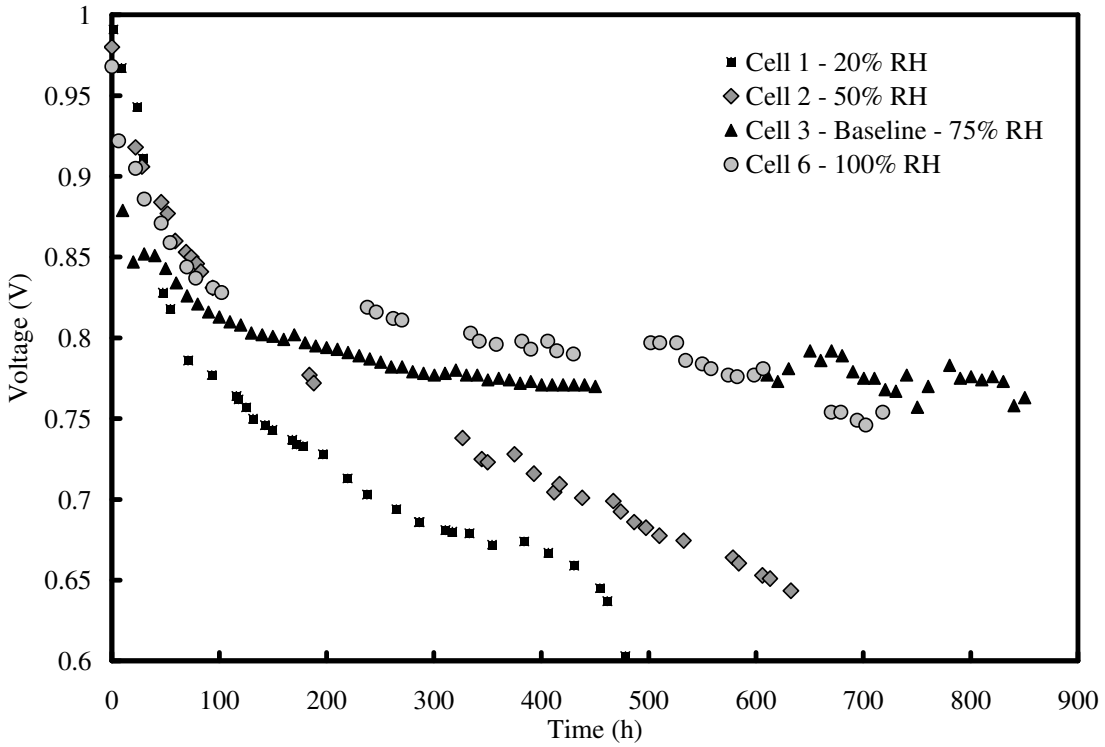

Figure 6-7: Open circuit voltage results with time for Cell 1 (20% RH), Cell 2 (50% RH), Cell 3 (75% RH), and Cell 6 (100% RH).

$$V_{Cell,OCV} = E^{\circ} - \eta_{reversible} - \eta_{irreversible} \tag{6-2}$$

Initially, reversible losses have no effect on the open circuit voltage and the voltage is determined only by the Nernst potential and crossover effects. The voltage at this time for Cells 1 to 4, Table 6-4, shows that the membranes operating at lower relative humidity generally have the higher open circuit potential. One exception is Cell 3, operated at 75% RH, which had a lower OCV than Cell 6, operated at 100% RH.

Table 6-4: OCV at 0 hours for Cells 1-6.

Cell	OCV at 0h V
1	1.018
2	0.98
3(Baseline)	0.930
6	0.968

The Nernst potential is influenced by relative humidity through its effect of lowering the hydrogen and oxygen partial pressures. An increase in relative humidity will result in a reduction in E_{eq} by reducing reactant partial pressures. The overpotential associated with crossover can be described by Equation (6-3) [3].

$$\eta_{ix} = \frac{RT}{F} \ln\left[\frac{i_{H_2}}{EAS \cdot i_o}\right] \tag{6-3}$$

The crossover overpotential is related to the amount of hydrogen crossover, which is influenced by relative humidity and membrane permeability as previously discussed, and electrochemically active surface area (EAS). Table 6-5 details the EAS and the ratio of crossover current to EAS. The differences in the initial open circuit voltage for Cell 3 and 4 is explained by the lower active surface area for Cell 3. This results in the higher than expected crossover overpotential and hence a lower voltage than Cell 6.

Table 6-5: EAS and crossover current measurements.

Cell	EAS (cm^2_{pt} / cm^2_{geo})	i_{H_2} (mA cm^{-2})	i_{H_2}/EAS
1	21.3	2.4	0.113
2	23.8	2.36	0.099
3	13.37	1.75	0.134
6	25.2	1.85	0.073

Figure 6-7 also shows that after a short time, cells operated at lower humidity have lower voltages than those operated at higher relative humidity. This result was also observed in other studies with similar membranes [12] and is caused by a combination of irreversible degradation and additional reversible losses. The steady degradation rate that becomes apparent after 100 hours of degradation can be used to estimate the rate of irreversible degradation and thus the magnitude of reversible degradation.

It is clear from the OCV curves that the steady degradation portions of each curve are not completely linear. In the case of Cell 3 (75% RH) the voltage degradation rate begins to

decrease after 450 hours. As such, for comparison purposes the average voltage degradation rate between 200 and 400 hours of degradation was used for comparison, as shown in Table 6-6. The results show that Cell 3 (75% RH) and Cell 6 (100% RH) had similar voltage degradation rates which were both lower than Cell 2 (50% RH) and Cell 1 (20% RH). The latter two cells also had similar degradation rates to each other. Overall the degradation rate decreased with increasing relative humidity.

Table 6-6: Voltage degradation rates for Cells 1-3, and 6.

Cell	Average Voltage Degradation Rate $\mu V\ h^{-1}$	Reversible Voltage Loss V
1	290	0.198
2	273	0.144
3 (Baseline)	115	0.145
6	108	0.126

The linear extension of the steady degradation trend to 0 hours allows the magnitude of reversible degradation to be estimated. They are listed in Table 6-6 for each cell. Reversible voltage loss makes up most of the initial drop in voltage and can be recovered by drawing current or changing operating conditions. From Table 6-6 it can be seen that the reversible voltage loss tends to decrease with increasing RH.

Although beyond the specific scope of this thesis, it is speculated that the mechanisms causing reversible degradation, such as platinum oxidation, become more dominant with decreasing relative humidity and hence are the dominant cause for the significantly different voltage values observed at times less than 100 hours.

The proposed second order degradation model was used to model voltage degradation. The model was not able to effectively predict the voltage degradation of Cell 1 (20% RH) and Cell 2 (50% RH). It is believed that even though chemical degradation may contribute the rate at which that voltage degrades, other factors such as catalyst layer and carbon support degradation also contribute to voltage degradation. Since these other

effects are not considered thoroughly in the model, it is not possible to conclude that the current model address all aspects of voltage degradation.

The above trends in key voltage data shows that the initial open circuit potential are linked to the crossover rate and EAS. Also, cells with high voltage degradation rates also exhibit high crossover rates. However, the voltage degradation rate and reversible voltage loss follows the relative humidity trends more than crossover trends. As discussed, voltage measurements result from a combination of factors. In this case, the voltage degradation rate is not only affected by the increase in crossover from membrane thinning, but also potentially from the effects of catalyst layer degradation.

6.4 CHAPTER SUMMARY

In this chapter the effect of changing reactant gas relative humidity was examined and the proposed semi-mechanistic model wyas used to explain the experimental results. Overall, fluoride release trends were consistent with measured initial crossover rates. When the semi-mechanistic degradation model was applied to the cell in this study, it was found that the first order dependence on hydrogen flux underestimated fluoride release. A second order dependence was able to better explain the data. Despite changing the model, after long degradation times the model still underestimated fluoride release. This was attributed to anode side degradation which is not captured by the model but clearly took place as seen in the SEM images.

Although fluoride release could be connected to initial crossover and modeled, voltage degradation behaviour could not. Initial voltage could be linked to initial crossover, but irreversible voltage degradation showed a weaker dependence. The proposed degradation model was also not able to capture the voltage degradation trends of cell 1 and 2.

CHAPTER 7 : MODEL PARAMETER SENSITIVITY

In order to better understand the model capabilities, parameter sensitivity analysis was performed using the proposed second order semi-mechanistic model. There are a number of causes to degradation that constitute the main parameters of the model. This section will use simulation results to examine how changing these parameters will impact degradation. The results of the parameter sensitivity will also be compared to experimental results available in the literature. Examination of the model will allow the main measurable parameters of interest to be identified. This methodology can be beneficial in materials selection since it provides a tool for rapid correlation of fuel cell parameters with materials properties and degradation. The focus of the sensitivity analysis is on two parameters: a) fluoride release and b) membrane thickness changes.

Key results of this chapter are:

- Model sensitivity analysis on material parameters such as material thickness, permeability, and reactivity are consistent with available literature.
- Model sensitivity analysis on operational parameters such as temperature, relative humidity, and hydrogen partial pressure are also consistent with the literature.
- Changes in fluoride diffusion coefficients significantly affect individual fluoride release rates from the anode and cathode but have minimal effect on the total fluoride release trends.

- The model shows that initial crossover and initial fluoride release rate are two measures which give a good indication of the overall durability of the membrane.

7.1 Model Sensitivity to Material Properties

The variables that will be investigated in the model sensitivity analysis are:

- initial membrane thickness (δ),
- initial membrane permeability (k_{H_2}), and
- membrane reactivity to peroxide (K_1).

The base case will be the fitted results presented in Chapter 3 with parameters changed by -50%, -20%, 0%, 20%, and 50% from the base case values. For the bulk of the analysis discussed, the fluoride release data will not be separated into the anode and cathode contributions. Instead, the total (anode + cathode) cumulative fluoride release results will be shown.

The effect of changing the thickness of the electrolyte membrane on the total cumulative fluoride release is shown in Figure 7-1. The results show that with increasing thickness the fluoride release behaviour changes. First, the initial lag time increases with increasing thickness. Further, degradation rate as seen by the slope of the cumulative release curves decreases with increasing thickness. With an increasing thickness, the hydrogen crossover rate decreases and hence the rate of degradation decreases.

The resulting thickness of the membrane can be plotted in terms of failure criteria, such as the time required for a loss of 50% of the cathode ionomer. The results show a linear relationship between the initial membrane thickness and the time to failure (Figure 7-2). The 50% loss criterion is an arbitrary value used here for demonstration purposes.

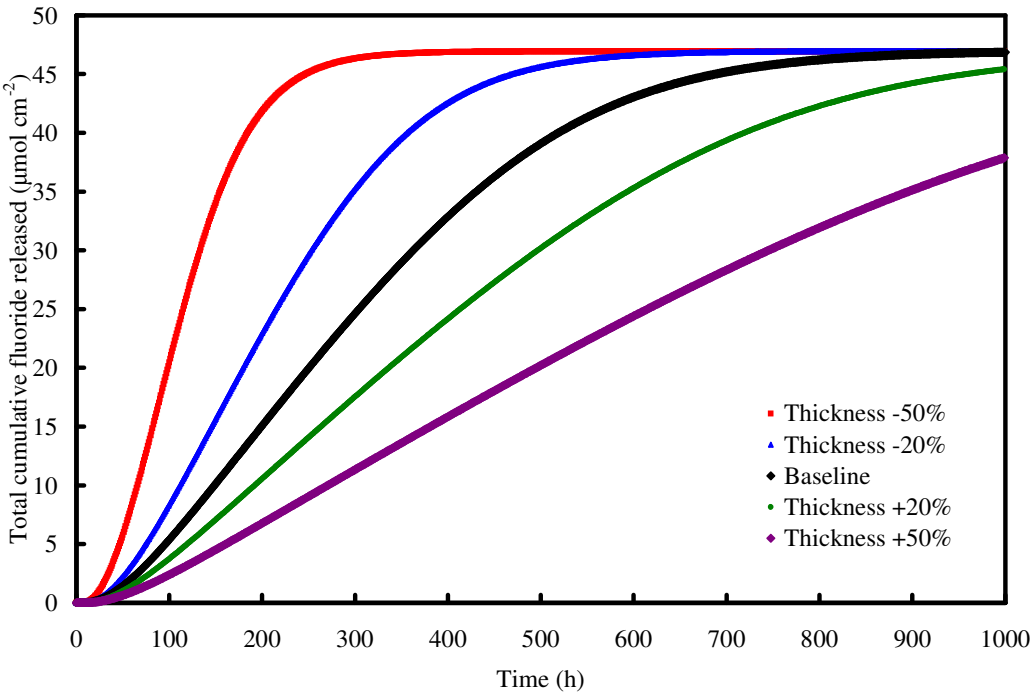

Figure 7-1: Modeled effect of thickness on cumulative fluoride ion release.

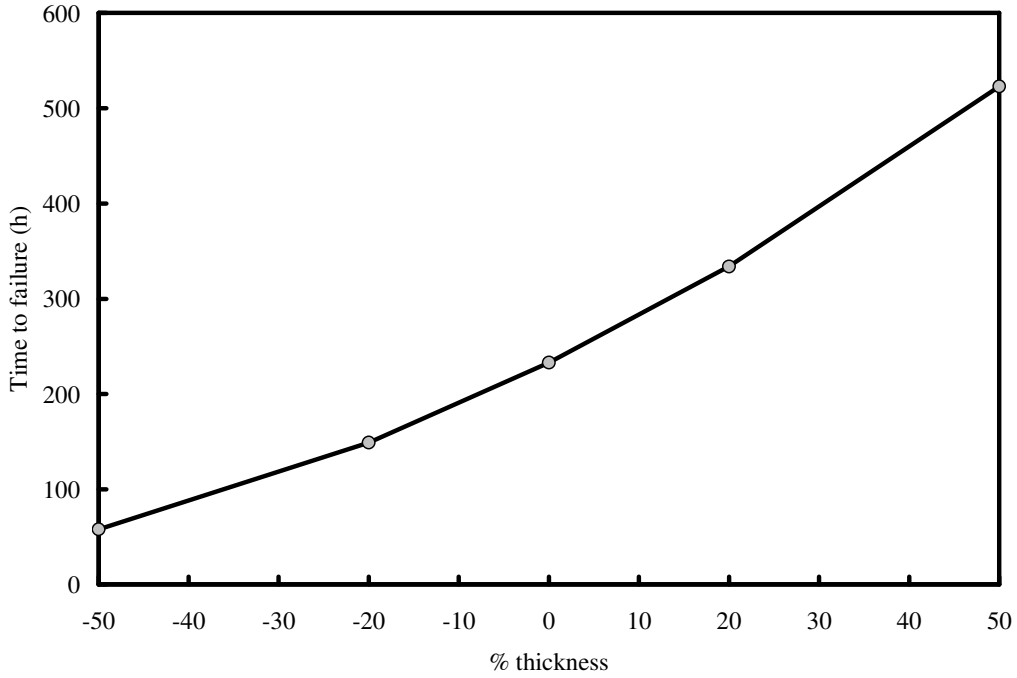

Figure 7-2: Effect of thickness on time to failure. Time to failure is defined as the time when the membrane has lost 50% of the cathode electrolyte layer.

Such a dependence of degradation on the thickness has been observed by Liu *et al* [43] who found the concentration of peroxide within a fuel cell membrane to increase with membrane thickness. As discussed above, this was attributed to changes in gas crossover resulting from thickness changes.

The change in permeability is another material property that will affect the degradation rate. There are few available literature data about this effect because the number of electrolytes studied in the literature is limited to mostly Nafion^{TM} derivatives. Thus, the membranes that have been studied have similar permeability to each other. Changes in permeability have a nonlinear effect on the time to failure as defined by the time when 50% if the cathode ionomer has been depleted as shown in Figure 7-3

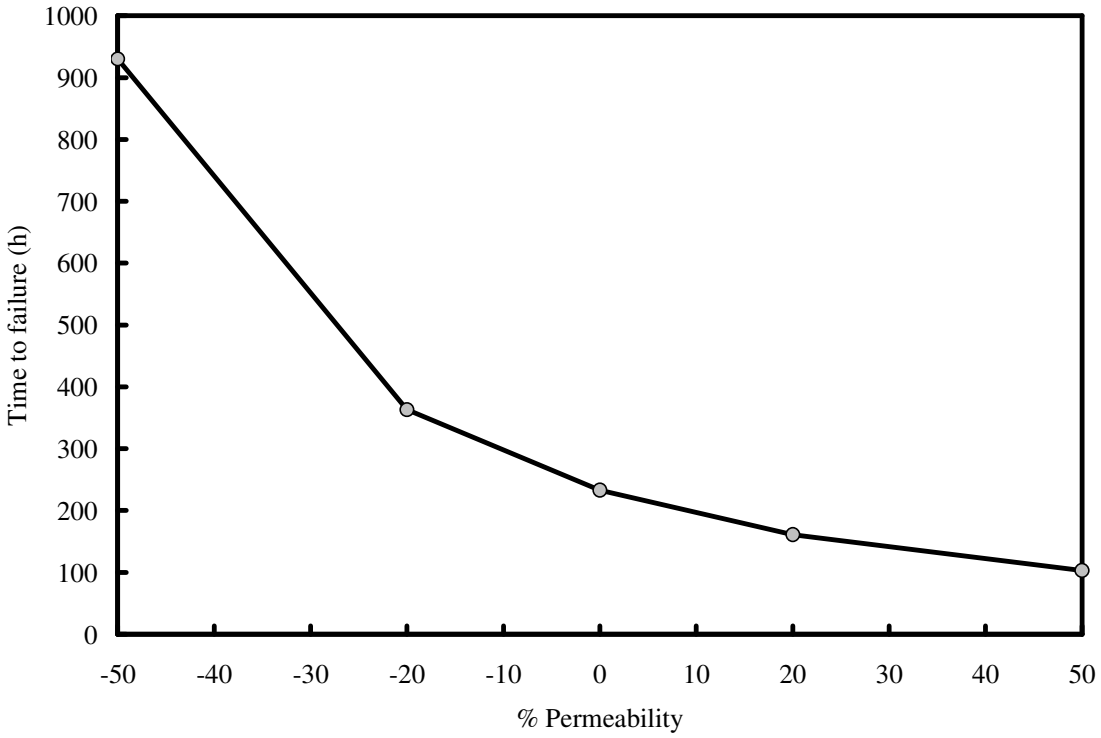

Figure 7-3: Effect of permeability on time to failure. Time to failure is defined as the time when the membrane has lost 50% of the cathode electrolyte layer

A decrease in permeability from the baseline conditions by 50% is shown to almost quadruple the time to failure. On the other hand, an increase in permeability by 50% only

decreases the time to failure by 56%.The final material property of interest is the degradation constant of the membrane (K_1). This characterizes the reactivity of the membrane and is therefore related to the nature of the material, the availability of carboxylic end groups, as well as operational conditions such as temperature which impact the rate of reaction. The effect of changing K_1 has a similar effect as changing the permeability, as shown in Figure 7-4.

As expected, the lower the reactivity of the membrane the longer it will last. From this result it is clear that one way to improve the durability of the membrane is to reduce the reactivity. This has been accomplished in next generation membranes such as those described by Curtin *et al* [28] which use different processing techniques to remove reactive endgroups from the polymer structure. These stabilized membranes showed significantly better resistance to Fenton's reagents as well as during in-situ durability tests.

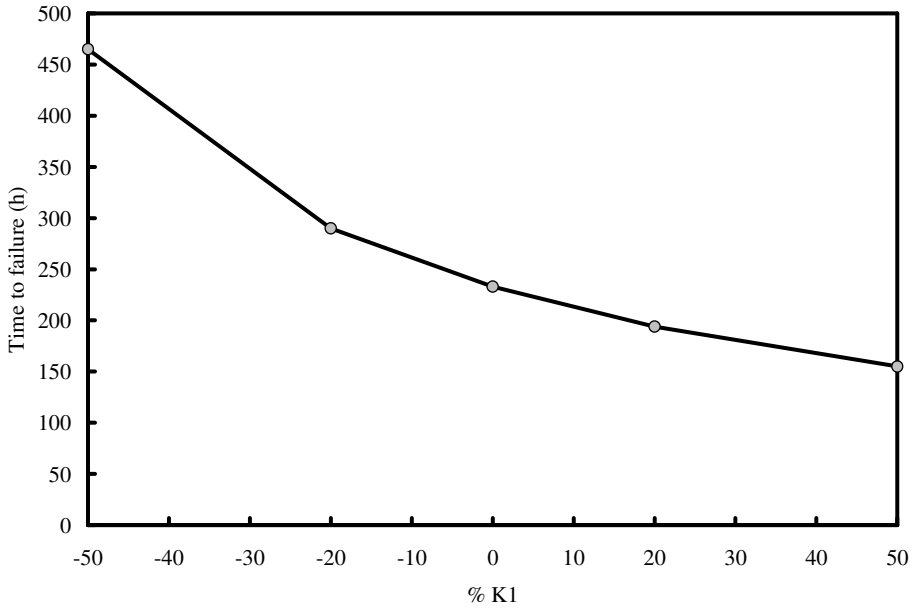

Figure 7-4: Effect of K_1 on time to failure. Time to failure is defined as the time when the membrane has lost 50% of the cathode electrolyte layer

7.2 Model Sensitivity to Operational Parameters

The parameters related to operational conditions that were investigated here are:

- temperature,
- gas partial pressure,
- relative humidity, and
- current density.

Although the current model being discussed is isothermal and as such the effect of temperature is not explored, it will be discussed in the context of how it would impact the degradation rate parameter. Relative humidity and gas partial pressure are related in the model. Relative humidity affects the permeability of the membrane. An increase in the water content in the membrane results in increased gas permeation. The effect of changing the permeability was examined above.

One of the effects of temperature on the degradation model is the contribution to the degradation rate. The rate of degradation has been shown to follow an Arrhenius type relationship with temperature [10]. As such, lower temperatures would reduce the K_1 term and result in longer times before failure, as shown in Figure 7-4. Temperature will also have an effect on other parameters such as diffusion coefficients and permeability.

Relative humidity is a second operational parameter of interest. The main effect of relative humidity is the contribution to water content within the electrolyte membrane. This causes the membrane properties to change, specifically the gas permeability. In general increasing relative humidity increases the permeability. This has been shown for Nafion^{TM} membranes [32,33] as well as Gore reinforced membranes [8]. The permeability of membranes used in this study was examined over a range of relative humidity values and the experimental permeability results are shown in Figure 7-5.

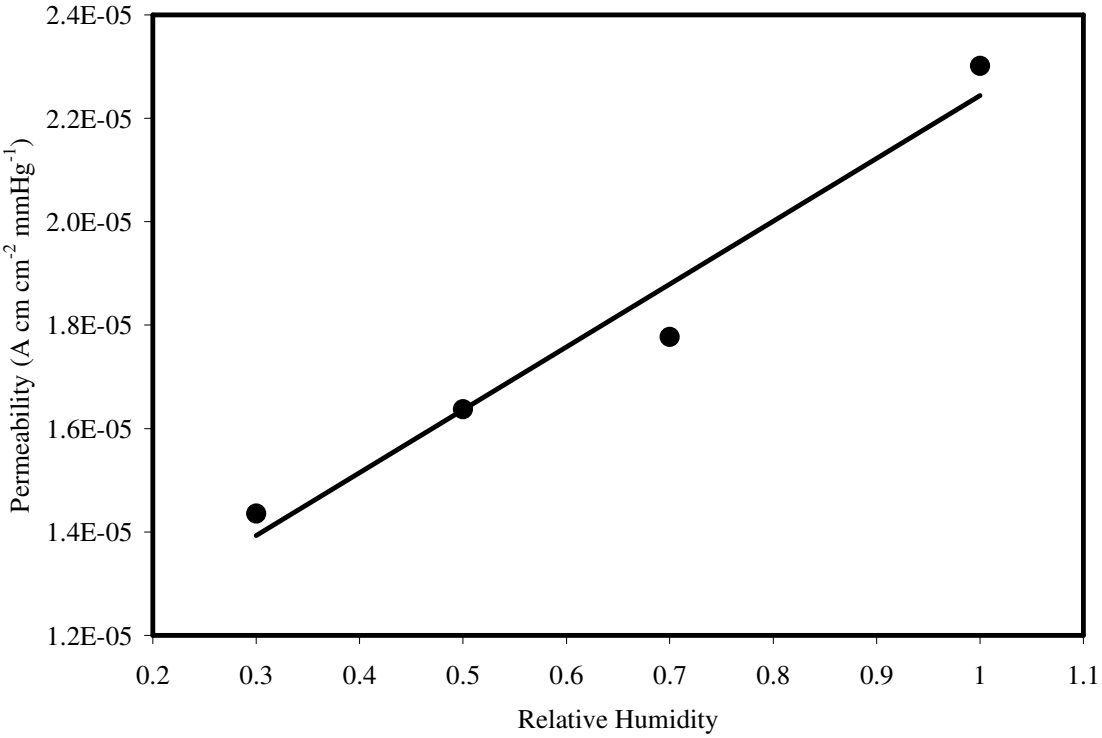

Figure 7-5: Effect of RH on hydrogen permeability from crossover current measurements (90°C).

The range in membrane permeability shows a doubling in permeability from 30% RH to 100% RH. In the model, relative humidity is not explicitly included as a variable. Instead, the permeability of the membrane in question at the desired relative humidity is specified. The effects of permeability on degradation as predicted by the model have been discussed above and are shown in Figure 7-3.

As with the membrane permeability and thickness, the hydrogen partial pressure controls the crossover rate across the membrane according to Fick's law. It is hydrogen crossover that is assumed to be the controlling factor to degradation in the model. As such, higher hydrogen partial pressures will lead to higher degradation rates and a lower time to failure, as shown in Figure 7-6.

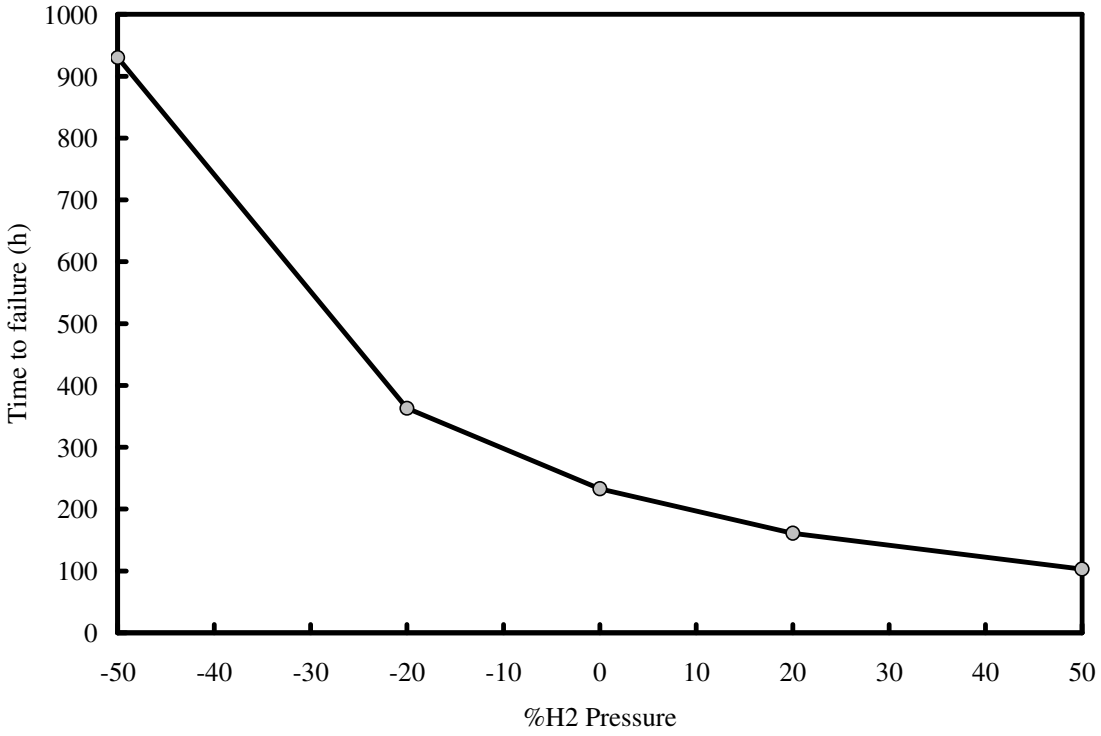

Figure 7-6: Effect of hydrogen partial pressure on time to failure. Time to failure is defined as the time when the membrane has lost 50% of the cathode electrolyte layer

Literature studies on the effect of hydrogen partial pressure on the fluoride release rate or peroxide concentration show an increase such as the work of Mittal *et al* [53]. Liu *et al* [55] found that the variation of the fluoride release rate with changing hydrogen partial pressure to follow second order behaviour.

The above discussion, with the exception of the membrane reactivity constant, revolves around material properties which are known at the onset of the durability experiments performed for this work. There are also two other parameters which influence the results but have not been discussed. Those are the fluoride diffusion coefficients through the membrane and gas diffusion layers. The diffusion coefficient of fluoride through the membrane has been measured in the literature and compares well to the fitted result as discussed in Chapter 5. The diffusion coefficient through the gas diffusion layer, on the other hand, has not been measured experimentally. The difficulty of measuring the diffusion through the GDL is that the water content will easily affect the result.

Furthermore, it is difficult to measure the water content, i.e. saturation, of the gas diffusion layer. These two diffusion coefficients have no bearing on the degradation itself. These coefficients influence the cumulative fluoride release curves, which is the way that degradation is monitored over the life of a cell.

Figure 7-7 and Figure 7-8 show the effect of the GDL and electrolyte diffusion coefficients. The results show that as the GDL diffusion coefficient decreases, the cathode cumulative fluoride release curves decrease while anode curves increase because the resistance to diffusion by both fluoride release paths become similar. Essentially, decreasing the GDL diffusion coefficient pushes the fluoride release towards the anode.

The decrease in GDL diffusion coefficient increases the lag time for both cathode and anode diffusion. Similarly, for a decrease in electrolyte fluoride diffusion coefficient, the lag time of the anode diffusion is seen with no change in the cathode lag time, as shown in Figure 7-8. As with the GDL diffusion coefficient, a decrease in the electrolyte diffusion coefficient essentially forces more fluoride through the cathode GDL.

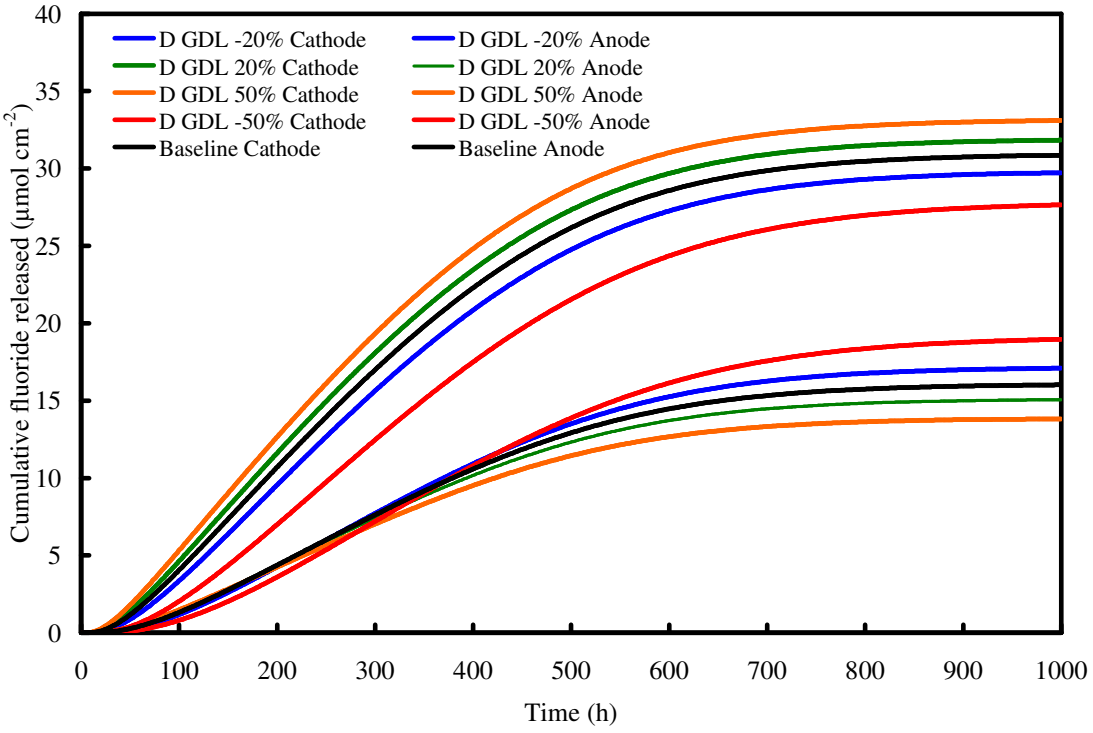

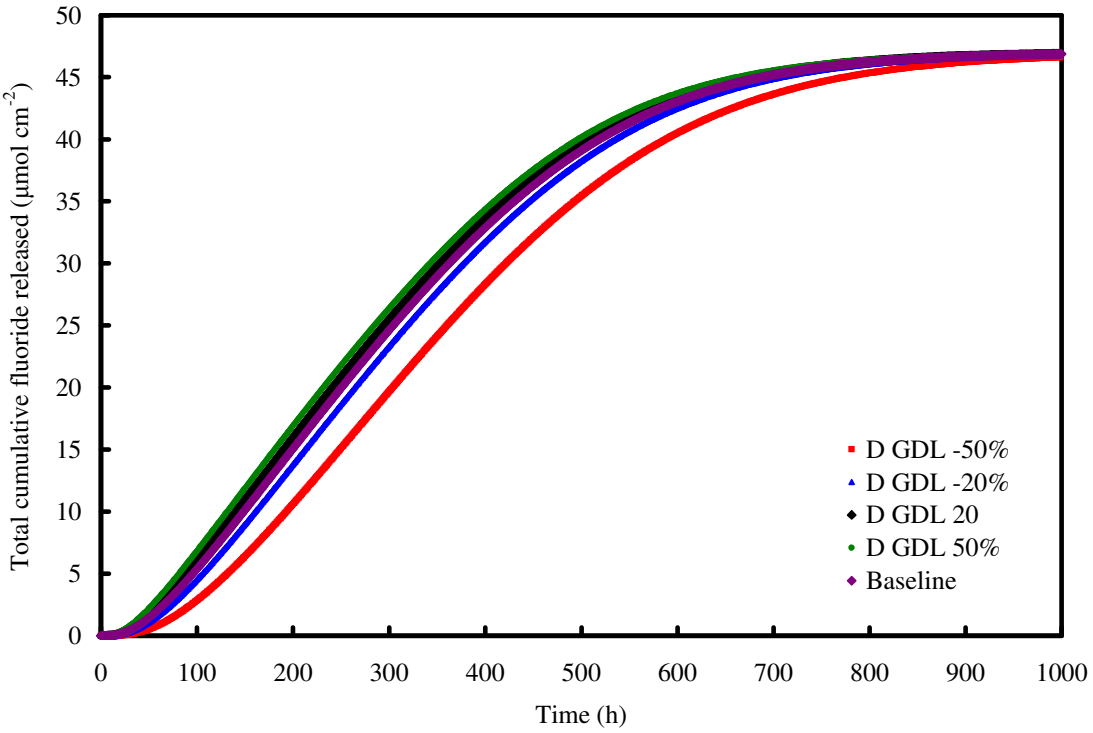

Figure 7-7: Effect of fluoride diffusion coefficient through the GDL (DGDL) on a) anode and cathode cumulative fluoride release and b) total (anode + cathode) cumulative fluoride release.

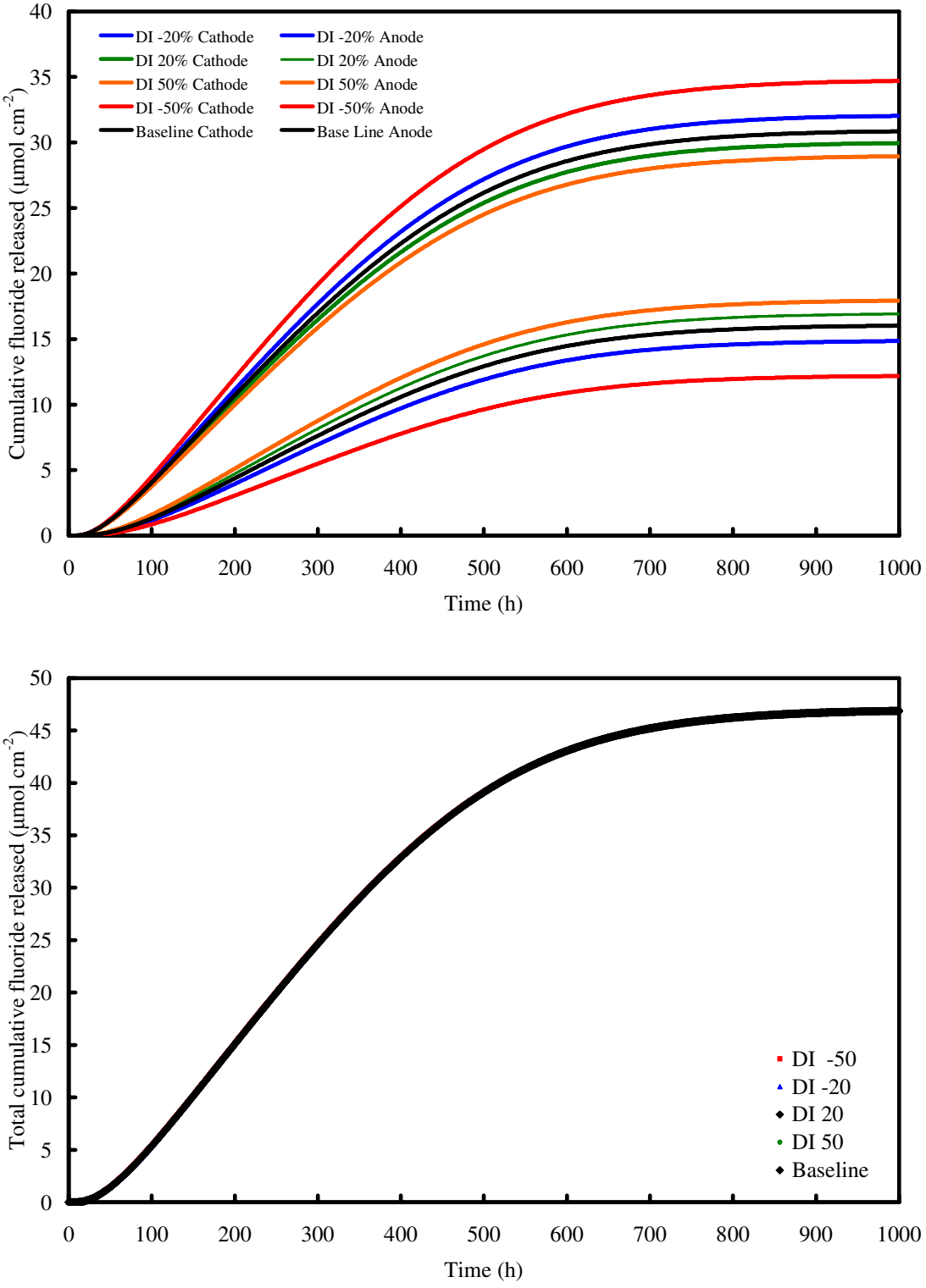

Figure 7-8: Effect of fluoride diffusion coefficient through the electrolyte (DI) on a) anode and cathode cumulative fluoride release and b) total (anode + cathode) cumulative fluoride release.

Based on the simulation results shown in Figures 7-7 and 7-8, it can be concluded that changes in the diffusion coefficients can affect the anode and cathode fluoride release trends. However, when the total (anode + cathode) fluoride trends are examined, there is only a moderate effect as shown in Figure 7-7b. The only significant deviation from the baseline curve occurs when there is a 50% decrease in the diffusion coefficient. Slight changes in the lag time can also be observed.

On the other hand, changes in the electrolyte diffusion coefficient show no effect on the total fluoride release curves as shown in Figure 7-8b. Overall, both figures show that if an experimenter is not concerned with the location of degradation, it is adequate to only collect information on the total cumulative fluoride release and not consider the effects of varying diffusion coefficients.

7.3 SIGNIFICANT QUANTITIES

From examination of the proposed semi-mechanistic model, two significant quantities should be discussed in terms of their importance to durability and estimating the time to failure. These quantities are the initial crossover and the initial fluoride release rate.

As was shown above, the membrane permeability, hydrogen partial pressure, and thickness all play a significant role in the durability of the membrane. Through Fick's law, shown in Equation (7-1), these parameters form the flux of hydrogen crossover through the electrolyte.

$$N_{H_2} = P_{M,H_2} \frac{\Delta p_{H_2}}{\delta} \tag{7-1}$$

The measurement of crossover at the experimental conditions of interest effectively summarizes the contribution of each of these terms and hence forms an excellent tool for determining if a membrane will degrade quickly or slowly before starting any testing. Combination of the above results tells us that high crossover will invariably lead to faster degradation and failure. This was shown in the results of Chapter 6.

One of the limitations of using the crossover alone to predict the degradation and time to failure is that it does not adequately represent the effect of temperature. Temperature will affect the permeability of the membrane but perhaps more importantly will change the degradation rate constant as well. Thus, to evaluate and predict degradation in a series of experiments over a range of temperatures and other material properties it is necessary to use a combination of crossover and the degradation rate.

According to the model, the crossover and the degradation rate constantly combine to determine the rate of electrolyte degradation (Equation (7-2)). The proportionality constant K_2 that describes fluoride release for every fraction percent of electrolyte that is lost is given in Equation (7-3).

$$-\frac{df_I}{dt} = K_1\left(N_{H_2}\right)^2\left(f_I\right) \tag{7-2}$$

$$\frac{dn_{F-}}{dt} = -K_2\frac{df_I}{dt} \tag{7-3}$$

Combination of Equations (7-4) – (7-3) gives

$$\frac{dn_{F-}}{dt} = K_2K_1\left(P_{M,H_2}\frac{\Delta p_{H_2}}{\delta}\right)^2\left(f_I\right) \tag{7-4}$$

Equation (7-4) describes the fluoride generated within the electrolyte. Initially, the cathode electrolyte fraction remaining in the membrane, f_I, is unity and Equation (7-4) then describes the initial amount of fluoride generated.

The initial fluoride generation rate best describes the trajectory of degradation of the membrane. It accounts for the effect of changes in operational conditions, including temperature, as well as the material properties themselves. In a practical situation the

generation rate is not known. However, the closest analogue is the initial fluoride release rate for a membrane. A recent study by Pierpoint *et al* [66] correlated the initial fluoride release rate to fuel cell material durability when subjected to a variety of accelerated stress tests. They found a direct relationship between the initial fluoride release rate and the time to failure for the cell. One drawback of using the initial fluoride release rate as an indicator of potential durability is that experimental variability resulting from start-up transients may influence initial fluoride release results.

Although the above two indicators are useful for predicting durability and failure in membranes, they are only truly useful for static experiments or comparing different conditions during similar experiments. They alone cannot be used to identify how widely varying conditions, such as those found in different drive cycles, will influence the durability of the electrolyte membrane. Only a fully dynamic model would be able to accomplish this.

7.4 CHAPTER SUMMARY

This chapter examined the effect of the various parameters involved in the proposed semi-mechanistic degradation model. The effect of differences in thickness, permeability, degradation rate constant, temperature, relative humidity and hydrogen partial pressure were discussed. Simulations with changes in these parameters were consistent with experimental results in the literature.

The observed model behaviour is reinforced by experimental data found in the literature. Examination of the model results revealed two quantities that can be used as indicators of potential durability: a) initial crossover and b) the initial fluoride release rate.

CHAPTER 8 : MODEL EXTENSION TO INCLUDE CURRENT DENSITY

This chapter expands the development and validation of a semi-mechanistic chemical degradation model presented previously to also include the effect of current density. The formulation of the model in the previous chapter incorporated the effects of material properties (permeability, thickness and reactivity) and operational conditions (relative humidity and hydrogen partial pressure). Parameter estimation was conducted using the second order dependence on hydrogen flux and a baseline condition open circuit voltage experiment at 75% relative humidity. Simulation results showed agreement with the fluoride release trends observed for membranes degraded at different relative humidity using an open circuit voltage (OCV) test. In this chapter, it is proposed that the effect of current on hydrogen concentration at the catalyst/electrolyte layer interface can explain fluoride release trends.

The results of this chapter are summarized as follows:

- Cell current density has a significant impact on fluoride emission rates.
- Increasing current density decreases fluoride release rates.
- With increasing current density, hydrogen concentration at the catalyst layer/electrolyte layer interface and its crossover will decrease.

- Modeling work shows that the reduction in hydrogen concentration can explain the observed degradation trends.

The model as described before is limited in usefulness because it is limited to OCV degradation. For the model to be useful when evaluating membrane durability in fuel cell applications, it must include the effects of current density. To this end, a study of voltage degradation and fluoride release from single cells operated at various current densities is presented here. Four cells were studied at the conditions given in Table 8-1.

Additionally, a mechanism describing the effect of current density on chemical degradation is also proposed and incorporated into the model.

Table 8-1: Current density and relative humidity conditions for Cell 2, and 7-9.

Cell	Anode/Cathode RH (%)	Current Density (mA cm^{-2})
2	50	0
7	50	300
8	50	500
9	50	700

8.1 VOLTAGE PLOTS

Voltage for each cell was monitored over time to yield the results shown in Figure 8-1. Between 0 and 200 hours, the effects of reversible voltage degradation can be seen in some of the curves, particularly under OCV conditions where there is an exponential drop in voltage over the first 200 hours followed by linear decline after 200 hours. OCV studies on the type of membrane used in this study have shown that this initial large drop is caused by reversible processes as well as irreversible degradation of the electrolyte layer. Reversible degradation effects are not as prominent in experiments at higher current densities.

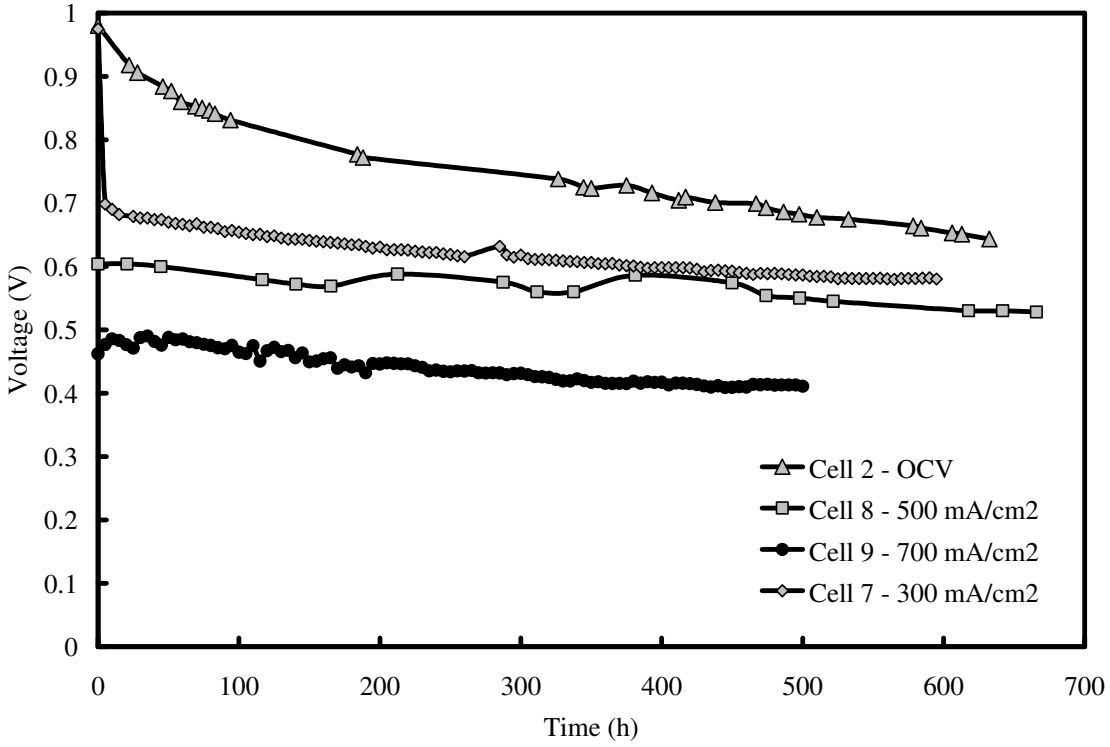

Figure 8-1: Voltage degradation plots for cells operated at different current densities (Cell 2 – 0 mA cm^{-2}, Cell 7 – 300 mA cm^{-2}, Cell 8 – 500 mA cm^{-2}, Cell 9 – 700 mA cm^{-2}).

The degradation rate for cases where there are significant reversible voltage effects was determined from the response between 200 and 500 hours of operation. The results are presented in Table 8-2.

Table 8-2: Voltage degradation rates at different current densities.

Membrane	Current Density	Voltage Degradation Rate mV h^{-1}
2	0	0.29
7	300	0.15
8	500	0.13
9	700	0.12

The above data shows that under open circuit voltage conditions there is a significantly higher voltage degradation rate than when current is flowing. Furthermore, under load the voltage degradation rate is similar for the range of current densities studied here. Overall the degradation rate under load ranged between 0.12 to 0.15 mV h^{-1} while at OCV

conditions the degradation rate was 0.293 mV h^{-1}. Voltage degradation can have many sources such as catalyst layer degradation. Additionally, when drawing current, increases in component resistances, such as the resistance to proton conduction or contact resistances, will contribute to the overall voltage degradation rate.

8.2 FLUORIDE RELEASE

The total cumulative fluoride released into the effluent water from both the cathode and anode sides was also measured over time (FFigure 8-2). The cumulative release is an indicator of overall membrane degradation due to chemical degradation. The curve for Cell 2, shows typical cumulative fluoride release behaviour for these membranes operating under OCV conditions [70].

There are three major parts to cumulative fluoride release curves as discussed previously. Initially there is some lag attributed to the time necessary to fully develop the fluoride concentration profile within the electrolyte membrane and the gas diffusion layers. This is followed by a linear region where degradation of the electrolyte progresses at a steady rate. Finally, as the electrolyte becomes scarcer within the electrolyte membrane, the rate of fluoride generation decreases causing the cumulative fluoride release curves to begin to plateau.

It is clear from Figure 8-2 that increasing the current density decreases fluoride release. Furthermore, the cumulative release curves at 300, 500, and 700 mA cm^{-2} are essentially linear in nature after the initial lag time. To more clearly show the effects of current density on degradation the cumulative amount of fluoride released after 500 hours for each membrane is plotted against current density in Figure 8-3. A linear decrease in degradation with increasing current density is observed. Comparison of fluoride data to voltage degradation trends showed no trends. This provides further evidence that the mechanism of voltage degradation is independent of hydrogen crossover.

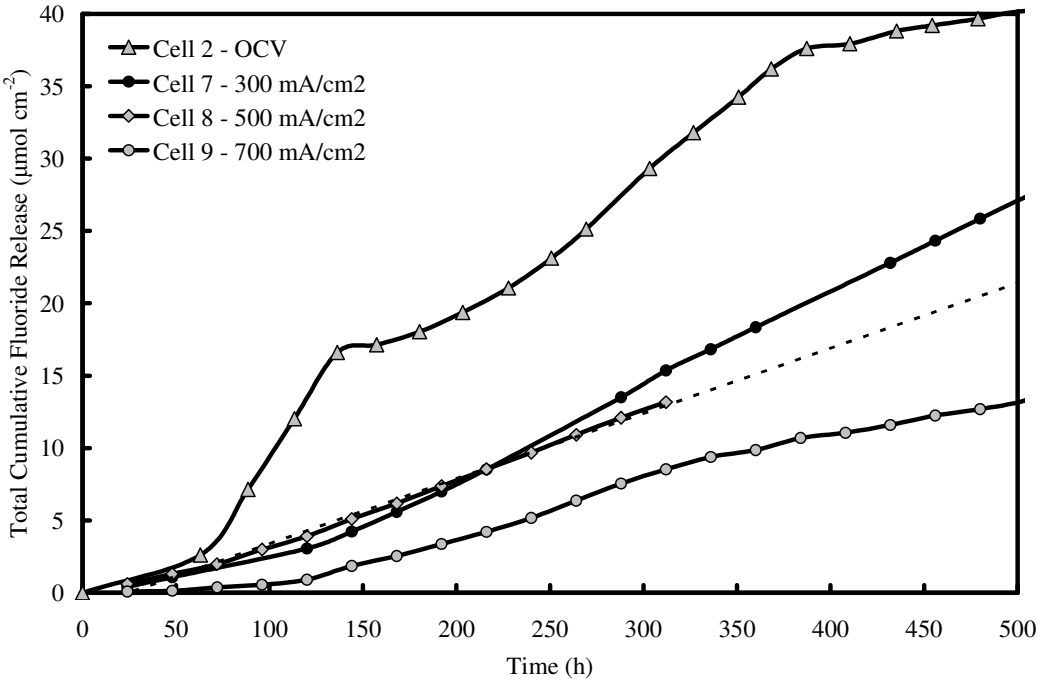

Figure 8-2: Total (anode + cathode) cumulative fluoride release for cells operated at different current densities (Cell 2 – 0 mA cm^{-2}, Cell 7 – 300 mA cm^{-2}, Cell 8 – 500 mA cm^{-2}, Cell 9 – 700 mA cm^{-2}). Dotted line indicates extrapolated fluoride release of Cell 8.

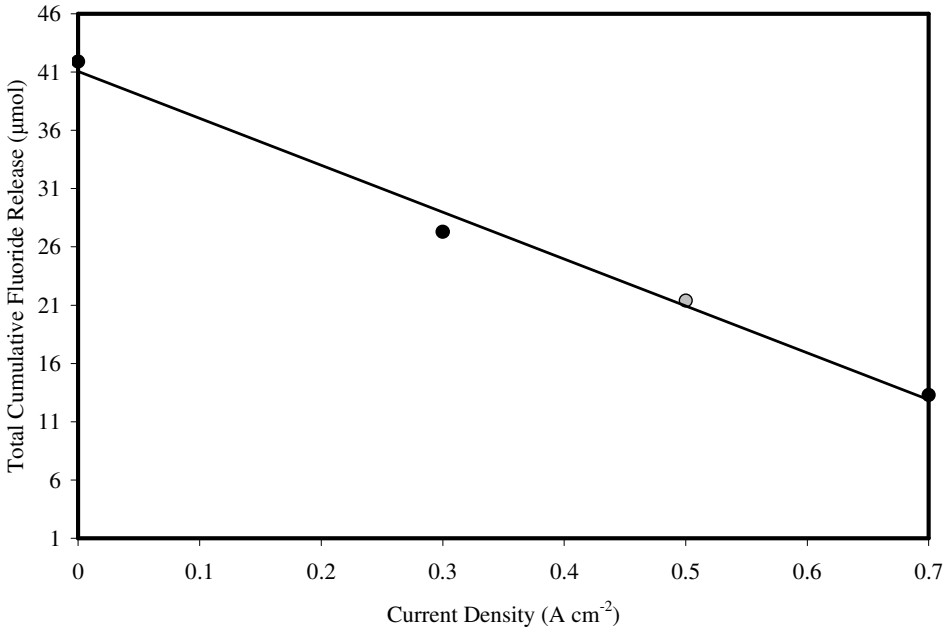

Figure 8-3: Total cumulative fluoride release at 500 hours of operation for Cells 2,7,8 and 9. Data for Cell 8 was extrapolated from the fluoride release curve.

8.3 PROPOSED MECHANISM AND MODEL

In Chapters 5 and 6, a semi-mechanistic model was proposed to describe the chemical degradation of the electrolyte layer. This model supposed that hydrogen crossover was a controlling factor in the degradation of the electrolyte membrane and hence the production of fluoride. Hydrogen permeation across the membrane was modeled using Fick's law and depends on the membrane permeability as well as the hydrogen driving force for permeation, hydrogen partial pressure or concentration at the electrolyte/catalyst layer interface.

Recent modeling work by Seddiq *et.al.*[38] and Rama [37] showed that increasing current density has the effect of reducing the hydrogen crossover across the membrane through the consumption of hydrogen at the catalyst layer and permeation resistance through the GDL. Both factors contribute to reducing reactant concentration, and hence the driving force for permeation. It is therefore proposed that the reduction in fluoride release with increasing current density measured experimentally in the experiments are the result of lower hydrogen driving force for crossover.

To explore this hypothesis, a model of the anode catalyst layer will be developed. The model will be used to calculate the concentration profile of molecular hydrogen in the anode catalyst layer. The concentration at the catalyst layer/ionomer interface, which is the driving force for hydrogen permeation across the electrolyte membrane, will then be compared to concentrations needed to explain the experimental results. The model domain and processes are shown in Figure 8-4. The main quantity of interest is the ratio of concentration at the catalyst/electrolyte interface and the feed concentration. The effects of the GDL are not considered at this stage. The model will be used to predict the quantity $C_{H_2,\delta}/C_{H_2,0}$ which will then be compared to estimated values of $C_{H_2,\delta}/C_{H_2,0}$ necessary as inputs to the semi-mechanistic degradation model to fit the experimental fluoride release data.

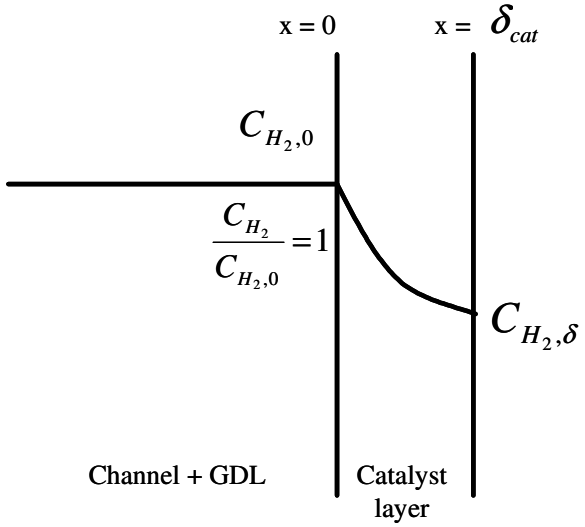

Figure 8-4: Schematic of the hydrogen concentration profile in the catalyst layer.

The water content within the pores of the anode catalyst layer plays a significant role in the final value of the ratio $C_{H_2,\delta}/C_{H_2,0}$. With low water content, gases are able to diffuse through the pores with a relatively high diffusion coefficient. On the other hand, if the pores of the catalyst layer are flooded with water or filled with electrolyte, gas must first dissolve into the medium before diffusing through the layer. Both conditions will be evaluated.

It is further assumed that because the hydrogen flux from the GDL into the catalyst layer is much larger than the crossover flux at the current densities of interest, the flux at the catalyst/ionomer interface can be assumed to be zero when solving the transport equations within catalyst layer. It assumed that neglecting the small amount of crossover at the catalyst layer/ionomer interface when solving the catalyst layer model will not dramatically impact the desired output of the simulation, the concentration profile within the catalyst layer.

For the simple geometry presented in Figure 8-4 the homogeneous reaction-diffusion phenomena within the catalyst layer can be described in 1-dimension by Equation (8-1).

$$\frac{dN_{H_2}}{dx} + R_v = 0 \tag{8-1}$$

The hydrogen flux can be described by Equation (8-2).

$$N_{H_2} = -D_{H_2}^{eff} \frac{dC_{H_2}}{dx} \tag{8-2}$$

Further, the reaction term can be related to the hydrogen concentration through the current being drawn and a simplified Butler-Volmer expression as shown in Equation (8-3).

$$R_v = \frac{1}{2F}\frac{di}{dx} = \frac{ai_\circ}{2F}\left(\frac{C_{H_2}}{C_{H_2}^{ref}}\right)^{1/2}\left[\exp\left(\frac{2F}{RT}\eta\right) - \exp\left(\frac{-2F}{RT}\eta\right)\right] \tag{8-3}$$

Substituting Equation (8-2) and (8-3) into (8-1) gives Equation (8-4).

$$D_{H_2}^{eff}\frac{d^2C_{H_2}}{dx^2} - kC_{H_2}^{1/2} = 0 \tag{8-4}$$

Where:

$$k = \frac{ai_\circ}{2F}\left(\frac{1}{C_{H_2}^{ref}}\right)^{1/2}\left[\exp\left(\frac{2F}{RT}\eta\right) - \exp\left(\frac{-2F}{RT}\eta\right)\right] \tag{8-5}$$

The boundary equations used to solve Equation (8-4) are:

$$x = 0, C_{H_2} = C_{H_2,o} \tag{8-6}$$

$$x = \delta_{cat}, N_{H_2} = 0 \tag{8-7}$$

When a flooded catalyst layer is assumed, the concentration of hydrogen dissolved into the liquid water is given by Henry's law, as shown in Equation (8-8).

$$C_{H_2} = \frac{p_{H_2}}{H_{H_2,w}} \tag{8-8}$$

$H_{H_2,w}$ is the Henry's law constant for hydrogen dissolved in water. The temperature dependence of $H_{H_2,w}$ is given by Equation (8-9) [74].

$$H_{H_2,w} = 8.34\times10^5 \exp(\frac{170}{T})(1+0.000071p^3) \tag{8-9}$$

In the above equation $H_{H_2,w}$ has units of atm cm^3 mol^{-1} and p has units of atm. The effective diffusion coefficient through the catalyst layer is a modification of the diffusion coefficient to account for the tortuous path of the porous layer. It is given in Equation (8-10)

$$D_{H_2}^{eff} = D_{H_2}\varepsilon^{1.5} \tag{8-10}$$

The parameters used to model the behaviour with current are given in Table 8-3.

Table 8-3: Parameters for macro-homogeneous model of the anode catalyst layer.

Parameter	Value	Reference
$ai_\circ$ (A m^{-3})	1x10^9	[75]
$c_{H_2}^{ref}$ (mol m^{-3})	40.88	[75]
F	96485	
R	8.314	
T (K)	363.15	
ε	0.4	[75]
δ_{cat} (m)	10X10^{-6}	
p_{H_2} (mmHg)	496.2	
D_{H_2} (through liquid phase) (m^2 s^{-1})	1.6 X10^{-8}	
D_{H_2} (through gas phase) (m^2 s^{-1})	2.0 X10^{-4}	

Simulation Results

The proposed second order chemical degradation model was used to simulate the experimental data. $C_{H_2,\delta}/C_{H_2,0}$ was estimated at each current density by modifying the hydrogen partial pressure in the degradation model. Graphs of the model fits are shown in Figure 8-5. All parameters are the same as in Chapter 6 with only the hydrogen partial pressure being modified to fit to experimental data (and this partial pressure change is as a result of the current flow). The ratio of the fitted hydrogen partial pressure with the hydrogen partial pressure at OCV provides the estimate for $C_{H_2,\delta}/C_{H_2,0}$.

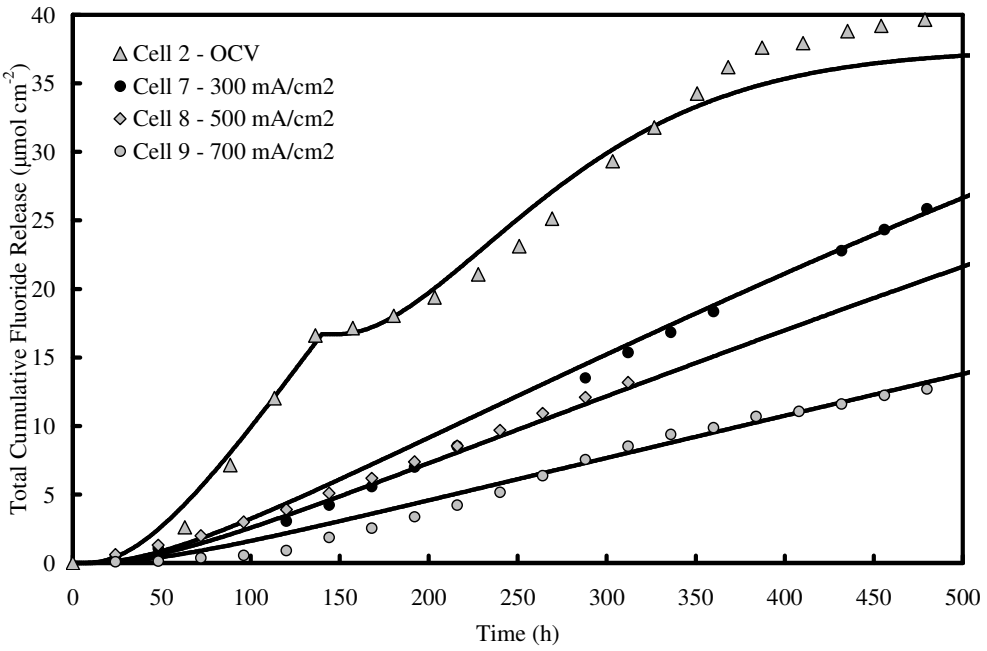

Figure 8-5: Experimental and simulated total (anode + cathode) cumulative fluoride release results for Cell 2 (OCV) ,Cell 7 (300 mA cm^{-2}), Cell 8 (500 mA cm^{-2}), and Cell 9 (700 mA cm^{-2}). Experimental results are shown as points and simulation results are shown as solid lines.

At open circuit potentials, there is no reaction and thus $C_{H_2,\delta}/C_{H_2,0}$ remains constant throughout the entire catalyst layer at a value of 1. With increasing current density, the models results showed a good fit to the experimental data by reducing $C_{H_2,\delta}/C_{H_2,0}$ to 60% at 300 mA cm^{-2}, and to 53% at 500 mA cm^{-2} and 34% at 700 mA cm^{-2}. These simulation results are presented in Figure 8-6.

Figure 8-6 also shows $C_{H_2,\delta}/C_{H_2,0}$ plotted against current density for the two cases explored in the above development, a dry catalyst layer and a fully flooded catalyst layer. The simulation results showed that a in a completely dry catalyst layer the diffusion coefficients and concentrations are very high in comparison to other conditions evaluated, thus leading to little change in concentration at that catalyst/electrolyte interface. On the other hand, when assuming a fully flooded catalyst layer the simulation results showed that after small currents the concentration at the electrolyte/catalyst layer interface is effectively zero. The results from the semi-mechanistic model fall between the two extremes. This can be explained by considering a catalyst layer that is partially flooded, and therefore the diffusion and concentration of hydrogen in this layer was reduced compared to the un-flooded example. Using the fully flooded catalyst layer model, the diffusion coefficient was modified to fit the model to the experimental estimates for $C_{H_2,\delta}/C_{H_2,0}$. The fitted diffusion coefficient, 1.9 X10^{-6} m^2s^{-1} was 2 orders of magnitude higher than the fully flooded case and 2 orders of magnitude lower than the water free case.

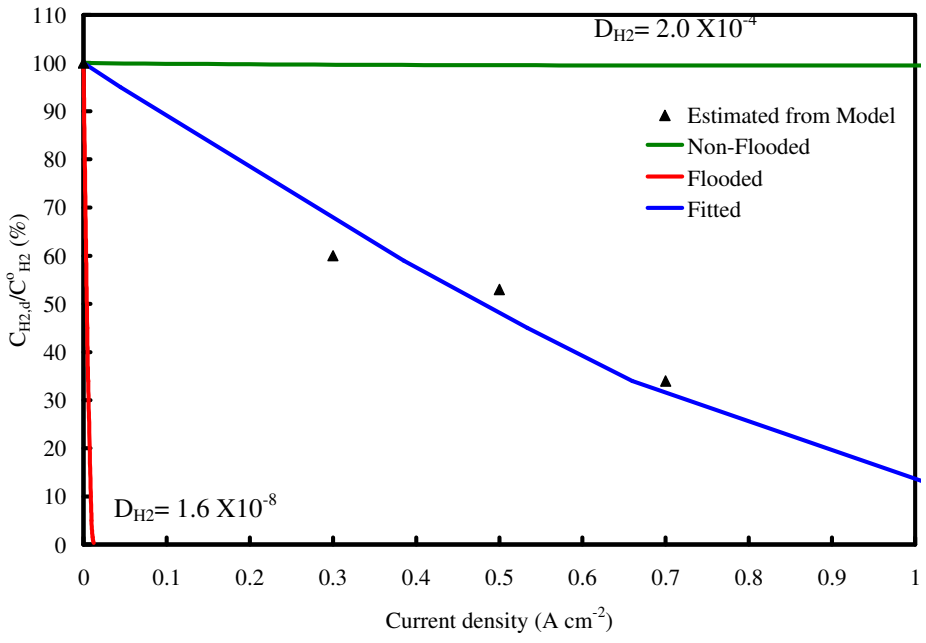

Figure 8-6: Comparison of the effect of current density on hydrogen concentration for flooded, non-flooded and fitted cases.

8.4 CHAPTER SUMMARY

This study has examined the effect of current density on the chemical degradation of the electrolyte membrane of a GORE PRIMEA series 5510 catalyst coated membrane as measured by fluoride release. Voltage degradation was also measured during the study. Four fuel cells were constructed and each was tested at a different current density, 0, 300, 500, and 700 mA cm^{-2}. An increase in current density from open circuit voltage conditions was seen to decrease the voltage degradation rate by a factor of two, however there was little difference in voltage degradation rates of each cell studied at different current densities. Increasing current density decreased cumulative fluoride release curves and fluoride release rates implying that there was less degradation. This was confirmed with SEM images which agreed with cumulative fluoride release results showing that higher release corresponded to thinner, more degraded, membranes. Membrane degradation was predominant on the cathode which is consistent for these membranes.

Previous chapters attributed the cathode electrolyte degradation to hydrogen crossover. It is proposed that with increasing current density the driving force for hydrogen crossover decreases because hydrogen within the catalyst layer is consumed by the reaction. This has the effect of lowering the hydrogen concentration at the catalyst/electrolyte interface where crossover happens. Using a macro-homogeneous model combined with the semi-mechanistic degradation model developed in Chapters 5 and 6, the effect of current density was modeled.

CHAPTER 9 : MODEL APPLICATIONS

Previous chapters have shown the development of a semi-mechanistic chemical degradation model for the electrolyte membrane and its validation against different relative humidity conditions and extension to include the effects of current density.

The main results from the following chapter are:

- In fuel cell systems for vehicle applications the amount of power delivered by the fuel cell varies with time.
- How the fuel cell is used and controlled will impact the power profile and therefore also degradation.
- The proposed chemical degradation model was applied to the dynamic conditions of three different drive cycles and was used to predict membrane thinning over the drive cycle period.
- The load profile will influence the rate of degradation.

9.1 LOAD PROFILES

The load profiles for a fuel cell under different drive cycles were created using a simulation tool known as PSAT (Powertrain System Analysis Toolkit). Using PSAT, a user may select a type of vehicle and powertrain architecture as well as drive cycle and the simulator, programmed with Matlab Simulink, and it is used to determine the amount

of power needed from engines and batteries in the system. The toolkit allows a user to examine and compare many different vehicle architectures without the need of physically building the vehicles. For the purposes of this work, the powertrain system modeled is a complete fuel cell power train where all electricity needed to power the motor is delivered from a fuel cell system.

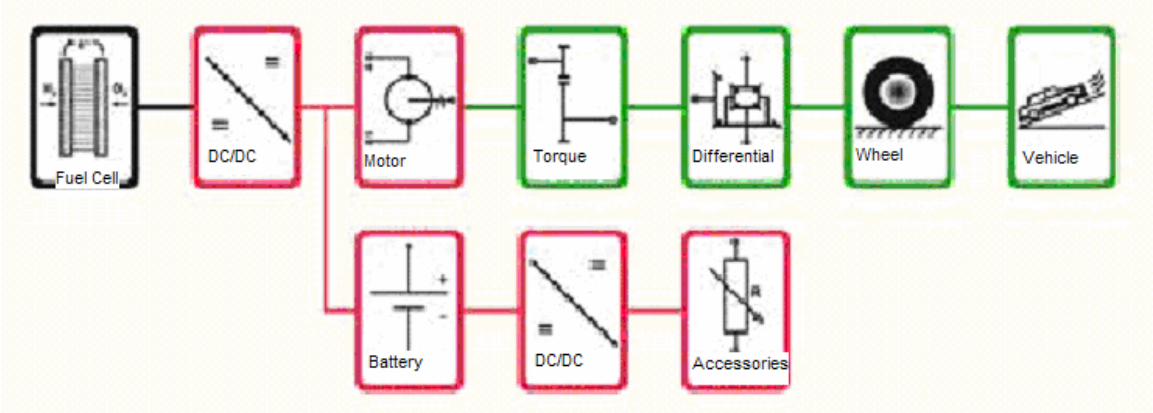

Figure 9-1: PSAT powertrain diagram for a fuel cell powertrain where all energy to move the vehicle comes from a fuel cell stack.

Figure 9-1 shows the main elements included in the vehicle simulation. The simulator models all major aspects of transferring power from an engine (in this case the fuel cell) to the vehicle wheels. The user is also able to define a drive cycle so that road grades, desired vehicle speeds, and driver aggressiveness can be considered.

Different powertrain architectures and driving situations may also influence degradation. One reason for hybridizing fuel cells with batteries within a vehicle is to protect the fuel cell from sharp spikes in load demand and thereby increase the life of the fuel cell system. However, there are currently no models to predict the benefit to fuel cell lifetime and thus no models to aid in the actual design and control of such systems.

The model presented in the previous chapters can be used to predict the effect of different drive cycles, and different hybrid strategies on the extent of chemical degradation (and hence thinning) of the electrolyte membrane. A full degradation model, which falls outside the scope of this work, would also include other degradation mechanisms that

affect catalyst layer durability and mechanical degradation of the fuel cell membrane. The work presented here will only focus on chemical degradation under different load profiles for an un-hybridized fuel cell power train.

Three load profiles are considered in this application of the semi-mechanistic model. Each drive cycle presents the power requirement for a 400 cell fuel cell (with each cell having an active area of 400 cm^2) when subjected to three standard drive cycles:

1) EPA Highway Fuel and Economy Test (HWFET)
2) EPA Urban Dynamometer Driving Schedule (UDDS)
3) Supplemental Federal Test Procedure US06 (US06)

The load profile of each cycle is presented in Figure 9-2 - Figure 9-4.

The main differences between each of the drive cycles are the maximum power achieved and the individual spikes and troughs which represent periods of acceleration and braking in a vehicle. For the purposes of this modeling effort, the fuel cell stack is considered to operate at 90°C and have inlet gas humidity of 75%. The current density of the fuel cell was determined using a polarization curve shown in Figure 9-5.

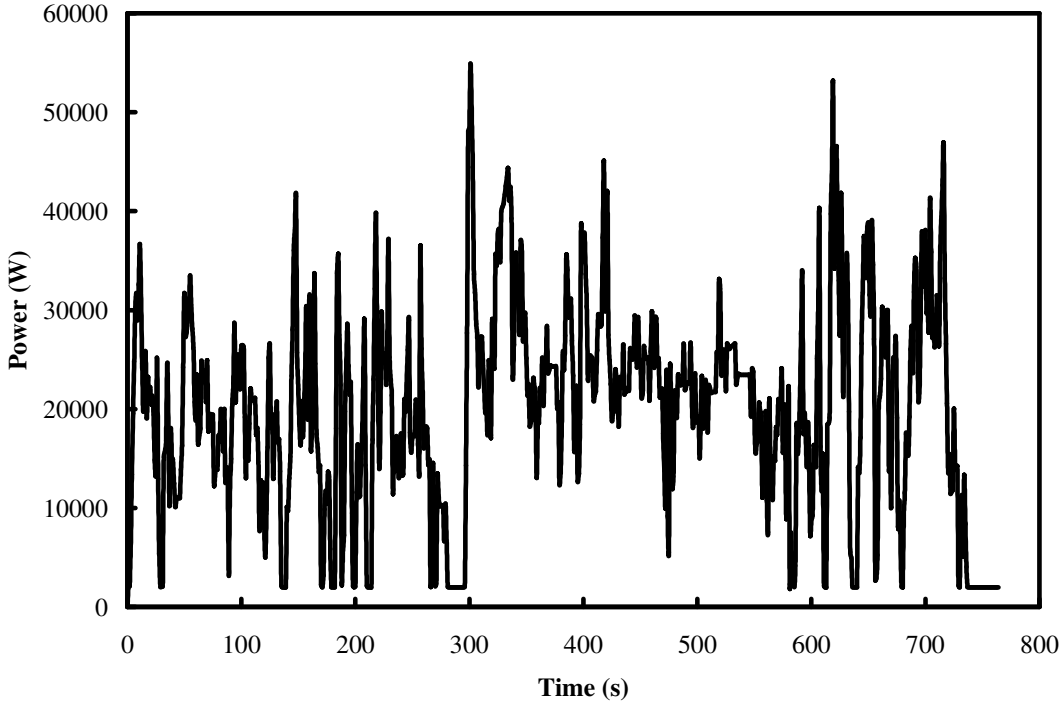

Figure 9-2: HWFET Drive Cycle

The average current density of each of the drive cycles was determined to be the following:

1) the HWFET cycle operates at an average current density of 177 mA cm^{-2};
2) the UDDS cycle operates at an average current density of 92 mA cm^{-2}; and
3) the US06 cycle operates at an average current density of 289 mA cm^{-2}.

From the results of Chapter 7, it is reasonable to estimate that the drive cycle that will cause the least chemical degradation is the US06 cycle due to its higher average current density followed by HWFET and the UDDS. The cycles ranged in time from 600 seconds to 1400 seconds.

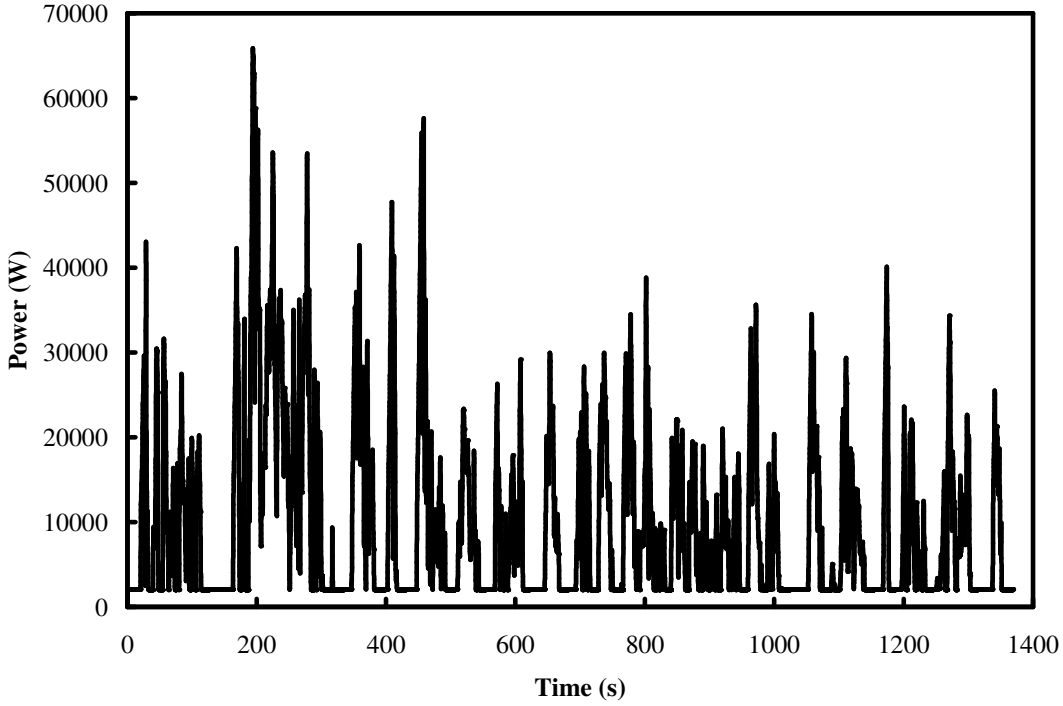

Figure 9-3: UDDS Drive Cycle

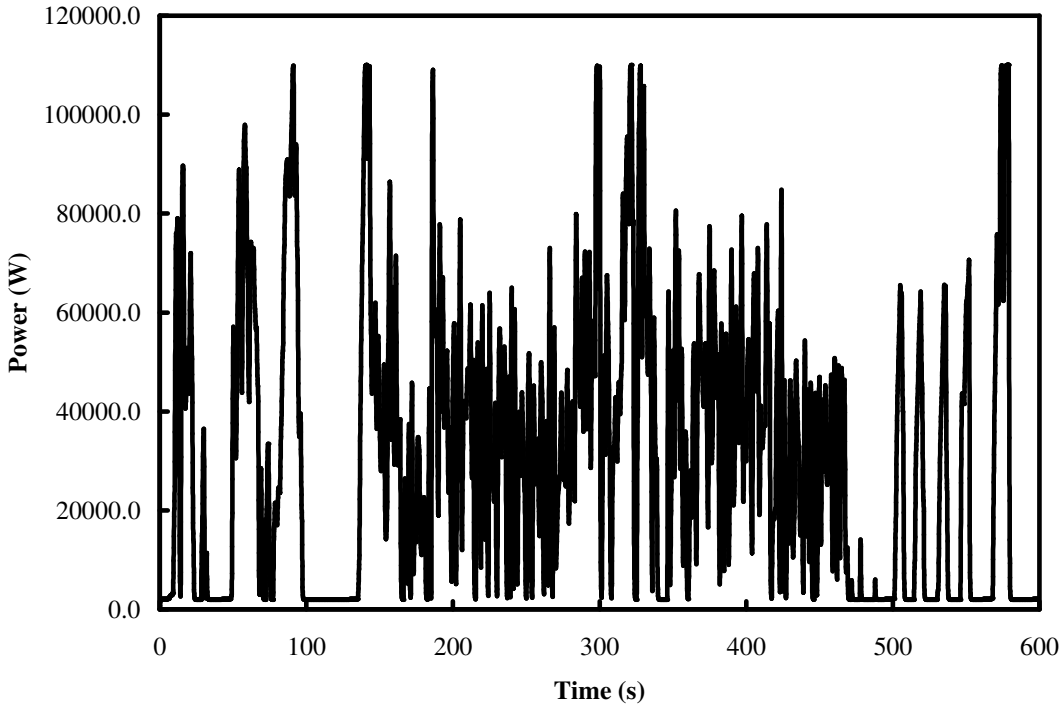

Figure 9-4: US06 Drive Cycle

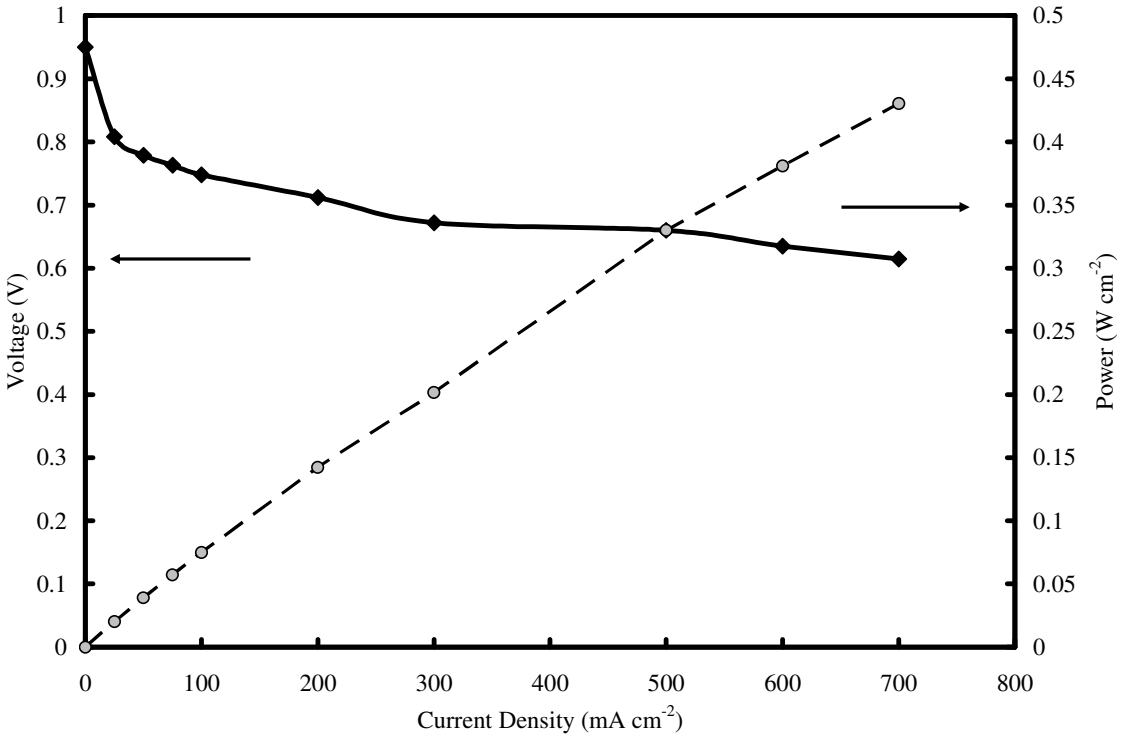

Figure 9-5: Typical polarization curve and power density curve.

9.2 MODEL RESULTS

Using the semi-mechanistic chemical degradation model, the anticipated degradation from one cycle of each drive cycle was estimated. These results are shown in Figure 9-6 as the percentage of cathode electrolyte remaining in the membrane. Though each degradation curve has a downward trend, they tend to plateau during periods where high currents are being drawn and hence decrease the degradation rate.

Note that degradation in Figure 9-6 is exaggerated because of the time scale used to plot these results. The actual degradation is only on the order of 0.1% of the cathode ionomer thickness. The magnitude of the degradation is expected to be small. This is due to the short cycle time, which is less than one hour in all cases. Nevertheless, the degradation from each cycle can be estimated. As expected from the average current densities for

each drive cycle, the UDDS cycle shows the most rapid degradation followed by HWFET and then US06.

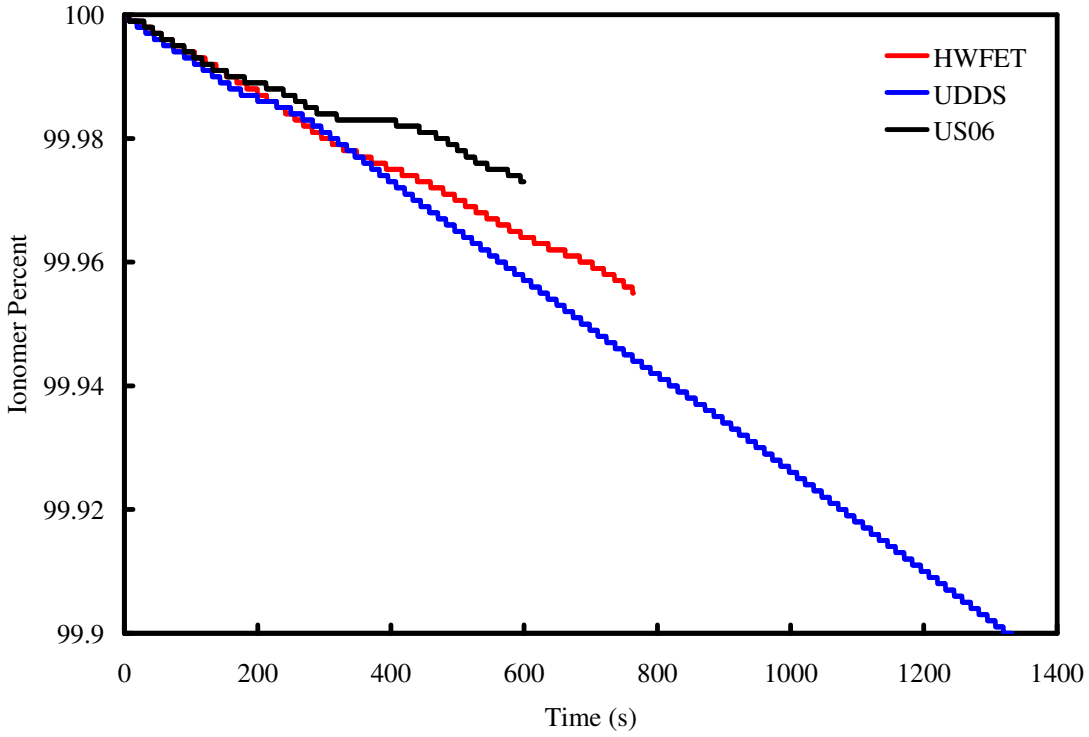

Figure 9-6: Simulated degradation of the cathode electrolyte membrane with time from different drive cycles.

Though on the surface the above results may seem trivial, however they show how the proposed degradation model can take a variety of inputs, including current density, and output information about degradation under dynamic conditions. The strength of the model lies in connecting it with more detailed fuel cell models that are able to dynamically predict humidity and pressure conditions dynamically as well. Further advances are also possible if the influence of temperature could also be added.

As discussed in the previous chapters, voltage degradation, though perhaps influenced by chemical degradation, is also influenced by other degradation mechanisms. As such, to be able to accurately describe how voltage and power curves will degrade the above model would necessarily need to be connected to a several catalyst layer models which describe

the different degradation mechanisms. One example of a suitable contribution to the modeling efforts would be inclusion of the catalyst layer degradation model proposed by Bi and coworkers [76].

CHAPTER 10 : CONCLUSIONS AND SUGGESTIONS FOR FUTURE WORK

10.1 CONCLUSIONS

This work described the development and application of a dynamic, semi-mechanistic chemical degradation model for reinforced fuel cell electrolyte membranes. The model was based on accelerated durability testing experiments conducted with Gore™ PRIMEA® series 5510 reinforced membranes in Hydrogenics Series 82 single cell hardware. This work specifically explored chemical degradation issues of the electrolyte membrane. The main objectives of this work were threefold:

1) To establish a mechanism of electrolyte degradation for GORE membranes.
2) To create a model that describes the degradation.
3) To apply the model to dynamic situations.

Fuel cell degradation can be described in three parts: causes, modes, and effects. Causes include material properties and operational condition that will influence degradation such as permeability, temperature, and reactant gas partial pressure. The degradation mode of interest in this study was chemical degradation. The main mechanism involves crossover gases reacting to form peroxide which can then become radical species. These radicals may then attack the polymer structure of the electrolyte membrane causing membrane

thinning, which results in increased crossover, as well as fluoride ion release. Finally, degradation causes performance loss and increased hydrogen crossover until failure.

Preliminary work showed that exposure of Nafion^{TM} PFSA ionomer membranes to a Fenton's solution that promotes the production of radicals will severely change the morphology and cause significant weight loss as well as fluoride release. Further preliminary work also examined how gas crossover characteristics change with degradation. Final preliminary experiments examined how degradation changed with operational conditions and materials. This work found that degradation, as measured by fluoride release rate, decreased with increasing current density. The above works have been published in the Journal of Power Sources.

Reversible and irreversible voltage degradation

Accelerated testing, in the form of open circuit voltage (OCV) durability experiments, were used to degrade cells by promoting chemical degradation. Initial results showed that voltage decay in OCV experiments was caused by reversible and irreversible sources. Reversible voltage degradation represents voltage decay that can be recovered once the fuel cell is shut-down or restarted while irreversible decay is a permanent loss of open circuit potential. Irreversible loss is generally attributed to changes in membrane integrity, such as membrane thinning, and changes in the catalyst layer. Hydrogen crossover and electrochemically active surface area (EAS) were the main membrane properties measured. It was shown that irreversible changes in these parameters, caused by degradation, could describe the irreversible voltage losses. Irreversible losses in the continuous open circuit voltage data were also consistent with voltage degradation seen in polarization curves. Since the irreversible performance losses could be explained by measuring crossover and EAS over time, a model which can link causes such as material properties and operational condition to crossover and EAS should be able to dynamically model voltage decay.

Dynamic semi-mechanistic degradation model

Such a model was developed based on the results of an OCV durability experiment (Cell 3) operated at 75% RH. During degradation of the fuel cell membrane, the cell voltage, fluoride ion release, and hydrogen crossover were monitored. Further, once testing was completed, the membrane was examined under a scanning electron microscope. The results showed that after degradation for 900 hours, the voltage degradation rate slowed as did the rate of fluoride release which was seen as a plateau on the cumulative fluoride release curves. Also, there was more fluoride release from the cathode than the anode. Examination of individual cumulative fluoride release curves from the anode and the cathode also revealed that the cumulative release reached a maximum at approximately the same time. SEM analysis showed that the electrolyte layer close to the cathode was significantly degraded while the anode electrolyte layer was not.

It was proposed that hydrogen crossover from the anode is the primary driver of degradation under these conditions. Crossover hydrogen reacts at the cathode to produce radical species which are then responsible for degradation at the cathode. It was also proposed that with time a degradation front would move through the cathode electrolyte layer and then slow at the non-reactive reinforcement layer until reaching the anode electrolyte layer where degradation, in the form of fluoride release, would recommence. It was further proposed that cathode side degradation was responsible for all the fluoride released and that once the cathode electrolyte was consumed the fluoride release rate dropped because there was no longer any reactant to participate in the degradation reactions that release fluoride ions. This explanation was consistent with anode and cathode cumulative fluoride release trends as well as SEM observations. Differences in fluoride release to the anode and the cathode were explained by differences in diffusion paths whereby anode side fluoride release took a long path from the generation point in the cathode, through the electrolyte membrane, anode electrode, and GDL to the anode channel. Released fluoride simply originated at the cathode and then diffused through the cathode electrode and GDL. Since the diffusion path to the cathode channel offered less resistance, cathode fluoride release was higher than anode release.

The above reaction and transport processes were modeled with a semi-mechanistic fuel cell chemical degradation model. The model inputs included hydrogen permeability and gas partial pressure with the main outputs being cumulative fluoride release. A first order dependence on the hydrogen flux was assumed for the initial model. Voltage was also modeled based on the chemical degradation of the electrolyte. The model also predicts information about electrolyte thickness and crossover with time. The simulations displayed an adequate fit to the experimental data. Further, the model was used to explain features of a second set of experimental data (Cell 4) which was operated under the same conditions of the baseline cell but differed in that cell operation was interrupted several times early in testing. Stoppage of the experiment caused concentration gradients to be interrupted within the cell layers and thus the fluoride release curves incurred lag times when starting up again. This had the effect of lowering the cumulative fluoride release as compared to the baseline case and could be simulated with the model.

Relative humidity and initial crossover effects on degradation

Further experiments examining the effect of relative humidity on degradation were also performed and compared with results from the chemical degradation model. Cells were run at 100%, 75%, 50%, and 20% RH in OCV tests (Cells 6, 3, 2, and 1 respectively). It was found that initial crossover rates were the best predictor of the rate of degradation. The cell running at 100% RH had a slightly higher permeability compared to the cell at 75% RH and accordingly the cumulative fluoride release curve was higher in the 100% RH case than the 75% RH case. Similarly, the cell running at 20% RH had a higher crossover rate than the cell at 50% RH, and both these cells had higher crossover than the 75 and 100 %RH cells, and cumulative fluoride release trends followed. The chemical degradation model was further refined with a second order dependence with respect to hydrogen flux (second order model). After long degradation times the experimental cumulative fluoride release for the 100%, 50%, and 20% RH cases exceeded model predictions. This discrepancy is thought to be caused by a limitation in the proposed model whereby only cathode side degradation is simulated. SEM analysis shows that with time the anode electrolyte will also degrade. Thus the discrepancy in model and experimental cumulative fluoride release curves is attributed to in onset of anode side

degradation and the resultant fluoride release. Note that in practical applications a fuel cell would likely be removed from service prior to undergoing anode degradation. It was also shown that the initial hydrogen crossover rate alone was not a good predictor for overall voltage degradation. This is thought to be because other degradation mechanisms, independent of chemical degradation of the membrane may be acting on the catalyst itself in catalyst layer.

Model sensitivity analysis

The proposed second order chemical degradation incorporates many different material causes to the degradation of the electrolyte membrane as measured by fluoride release and thinning. The considered properties are mostly measurable quantities that influence degradation. Material properties included in the model are the initial membrane thickness (δ), initial membrane permeability (k_{H_2}), and the membrane reactivity to peroxide (K_1). Operational conditions that can be incorporated into the model are gas partial pressure and relative humidity. The effect of temperature was not considered although it is believed that temperature would most significantly affect membrane reactivity. Fluoride diffusion coefficients through the GDL and electrolyte layers are also included in the model. Sensitivity analysis to the different parameters showed that the model behaved in a manner consistent with reported results. The sensitivity analysis also showed that initial crossover rate and initial fluoride release rate should be good indicators of membrane durability.

Effect of current density on degradation

A final significant operational condition is the electrochemical production of current in the fuel cell. The chemical degradation model described thus far had been based on and only been used in situations where no current was drawn from the cell. Studies have shown that one of the implications of drawing current is that hydrogen crossover will decrease since the partial pressure at the catalyst layer – electrolyte layer interface decreases due to reaction-diffusion transport within the catalyst layer. Experimental data showed that with increasing current density, the fluoride release rates decreased. Using the proposed fuel cell degradation model the driving force of hydrogen at the catalyst

layer – electrolyte was determined by fitting the experimental data. A macro-homogeneous model of the fuel cell catalyst layer was then proposed to describe the behaviour of the hydrogen driving force at the electrolyte membrane interface. It was found that this model depends heavily on the initial assumptions for the state of the catalyst layer. The predictions based on fitting experimental data were found to lie between two extremes, a fully flooded catalyst layer and a completely open catalyst layer. It is suggested that the anode catalyst layer is therefore only partially flooded and that a reduction of hydrogen concentration through the catalyst layer may explain why chemical degradation of the electrolyte membrane is reduced with current density. Current density did not seem to have a significant impact on the voltage degradation rate except between OCV conditions and 300 mA cm^{-2}.

Application to dynamic conditions

In order to demonstrate the dynamic capabilities of the fluoride release model, which has been used in situations where operational conditions did not change with time, the model was applied to a situation where current density changed rapidly with time. Three different drive cycles were examined and the proposed model was used to estimate the variation in cathode electrolyte thickness with time over the course of the drive cycle. The model predicted different degradation profiles for each drive cycle. Overall, the drive cycle with the lowest average current density over the test time had more degradation than those with higher current densities. The model only predicts chemical degradation of the electrolyte membrane and therefore it must be connected with other models such as a catalyst layer degradation model before being used to predict performance.

10.2 CONTRIBUTIONS

There have been many contributions to the literature from this work. The preliminary work described in Chapter 2 has been published as three different articles [1,46,47], further, the contents of Chapter 4 and 5 have also been recently published or accepted for publication [68,70].

The main contribution of this work is a semi-mechanistic chemical degradation model of the electrolyte membrane which dynamically links important material properties and operational conditions to meaningful and measurable material changes and effects such as membrane thinning, changes in crossover, and especially fluoride ion release.

Other contributions of this work to the scientific community are as follows, where this work:

- Revealed the extent of reversible and irreversible voltage degradation.
- Linked open circuit voltage degradation to crossover and EAS degradation.
- Showed that the cathode side is the principle site degradation in a fuel cell.
- Showed the link between initial reactant crossover and degradation in RH studies.
- Showed the potential relationship between current density, hydrogen crossover, and chemical degradation.
- Estimated the chemical degradation of the polymer electrolyte under three dynamic drive cycles, demonstrating the use of material degradation models in system reliability models.

10.3 SUGGESTION FOR FUTURE WORK

Research can continue in the future and expand the following topics:

- Extra repeat experimentation including stopping experiments at different times to establish how the degradation front moves through the membrane.
- Study of anode side degradation and establish rates of degradation once the cathode ionomer is consumed. Although continued operation of the cell beyond this point of degradation is not representative of practical applications, this study will aid in understanding overall membrane degradation.
- Study partial pressure effects of hydrogen, with the total pressure remaining the same to determine the rate of peroxide generation on the anode or cathode side.
- Conduct studies at different temperatures to determine its effect on degradation and extend model for operations at different temperatures.

REFERENCES

[1] S.Kundu, L.C.Simon, M.Fowler. Comparison of two accelerated Nafion™ degradation experiments. *Polymer Degradation and Stability*, 93(2008) 214-224.

[2] M.W.Fowler, R.F.Mann, J.C.Amphlett, B.A.Peppley, P.R.Roberge. Incorporation of voltage degradation into a generalised steady state electrochemical model for a PEM fuel cell. *Journal of Power Sources* 106(2002), 274-283.

[3] K.C.Neyerlin, H.A.Gasteiger, C.K.Mittelsteadt, J.Jorne, W.Gu. Effect of relative humidity on oxygen reduction kinetics in a PEMFC. *Journal of The Electrochemical Society* 152(2005) 1073-1080.

[4] J.Larminie, A.Dicks. "Fuel Cell Systems Explained." 2 edn. John Wiley & Sons, 2003.

[5] M.Fowler, R.F.Mann, J.C.Amphlett, S.Kundu, I.Wheeldon, B.A.Peppley. Chapter 9: Issues Associated with Material Characteristics in PEM Fuel Cells. In: Thring RH, ed. Fuel Cells for Automotive Applications. ASME Press, 2004.

[6] T.R.Ralph, D.E.Barnwell, P.J.Bouwman, A.J.Hodgkinson, M.I.Petch, M.Pollington. Reinforced membrane durability in proton exchange membrane fuel cell stacks for automotive applications. *Journal of The Electrochemical Society* 155(2008) 411-422.

[7] L.Fuqiang, Y.Baolian, X.Danmin, Y.Jingrong, Z.Huamin. Nafion®/PTFE composite membranes for fuel cell applications. *Journal of Membrane Science* 212(2003) 213-223.

[8] S. Cleghorn, J. Kolde, W. Liu in: W. Vielstich, H. Gasteiger, A. Lamm (Eds.), Handbook of Fuel Cells—Fundamentals, Technology and Applications, vol. 3, John Wiley & Sons, New York, 2003, pp. 566–575.

[9] S.Kundu, M.W.Fowler, L.C.Simon, S.Grot. Morphological features (defects) in fuel cell membrane electrode assemblies. *Journal of Power Sources* 157(2006) 650-656.

[10] A.B. LaConti, M. Hamdan, R.C. McDonald, in: W. Vielstich, H. Gasteiger, A. Lamm (Eds.), Handbook of Fuel Cells—Fundamentals, Technology and Applications, vol. 3, John Wiley & Sons, New York, 2003, pp. 647–663.

[11] A.Collier, H.Wang, X.Zi Yuan, J.Zhang, D.P.Wilkinson. Degradation of polymer electrolyte membranes. *International Journal of Hydrogen Energy* 31(2006) 1838-1854.

[12] C.H. Paik, T. Skiba, V. Mittal, S. Motupally, T.D. Jarvi, *207th Meeting of the Electrochemical Society - Meeting Abstracts*, 2005, 771.

[13] M. F. Mathias, R. Makharia, H. A.Gasteiger, J. J. Conley, T. J. Fuller, C. J. Gittleman, S. S. Kocha, D. P. Miller, C.K. Mittelsteadt, T. Xie, S.G. Yan, P. T. Yu. *The Electrochemical Society Interface* 14 (2005) 24-36.

[14] T.Kinumoto, M.Inaba, Y.Nakayama, K.Ogata, R.Umebayashi, A.Tasaka, Y.Iriyama, T.Abe, Z.Ogumi. Durability of perfluorinated ionomer membrane against hydrogen peroxide. *Journal of Power Sources* 158(2006) 1222-1228.

[15] X.Cheng, Z.Shi, N.Glass, L.Zhang, J.Zhang, D.Song, Z.S.Liu, H.Wang, J.Shen. A review of PEM hydrogen fuel cell contamination: Impacts, mechanisms, and mitigation. *Journal of Power Sources* 165(2007) 739-756.

[16] J.J.Baschuk, X.G.Li. Carbon monoxide poisoning of proton exchange membrane fuel cells. *International Journal of Energy Research* 25(2001) 695-713.

[17] K.Narusawa, M.Hayashida, Y.Kamiya, H.Roppongi, D.Kurashima, K.Wakabayashi. Deterioration in fuel cell performance resulting from hydrogen fuel containing impurities: poisoning effects by CO, CH4, HCHO and HCOOH. *JSAE Review* 24(2003) 41-46.

[18] D.Liu, S.Case. Durability study of proton exchange membrane fuel cells under dynamic testing conditions with cyclic current profile. *Journal of Power Sources* 162(2006) 521-531.

[19] L.Jing, H.Ping, W.Keping, M.Davis, Y.Siyu. Characterization of catalyst layer structural changes in PEMFC as a function of durability testing. *ECS Transactions* 3(2006) 743-751.

[20] Y.Fujii, S.Tsushima, K.Teranishi, K.Kawata, T.Nanjo, S.Hirai. Degradation investigation of PEMFC by scanning electron microscopy and direct gas mass spectroscopy. *ECS Transactions* 3(2006) 735-741.

[21] J.Hou, H.Yu, S.Zhang, S.Sun, H.Wang, B.Yi, P.Ming. Analysis of PEMFC freeze degradation at -20 [deg]C after gas purging. *Journal of Power Sources* 162(2006) 513-520.

[22] Q.Guo, Z.Qi. Effect of freeze-thaw cycles on the properties and performance of membrane-electrode assemblies. *Journal of Power Sources* 160(2006) 1269-1274.

[23] M.Oszcipok, D.Riemann, U.Kronenwett, M.Kreideweis, A.Zedda. Statistic analysis of operational influences on the cold start behaviour of PEM fuel cells. *Journal of Power Sources* 145(2005) 407-415.

[24] R.C.McDonald, C.K.Mittelsteadt, E.L.Thompson. Effects of deep temperature cycling on Nafion 112 membranes and membrane electrode assemblies. *Fuel Cells* 4(2004) 208-213.

[25] Y.Tang, M.H.Santare, A.M.Karlsson, S.Cleghorn, W.B.Johnson. Stresses in proton exchange membranes due to hygro-thermal loading. *Journal of Fuel Cell Science and Technology* 3(2006) 119-124.

[26] X.Huang, R.Solasi, Y.Zou, M.Feshler, K.Reifsnider, D.Condit, S.Burlatsky, T.Madden. Mechanical endurance of polymer electrolyte membrane and PEM fuel cell durability. *Journal of Polymer Science, Part B: Polymer Physics* 44(2006) 2346-2357.

[27] D.A.Stevens, J.R.Dahn. Thermal degradation of the support in carbon-supported platinum electrocatalysts for PEM fuel cells. *Carbon* 43(2005) 179-188.

[28] D.E.Curtin, R.D.Lousenberg, T.J.Henry, P.C.Tangeman, M.E.Tisack. Advanced materials for improved PEMFC performance and life. *Journal of Power Sources* 131(2004) 41-48.

[29] A.Panchenko, H.Dilger, J.Kerres, M.Hein, A.Ullrich, T.Kaz, E.Roduner. In-situ spin trap electron paramagnetic resonance study of fuel cell processes. *Physical Chemistry Chemical Physics* 6(2004) 2891-2894.

[30] M.Inaba. Degradation Mechanism of Polymer Electrolyte Membrane Fuel Cells. 14th International Conference on the Properties of Water and Steam in Kyoto(2005), 395-402.

[31] J.Healy, C.Hayden, T.Xie, K.Olson, R.Waldo, M.Brundage, H.Gasteiger, J.Abbott. Aspects of the chemical degradation of PFSA ionomers used in PEM fuel cells. *Fuel Cells* 5(2005) 302-308.

[32] K.Broka, P.Ekdunge. Oxygen and hydrogen permeation properties and water uptake of Nafion 117 membrane and recast film for PEM fuel cell. *Journal of Applied Electrochemistry* 27(1997) 117-123.

[33] P.Gode, G.Lindbergh, G.Sundholm. In-situ measurements of gas permeability in fuel cell membranes using a cylindrical microelectrode. *Journal of Electroanalytical Chemistry* 518(2002) 115-122.

[34] J.S.Chiou, D.R.Paul. Gas permeation in a dry nafion membrane. *Industrial & Engineering Chemistry Research* 27(1988) 2161-2164.

[35] X.Cheng, J.L.Zhang, Y.H.Tang, C.J.Song, J.Shen, D.T.Song, J.J.Zhang. Hydrogen crossover in high-temperature PEM fuel cells. *Journal of Power Sources* 167(2007) 25-31.

[36] P.Pandey, R.S.Chauhan. Membranes for gas separation. *Progress in Polymer Science* 26(2001) 853-893.

[37] P.Rama, R.Chen, R.Thring. Polymer electrolyte fuel cell transport mechanisms: a universal modelling framework from fundamental theory. Proceedings of the Institution of Mechanical Engineers, Part A (Journal of Power and Energy) 2006, 220 535-550.

[38] M.Seddiq, H.Khaleghi, M.Mirzaei. Numerical analysis of gas cross-over through the membrane in a proton exchange membrane fuel cell. *Journal of Power Sources* 161(2006) 371-379.

[39] K.Broka, P.Ekdunge. Modelling the PEM fuel cell cathode. *Journal of Applied Electrochemistry* 27(1997) 281-289.

[40] Ryan J.Wane. Durability Studies on Polymer ELectrolyte Membrane Fuel Cells. PhD. Thesis, 2004. Case Western Reserve University.

[41] V.O.Mittal, H.R.Kunz, J.M.Fenton. Membrane degradation mechanisms in pemfcs. *ECS Transactions* 3(2006) 507-517.

[42] C.Chen, T.F.Fuller. H2O2 Formation under Fuel-cell Conditions. *ECS Transactions* 11(2007) 1127-1137.

[43] L.Wen, D.Zuckerbrod. In situ detection of hydrogen peroxide in PEM fuel cells. *Journal of The Electrochemical Society* 152(2005) 1165-1170.

[44] M.K.Kadirov, A.Bosnjakovic, S.Schlick. Membrane-derived fluorinated radicals detected by electron spin resonance in UV-irradiated nafion and dow ionomers: Effect of counterions and H2O2. *Journal of Physical Chemistry B* 109(2005) 7664-7670.

[45] S.J.C.Cleghorn, D.K.Mayfield, D.A.Moore, J.C.Moore, G.Rusch, T.W.Sherman, N.T.Sisofo, U.Beuscher. A polymer electrolyte fuel cell life test: 3 years of continuous operation. *Journal of Power Sources* 158(2006) 446-454.

[46] S.Kundu, K.Karan, M.Fowler, L.C.Simon, B.Peppley, E.Halliop. Influence of micro-porous layer and operating conditions on the fluoride release rate and degradation of PEMFC membrane electrode assemblies. *Journal of Power Sources* 179(2008) 693-699.

[47] S.Kundu, M.Fowler, L.C.Simon. Gas Selectivity Measurements as a Diagnostic Tool for Fuel Cells. *Journal of Power Sources* 180(2008) 760-766.

[48] S.Hommura, K.Kawahara, T.Shimohira. Degradation mechanism of perfluorinated membrane in fuel cell environment. Electrochemical Society 2005 Meeting Abstracts, Quebec, Canadam p 803.

[49] T.A.Aarhaug, A.M.Svensson. Degradation rates of PEM fuel cells running at open circuit voltage. *ECS* Transactions 3(2006) 775-780.

[50] A.Ohma, S.Suga, S.Yamamoto, K.Shinohara. Membrane degradation behavior during open-circuit voltage hold test. *Journal of The Electrochemical Society* 154(2007) 757-760.

[51] A.Ohma, S.Yamamoto, K.Sinohara. Analysis of Membrane Degradation Behavior During OCV Hold Test. *ECS Transactions* 11(2007) 1181-92.

[52] V.O.Mittal, H.R.Kunz, J.M.Fenton. Is H_2O_2 involved in the membrane degradation mechanism in PEMFC? *Electrochemical and Solid-State Letters* 9(2006) 299-302.

[53] V.O.Mittal, H.R.Kunz, J.M.Fenton. Effect of catalyst properties on membrane degradation rate and the underlying degradation mechanism in PEMFCs. *Journal of The Electrochemical Society* 153(2006) 1755-1759.

[54] E.Arato, P.Costa. Transport mechanisms and voltage losses in PEMFC membranes and at electrodes: A discussion of open-circuit irreversibility. *Journal of Power Sources* 159(2006) 861-868.

[55] H.Liu, J.Zhang, F.D.Coms, W.Gu, B.Litteer, H.A.Gasteiger. Impact of gas partial pressure on PEMFC chemical degradation. *ECS Transactions* 3(2006) 493-505.

[56] W.Bi, G.E.Gray, T.F.Fuller. PEM fuel cell Pt/C dissolution and deposition in nafion electrolyte. *Electrochemical and Solid State Letters* 10(2007) B101-B104.

[57] A.Ohma, S.Suga, S.Yamamoto, K.Shinohara. Phenomenon analysis of PEFC for automotive use (1): Membrane degradation behavior during OCV hold test. *ECS Transactions* 3(2006) 519-529. 2006.

[58] E.Endoh, S.Hommura, S.Terazono, H.Widjaja, J.Anzai. Degradation Mechanism of the PFSA Membrane and Influence of Deposited Pt in the Membrane. *ECS Transactions* 1(2008) 1083-1091.

[59] S.J.Lee, C.D.Hsu, C.H.Huang. Analyses of the fuel cell stack assembly pressure. *Journal of Power Sources* 145(2005) 353-361.

[60] L.M.Roen, C.H.Paik, T.D.Jarvi. Electrocatalytic Corrosion of Carbon Support in PEMFC Cathodes. *Electrochemical and Solid-State Letters* 7(2004) 19-22.

[61] S.D.Knights, K.M.Colbow, J.St Pierre, D.P.Wilkinson. Aging mechanisms and lifetime of PEFC and DMFC. *Journal of Power Sources* 127(2004) 127-34.

[62] T.F.Fuller, G.Gray. Carbon corrosion induced by partial hydrogen coverage. *ECS Transactions* 1(2005) 345-353.

[63] B.Wahdame, D.Candusso, X.Francois, F.Harel, A.De Bernardinis, J.M.Kauffmann, G.Coquery. Study of a 5 kW PEMFC using experimental design and statistical analysis techniques. *Fuel Cells* 7(2007) 47-62.

[64] A.S.Feitelberg, J.Stathopoulos, Q.Zhigang, C.Smith, J.F.Elter. Reliability of Plug Power GenSys™ fuel cell systems. *Journal of Power Sources* 147(2005) 203-207.

[65] K.Astrom, E.Fontell, S.Virtanen. Reliability analysis and initial requirements for FC systems and stacks. *Journal of Power Sources* 171(2007) 46-54.

[66] D.Pierpont, M.Hicks, T.Watschke, P.Turner. Accelerated testing and lifetime modeling for the development of durable fuel cell MEAs. *ECS Transactions* 1(2005) 229-237.

[67] R.Z.Jiang, D.Chu. Voltage-time behavior of a polymer electrolyte membrane fuel cell stack at constant current discharge. *Journal of Power Sources* 92(2001) 193-198.

[68] S.Kundu, M.Fowler, L.C.Simon, R.Abouatallah. Reversible and Irreversible Voltage Degradation at OCV. Accepted to *Journal of Power Sources* June 2008.

[69] K.Teranishi, K.Kawata, S.Tsushima, S.Hirai. Degradation mechanism of PEMFC under open circuit operation. *Electrochemical and Solid-State Letters* 9(2006) 475-477.

[70] S.Kundu, M.Fowler, L.C.Simon. Degradation and Modeling of GORE membrane at OCV. Accepted to *Journal of Power Sources* July 2008.

[71] S.S.Kocha, J.D.Yang, J.S.Yi. Characterization of gas crossover and its implications in PEM fuel cells. *AIChE Journal* 52(2006) 1916-1925.

[72] W.Liu, K.Ruth, G.Rusch. Membrane Durability in PEM Fuel Cells. *Journal of New Materials for Electrochemical Systems* 4(2001) 227-231.

[73] E.K.Unnikrishnan, S.D.Kumar, B.Maiti. Permeation of inorganic anions through Nafion ionomer membrane. *Journal of Membrane Science* 137(1997) 133-137.

[74] R.F.Mann, J.C.Amphlett, B.A.Peppley, C.P.Thurgood. Henry's Law and the solubilities of reactant gases in the modelling of PEM fuel cells. *Journal of Power Sources* 161(2006) 768-774.

[75] H.Ju, C.Y.Wang. Experimental validation of a PEM fuel cell model by current distribution data. *Journal of The Electrochemical Society* 151(2004) 1954-1960.

[76] B.Wu, T.F.Fuller. Modeling of PEM fuel cell Pt/C catalyst degradation. *Journal of Power Sources* 178(2008) 188-196.

APPENDIX A – PUBLICATION LIST

Refereed Publications

Kundu, S., Fowler, M.W., Simon, L. C., Abouatallah, R., "Analysis and Degradation Modeling of Gore™ Catalyst Coated Membranes Operated Under OCV Conditions", *Journal of Power Sources.* Accepted July, 2008.

Kundu, S., Fowler, M.W., Simon, L. C., Abouatallah, R., "Reversible and Irreversible Degradation in Fuel Cells during OCV Durability Test", *Journal of Power Sources.* Accepted June, 2008.

Kundu, S., Fowler, M.W., "Use of Engineering Design Competitions for Undergraduate Research and Capstone Projects", Submitted to *Chemical Engineering Education.* Accepted - March, 2008.

Kundu, S., Fowler, M.W., Simon, L. C., "Gas Selectivity Measurements as a Diagnostic tool for Fuel Cells", *Journal of Power Sources* 180 (2008) 760 - 766.

Kundu, S., Karan, K., Fowler, M.W., Simon, L. C., Peppley, B., Haliop, E., "Influence of Micro-porous Layer and Operating Conditions on the Fluoride Release Rate and Degradation of PEMFC Membrane Electrode Assemblies", *Journal of Power Sources* 179(2008) 693-699.

Kundu, S., Simon, L. C. Fowler, M.W., "Comparison of Two Accelerated Nafion™ Degradation Experiments", *Polymer Degradation and Stability*, 93(2008) 214-224.

Kundu, S., Fowler, M., Simon., L., Grot S., "Morphological Features (Defects) in Fuel Cell Membrane Electrode Assemblies", *Journal of Power Sources*, 157(2006) 650-656.

Kundu, S., Fowler, M. W., Simon, L. C., Grot S., "Mechanical Properties of Nafion™ Electrolyte Membranes Under Hydrated Conditions", *Polymer*, 46(2005), 11707 – 11715.

M.W. Fowler, R.F. Mann, J.C. Amphlett, **S. Kundu**, I. Wheeldon, and B.A. Peppley, "Chapter 9: Issues Associated with Material Characteristics in PEM Fuel Cells", Fuel Cells for Automotive Applications, Thring, R.H. editor, ASME Press 2004.

Posters and Presentations

Kundu, S., Fowler, M.W., Simon, L. C., Abouatallah, R., "Fuel Cell Membrane Degradation", Poster presentation at the 3rd Fuel Cell Durability Conference, Miami FL, November 2007.

Kundu, S., Fowler, M.W., "Fuel Cell Material Degradation", Poster Presentation at the Energy Days Conference, Waterloo ON October, 2007

Kundu, **S**., Fowler, M. W., Simon, L.C., "Gas Selectivity as a Diagnostic Tool for Fuel Cell Degradation Studies" Oral presentation at Hydrogen and Fuel Cells 2007, Vancouver, Canada April 29 – May 2 2007.

Kundu, **S**., Fowler, M. W., Simon, L.C., "Reversible and Irreversible Degradation at OCV Conditions", poster presentation at the Gordon Fuel Cell Conference, Smithfield Rhode Island, July 17 – 22, 2006.

Kundu, **S**., Fowler, M. W., Simon, L.C., "PEMFC Degradation at OCV Conditions", poster presentation at the Fuel Cell Research Centre, Kingston ON, May, 2006.

Kundu, **S**., Fowler, M. W., Simon, L.C., "Degradation of Fuel Cell Membranes by Various Mechanism", oral presentation at the 55th Canadian Chemical Engineering Conference, Toronto Ontario, October 16 - 19, 2005.

Kundu, S., Fowler, M. W., Simon, L. C., Chan, K.W., Grot S., "Morphological Anomalies (Defects) in PEMFC MEAs", poster presentation at the Ninth Grove Fuel Cell Symposium, London UK, October 4 – 6, 2005.

Kundu, **S**., Fowler, M. W., Simon, L.C., "Morphological Anomalies (Defects) in PEMFC MEAs", oral presentation at the 1st Symposium on Manufacturing MEAs for Hydrogen Applications, Dayton Ohio, August 9 – 11, 2005.

Kundu, **S**., Fowler, M. W., Simon, L.C., "Degradation Mechanisms in Fuel Cells", poster presentation at the Gordon Fuel Cell Conference, Smithfield Rhode Island, July 17 – 22, 2005.

Kundu, S., Fowler, M. W., Simon, L. C., Grot S., "Durability Issues in PEM Fuel Cell Materials", poster presentation at the Hydrogen and Fuel Cells 2004 Conference and Trade Show, Toronto Ontario, September 25-28, 2004.

Kundu, S., Simon, L.C., Fowler, M. W., , "Mechanical Properties of Nafion^{TM} Electrolyte Membranes Under Hydrated Conditions", oral presentation at the 87th Canadian Chemistry Conference and Exhibition, London Ontario, May 29 – June 2, 2004.

Kundu, S., Simon, L.C., Fowler, M. W., , "Mechanical Properties of Nafion^{TM} Electrolyte Membranes Under Hydrated Conditions", poster presentation at the IPR 26th Annual Symposium on Polymer Science/Engineering, Waterloo Ontario, May 11 - 12 , 2004.

Kundu, S., Fowler, M. W., Simon, L.C., "Structure Property Relationships in Fuel Cell Materials", oral presentation at the 2003 Masters Research Seminar, University of Waterloo, Ontario, November 27, 2003.

Kundu, S., Fowler, M. W., Lam, A. Simon, L.C., "Gas Diffusion Layer Aging", oral presentation at the 53rd Canadian Chemical Engineering Conference, Hamilton Ontario, October 26-29, 2003.

Kundu, S., Fowler, M. W., Simon, L.C., "Materials and Performance of Fuel Cells", poster presented at the Gordon Research Conference, July 27 – August 1, 2003.

Kundu, S., Fowler, M. W., Simon, L.C., "Characterization of Polymeric Materials in Fuel Cells", poster presentation at MMO Partnerships 2003, June 19, 2003.

Kundu, S., Fowler, M. W., Simon, L. C., Grot S., "Characterization of Morphology in the Catalyst Layer of Membrane Electrode Assemblies", oral presentation at the New Materials for Electrochemical Systems 5th International Symposium, July 6 – 11, 2003.

Kundu, S., Fowler, M. W., "Fuel Cell Material Defects and Reliability", Invited Presentation at King Mongkut's University of Technology Thonburi (KMUTT), Chemical Engineering Practice School (CHEPS), Bangkok, Thailand, June 2003.

Kundu, S., Fowler, M. W., Simon, L.C., "Characterization of Polymeric Materials in Fuel Cells", poster presented at SPE University Industry Dinner night, Mississauga April 2003.

Kundu, S., Fowler, M.W., "Fuel Cells in Developing Countries", oral and poster presentation at the 2nd National Engineers Without Borders Conference, Waterloo April 2003.

APPENDIX B – TEST STATION PROCEDURES

B 1Commissioning

The goal of commissioning is to break in a new cell and ease the cell into drawing current. This is accomplished at high temperatures and pressures but with a low current draw

Start-up See Test Station Start up

Temperature Settings

F2 – Temperature Setpoints

Temperature settings for the test station will be given in the following format Cell.Anode.Cathode. This corresponds to the cell temperature (F2 – E), the anode dew point temperature (F2 –A) and the cathode dew point temperature (F2 – C) respectively. The temperature settings for F2 - B, D, F and G should all be set to the cell temperature settings.

Commissioning temperature settings are 80.80.80. Set F2 - B, D, E, F and G to 80ºC and as the cell temperature rises increases the anode and cathode dew point temperatures (F2 - A and C) to follow. All temperatures should end up set to 80ºC

Set water bath to 88ºC to maintain cell temperature

Pressure Settings

Raise both the anode and cathode pressures using the manual control knobs up to 100 kPa without exceeding a differential pressure of 10 kPa (a differential pressure of 30 kPa will result in an automatic shutdown)

Current Settings

F1 – A - Current should be ramped up in increments of 8.2A to 16.4A (current density = 0.2). though it is in fact more customary to run in constant voltage mode at 0.6 volts – unless currents are over 0.7 A/cm^2 at that point.

Flow Settings

F4 – K,L – STOICHIOMETRIC RATIOS should be set to 1.5/2.5 (anode/cathode)

M - Min flow should be set to 0.4 A/cm^2

Time

Commissioning settings must run for 8 hours, after commissioning the fuel cell a polarization curve will be conducted to test the cells performance.

Logging Interval

F4 – C – LOGGING INTERVAL = 60

B 2 Polarization Curves

1. Start up – See Test Station Start up
2. F4 – C - LOGGING INTERVAL = 1 s
3. F4 – K,L - STOICHIOMETRIC RATIOS to 1.2:2 (anode:cathode)
4. Set temperatures to 80.73.64 (cell.andoe.cathode). To achieve these temperatures both saturators must be set at a temperature 1 degree above the desired temperature. F2 - A-74, B – 80, C – 65, D: G – 80 (move the anode and cathode saturator temperatures up in increments matching the cell temperature)
5. Set the water bath to 88ºC
6. Raise pressures using control knobs to 100 kPa (Anode and Cathode) maintaining a differential of 10 kPa
7. Once temperatures have reached set points you may begin raising the current by increments of 8.2A in preparation of the polarization curve.
8. Continue raising current until the voltage becomes slightly unstable (varying by over 5mV in a minute) or cell voltage drops below 0.3V. This usually corresponds to a current density of about 1.2
9. Start the timer for 4 minutes
10. At 4 minutes record the cell voltage and continue at that setting for 2 more minutes

11. After the 2 minutes compare your recorded value with the current cell voltage if the cell voltage is the same you may reduce the current and repeat steps 8-10 on the next step down in current density. If voltage is not stable (varying by more then 2mV) record voltage and continue testing for 1 minute intervals until stable. If stability is not reached in 15 minutes drop current and continue with polarization curve
12. The current densities to be tested are 1.4*, 1.3*, 1.2, 1.1, 1, 0.9, 0.8, 0.7, 0.6, 0.5, 0.4, 0.3, 0.2, 0.1, 0.05, 0.
13. Once a current density of 0.3 is reached the min flow must be adjusted to match each current density so as to maintain the correct stoichiometric ratios in the cell (F4 – M - A/CM2 ZERO LOAD FLOW 0.3, 0.2)
14. Lowering the ZERO LOAD FLOW BELOW 0.2 is not recommended as the controllers have difficulty with low flow rates
15. After 8.2A drop to 4.1A and then finally 0 A to test OCV (open current voltage). OCV only needs to be tested for 2 minutes.
16. Repeat these step for temperature settings of 65.59.50 and a pressure of 20 kPa
17. Once these polarization curves are complete two additional polarization curves must be completed at the previous settings with a helium/oxygen mixture (see Helox Setup).

*Only test these if the voltage is sufficient. Maintaining too high a current density could burn the cell. If at high current density a steep decline is observed reduce current density immediately.

B 3 Leak Checks

Leak checks are used to determine if there is a hole in the membrane. Holes can be caused by current burning through the cell, improper compression or even a large pressure gradient rupturing the membrane. (K.Chan)

1. External Leak Check
    1. Shutdown cell
    2. Plug bottom three ports of the cell (anode out, water out and cathode out)
    3. Hook up top three inlet ports together with a triple connection
    4. Attach top of rotameter to open end of triple port
    5. Turn small knob on nitrogen regulator fully open and large knob fully closed.
    6. Shut off nitrogen line to machine and vent line attached to pressure gauge using the black knobs after the regulator.
    7. Attach bottom of rotameter to pressure gage attached to nitrogen tank ensuring both are upright (you may need additional piping to help with this)
    8. Pressurize cell to 30 psi using the large knob on the nitrogen regulator.
    9. If rotameter is recording a flow rate drip soapy water over all connections to identify leaks
    10. Once all connections are sealed record rotameter value as External Leak
    11. Turn large nitrogen regulator knob fully closed and vent nitrogen line

2. Coolant Leak Checks
    1. Disconnect triple port leaving bottom ports of cell plugged
    2. Plug cathode inlet, attach pressure gauge to water inlet and bottom of rotameter to anode inlet
    3. Pressurize up to 20 psi using the same method as above and record under Coolant to Anode Leak
    4. Turn large nitrogen regulator knob fully closed
    5. Switch the plug and the rotameter
    6. Pressurize up to 20 psi as above and check for leaks
    7. Record value under Coolant to Cathode Leak

8. Turn large nitrogen regulator knob fully closed and vent nitrogen line

3. Crossover Leak Checks

   Take extra care here as a large pressure gradient can burst the cell membrane

   1. Plug cooling water inlet port, connect pressure gauge to anode and rotameter to cathode
   2. Pressurize up to 5 psi using the same method as above and check for leaks
   3. Record value as Anode to Cathode Crossover
   4. Turn large nitrogen regulator knob fully closed
   5. Switch pressure gauge and rotameter
   6. Pressurize up to 5 psi and record as Cathode to Anode Crossover
   7. Turn large nitrogen regulator knob fully closed

APPENDIX C – SAMPLE DATA AND SAMPLE CALCULATIONS

C 1. Cumulative fluoride release

C 1.1 List of terms

Variable	Description	Units
$t_{s,i-start}$	Start time of degradation segment "*i*"	h
$t_{s,i-end}$	End time of degradation segment "*i*"	h
$t_{w,i-start}$	Start time of water collection segment "*i*"	h
$t_{w,i-end}$	Start time of water collection segment "*i*"	h
$C_{F-,i,j}$	Fluoride ion concentration for water sample "*i*" on side "*j*"	mg L^{-1}
$V_{w,i,j}$	Collected water volume for water sample "*i*" on side "*j*"	L
$n_{F-,w,i,j}$	Mols of fluoride in water sample "*i*" on side "*j*"	mol
$n_{F-,i,j}$	Estimated mols of fluoride in degradation segment "*i*" on side "*j*"	
$\dot{n}_{F-,i,j}$	Estimated fluoride release rate in segment "*i*" on side "*j*"	mol h^{-1}
$n_{Cu,F-,i,j}$	Cumulative fluoride released from t = 0 to the end of water collection segment "*i*" on side "*j*"	mol, mol cm^{-2}
$m_{w,i,j}$	Collected water mass for water sample "*i*" on side "*j*"	g

Calculations for cumulative fluoride release are shown below. Calculations are based on the following data set:

Segment "*i*"	Start Time	Water start	Water end	Mass water collected	Fluoride concentration
	$t_{s,\,i-start}$	$t_{w,i-start}$	$t_{w,i-end}\,, t_{s,i-end}$	$m_{w,i,C}/m_{w,i,A}$	$C_{F-,i,C}/C_{F-,i,A}$
1	0	29.5	35.27	124.8/36.9	0.839/0.284
2	35.27	54.18	64.4	355/126	1.51/0.825

Experimental data includes the testing time, water collection period, mass of water, as well as the fluoride concentration in the water. From this data the fluoride release rate and the cumulative release is calculated.

C 1.2 Segment time and water collection time

Due to the capacities of the knockout drums which collected water, it was not always possible to collect water throughout an entire time segment. Therefore there can be a difference between segment times and water collections times. A segment will run from the start time to the end of a water collection period. The start time for subsequent segments is the end of the water collection period of the previous segment. In the above data the first segment runs from 0 to 35.27 hours, and the second segment is from 35.27 to 64.4 hours. The water collection time is the time for which water was allowed to collect in the knockout drums before sampling and weighing.

The first segment time is given by

$$\Delta t_{s,1} = t_{s,1-end} - t_{s,1-start}$$
$$\Delta t_{s,1} = 35.27h - 0h = 35.27h$$

The water collection time is

$$\Delta t_{w,1} = t_{w,1-end} - t_{w,1-start}$$
$$\Delta t_{w,1} = 35.27h - 29.5h = 5.77h$$

C 1.3 Average fluoride release rate

The average fluoride release rate of the cathode is given by first calculating the total amount of fluoride in the water sample and then dividing by the water collection time. In this way cathode fluoride release rate for the first segment is:

$$C_{F-,1,C} = (0.839\frac{mg}{L})\frac{1g}{1000mg}\frac{1mol}{19g} = 4.42\times10^{-5}\frac{mol}{L}$$
$$V_{w,1,C} = (124.8g)\frac{1cm^3}{g}\frac{1L}{1000cm^3} = 0.1248L$$
$$n_{F-,w,1,C} = C_{F-,1,C}V_{w,1,C} = (4.42\times10^{-5}\frac{mol}{L})(0.1248L) = 5.51\times10^{-6}mol$$

The average fluoride release rate from the cathode in segment one is therefore:

$$\dot{n}_{F-,1,C} = \frac{n_{F-,1,C}}{\Delta t_{w,1}} = \frac{5.51\times10^{-6}mol}{5.77h} = 9.55\times10^{-7}\frac{mol}{h}$$

C 1.4 Cumulative fluoride release

Calculation of cumulative fluoride release is done in the following way. The main assumption is that the average rate of fluoride release is constant for a segment time. This assumption is fully valid in experiments where all water from a segment is collected. In cases where only part of the effluent water is collected this assumption becomes invalid when the water collection time is much smaller than the segment time. Given the data below where cathode fluoride release rate for the two data points is calculated as shown above.

Segment "*i*"	Cathode release Rate $\dot{n}_{F-,i,C}$
1	9.55E-07
2	2.76E-06

The estimated fluoride released in segment 1 is

$$n_{F-,1,C} = \dot{n}_{F-,1,C}\Delta t_{s,1} = 9.55\times10^{-7}\,\frac{mol}{h}35.27h = 3.37\times10^{-5}mol$$

On a per cm^{-2} basis the above number is divided by the active surface area.

$$n_{F-,1,C} = \frac{3.37\times10^{-5}mol}{80.1cm^2} = 4.21\times10^{-7}\,\frac{mol}{cm^2}$$

The cumulative fluoride release, which is calculated for the end of a test segment, for a measurement segment is found by calculating the fluoride release for each segment up to and including the desired segment and then summing these values.

For the first segment, the cumulative fluoride release is simply the fluoride released during that segment since at t = 0, there is no cumulative release.

$$n_{Cu,F-,1,C} = \sum_{1} n_{F-,i,C}$$

$$n_{Cu,F-,1,C} = 0 + 4.21\times10^{-7}\,\frac{mol}{cm^2} = 4.21\times10^{-7}\,\frac{mol}{cm^2}$$

For the second segment:

$$n_{Cu,F-,2,C} = \sum_{2} n_{F-,i,C}$$

$$n_{Cu,F-,2,C} = 0 + 4.21\times10^{-7}\,\frac{mol}{cm^2} + 1.00\times10^{-6}\,\frac{mol}{cm^2} = 1.42\times10^{-6}\,\frac{mol}{cm^2}$$

C 2 Water Balance Calculations

Water balance calculations for a cell with reaction is presented here. The experimental data used is from Cell 9 which was operated at 700 mA cm^{-2}.

C 2.1List of terms

Variable	Description	Units
$Q_{j,i}$	Volumetric flow rate of component "*j*" in stream "*i*"	SLPM
$y_{j,i}$	Mole fraction of components "*j*" in stream "*i*"	
n_i	Molar flow rate of stream "*i*"	mol min^{-1}
$n_{j,i}$	Molar flow rate of component "*j*" in stream "*i*"	mol min^{-1}
RH_i	Relative humidity of stream "*i*"	%
m_i	Mass flow rate of stream "*i*"	mol min^{-1}
$m_{j,i}$	Mass flow rate of component "*j*" in stream "*i*"	mol min^{-1}
$p_{j,i}$	Partial pressure of component "*j*" in stream "*i*"	mmHg
$p^*_{j,i}(T)$	Vapour pressure of component "*j*" in stream "*i*" at temperature "*T*"	mmHg
T_i	Temperature of Stream "*i*"	°C
$P_{tot,i}$	Total pressure of Stream "*i*"	mmHg
i	Current Density	mA cm^{-2}
F	Faraday's Constant	C mol^{-1}
A_{geo}	Fuel Cell Geometric Active Area	cm^2

Considering the following system :

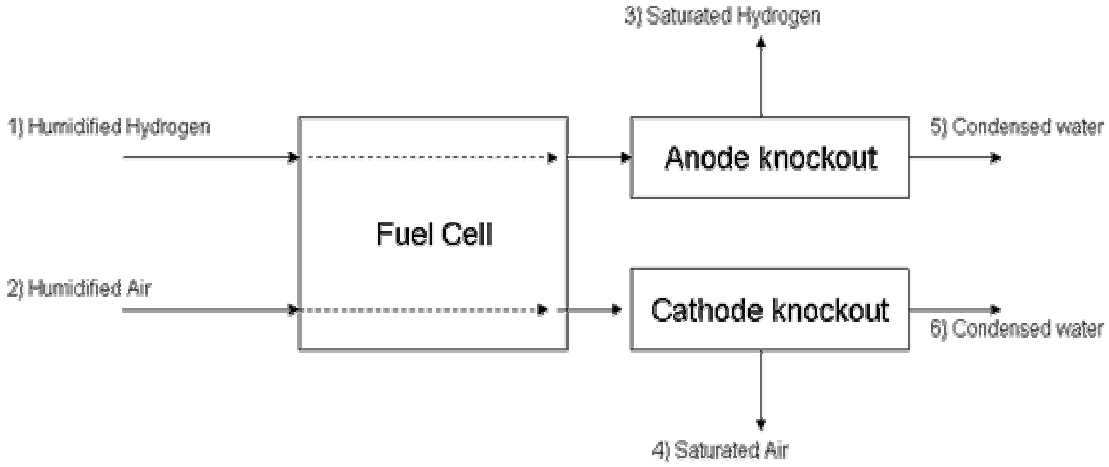

C 2.2Mass flow of water into the fuel cell

Calculation of the amount of water entering the fuel cell system with humidified anode and cathode flows is calculated by performing material balances on the respective inlet streams.

Given the following data:

Variable	Value
$Q_{H_2,1}$	0.51 SLPM
$Q_{Air_2,2}$	1.95 SLPM
T_1	90°C
T_2	90°C
RH_1	50%
RH_2	50%

Molar flow rate of hydrogen and air

$$n_{i,j} = \frac{Q_{i,j}}{22.4 molL^{-1}}$$

$$n_{H_2,1} = \frac{0.51 L \min^{-1}}{22.4 molL^{-1}} = 0.0228 \frac{mol}{\min}$$

$$n_{Air,2} = \frac{1.95 L \min^{-1}}{22.4 molL^{-1}} = 0.0871 \frac{mol}{\min}$$

Mol fraction of water in stream 1 and 2

$$y_{j,i} = \frac{p_j}{P_{tot,i}} = \frac{RH_i}{100\%} \frac{p^*_{j,i}(T)}{P_{tot,i}}$$

$$y_{H_2O,1} = y_{H_2O,2} = \frac{50\%}{100\%} \frac{p^*_{H_2O,i}(90^\circ C)}{760}$$

$p^*_{H_2O,i}(90^\circ C)$ is obtained from Antoine's equation where:

$$Log_{10}(p^*_{H_2O,i}(90^\circ C)) = 7.96681 - \frac{1668.210}{90 + 228.000} = 2.721$$

$$p^*_{H_2O,i}(90^\circ C) = 525.85 mmHg$$

Thus,

$$y_{H_2O,1} = y_{H_2O,2} = \frac{50\%}{100\%} \frac{525.85 mmHg}{760 mmHg} = 0.35$$

Molar flow rate of water into the cell with hydrogen and air streams

From non-condensable phase (H_2 and Air) and water balances

$$n_{H_2O,1} = \frac{y_{H_2O,1}}{(1 - y_{H_2O,1})} n_{H_2,1} = \frac{0.35}{(1 - 0.35)} 0.0228 \frac{mol}{\min} = 0.0123 \frac{mol}{\min}$$

$$n_{H_2O,2} = \frac{y_{H_2O,2}}{(1 - y_{H_2O,2})} n_{Air,2} = \frac{0.35}{(1 - 0.35)} 0.0871 \frac{mol}{\min} = 0.0469 \frac{mol}{\min}$$

Converting molar flow to mass flow gives

$$m_{H_2O,1} = 0.0123 \frac{mol}{\min} \frac{18 g}{mol} \frac{60 \min}{1 h} = 13.24 \frac{g}{h}$$

$$m_{H_2O,2} = 0.0469 \frac{mol}{\min} \frac{18 g}{mol} \frac{60 \min}{1 h} = 50.63 \frac{g}{h}$$

C 2.3Mass flow of water exiting the fuel cell knockout drum with gas streams

The main assumption for water exiting the fuel cell with the gas streams is that the gas streams are at room temperature (30°C) and that these streams are saturated. The latter assumption is suitable when water collects in the knockout drums, which will only happen at the dew point temperature of the gas stream.

Variable	Value
$Q_{H_2,3}$	0.51 SLPM
$Q_{Air_2,4}$	1.95 SLPM
T_3	30°C
T_4	30°C
RH_3	100%
RH_4	100%

The same calculation as for the inlet water flow rates are used. Briefly, mol fraction of water in stream 3 and 4

$$y_{j,i} = \frac{p_j}{P_{tot,i}} = \frac{RH_i}{100\%}\frac{p^*_{j,i}(T)}{P_{tot,i}}$$

$$y_{H_2O,1} = y_{H_2O,2} = \frac{100\%}{100\%}\frac{p^*_{H_2O,i}(30^\circ C)}{760}$$

$p^*_{H_2O,i}(30^\circ C)$ is obtained from Antoine's equation where:

$$Log_{10}(p^*_{H_2O,i}(30^\circ C)) = 8.10765 - \frac{1750.286}{30 + 235.000} = 1.503$$

$$p^*_{H_2O,i}(30^\circ C) = 31.83\,mmHg$$

$$y_{H_2O,1} = y_{H_2O,2} = \frac{100\%}{100\%}\frac{31.83mmHg}{760mmHg} = 0.042$$

$$n_{H_2O,3} = \frac{y_{H_2O,3}}{(1-y_{H_2O,3})} n_{H_2,3} = \frac{0.042}{(1-0.042)} 0.0089 \frac{mol}{\min} = 0.0010 \frac{mol}{\min}$$

$$n_{H_2O,4} = \frac{y_{H_2O,2}}{(1-y_{H_2O,2})} n_{Air,2} = \frac{0.042}{(1-0.042)} 0.0357 \frac{mol}{\min} = 0.0038 \frac{mol}{\min}$$

$$m_{H_2O,3} = 0.0010 \frac{mol}{\min} \frac{18g}{mol} \frac{60\min}{1h} = 1.1 \frac{g}{h}$$

$$m_{H_2O,4} = 0.0038 \frac{mol}{\min} \frac{18g}{mol} \frac{60\min}{1h} = 4.1 \frac{g}{h}$$

C 2.4Cathode Water Production from Reaction

Variable	Value
i	700 mA cm^{-2}
A_{geo}	80.1 cm^2

The mols of water produced at the cathode through the cathode reaction:

$$2H^+ + ½\ O_2 + 2e^- \rightarrow H_2O$$

Is given by

$$n_{H_2O,rxn} = i \frac{A}{1000mA} \frac{A_{geo}}{2F}$$

$$n_{H_2O,rxn} = 700 \frac{mA}{cm^2} \frac{A}{1000mA} 80.1 cm^2 \frac{\frac{1C}{s}}{1A} \frac{1}{96485 \frac{C}{mol\,e^-}} \frac{1mol\,H_2O}{2mol\,e^-} \frac{3600s}{1h} = 1.05 \frac{mol}{h}$$

Thus the mass flow is

$$m_{H_2O,rxn} = 1.05 \frac{mol}{h} \frac{18g}{mol} = 18.8 \frac{g}{h}$$

C 2.5Condensed water collection rates

Water condensation rates are determined by the mass of water collected in the knockout drums and were found to be as follows:

Variable	Value
$m_{H_2O,5}$	4.60 g/h
$m_{H_2O,6}$	69.28 g/h

C 2.6Total Water Balance

Theoretical anode and cathode water collection rates

The theoretical anode and cathode water condensation/collection rates is given by the amount of anode or cathode water introduced into the cell minus the water exiting in the gas phase from the knockout drums.

For the anode:

$$m_{H_2O,5} = m_{H_2O,1} - m_{H_2O,3} = 13.24\frac{g}{h} - 1.1\frac{g}{h} = 12.14\frac{g}{h}$$

For the cathode the water produced during the reaction must be accounted for as follows:

$$m_{H_2O,6} = m_{H_2O,1} + m_{H_2O,rxn} - m_{H_2O,4} = 50.63\frac{g}{h} + 18.8\frac{g}{h} - 4.1\frac{g}{h} = 65.33\frac{g}{h}$$

Comparison of the measured anode and cathode water collection rates indicates that some water back diffusion occurred from the cathode to the anode.

The overall water balance:

$$m_{H_2O,5} + m_{H_2O,6} = 12.14\frac{g}{h} + 65.33\frac{g}{h} = 77.47\frac{g}{h}$$

Compared to the measured water collection

$$4.6\frac{g}{h} + 69.28\frac{g}{h} = 73.88\frac{g}{h}$$

Thus the error between the measured and theoretical water collection rates is:

$$Error = 100\% \left[\frac{77.47 \frac{g}{h} - 73.88 \frac{g}{h}}{73.88 \frac{g}{h}} \right] = 4.9\%$$

C 3Fuel Cell current density Calculations for Drive Cycle power data

C 3.1List of Terms

Variable	Description	Units
P_{FC}	Fuel cell stack power	W
i	Current density	A cm^{-2}
F	Faraday's Constant	C mol^{-1}
n_{cell}	Number of Cells	
A_{geo}	Geometric Surface area of each cell	cm^2
V_{cell}	Voltage	V

Given the following data and polarization/power curve

Variable	Description
P_{FC}	2064W
n_{cell}	400
A_{geo}	400 cm^2

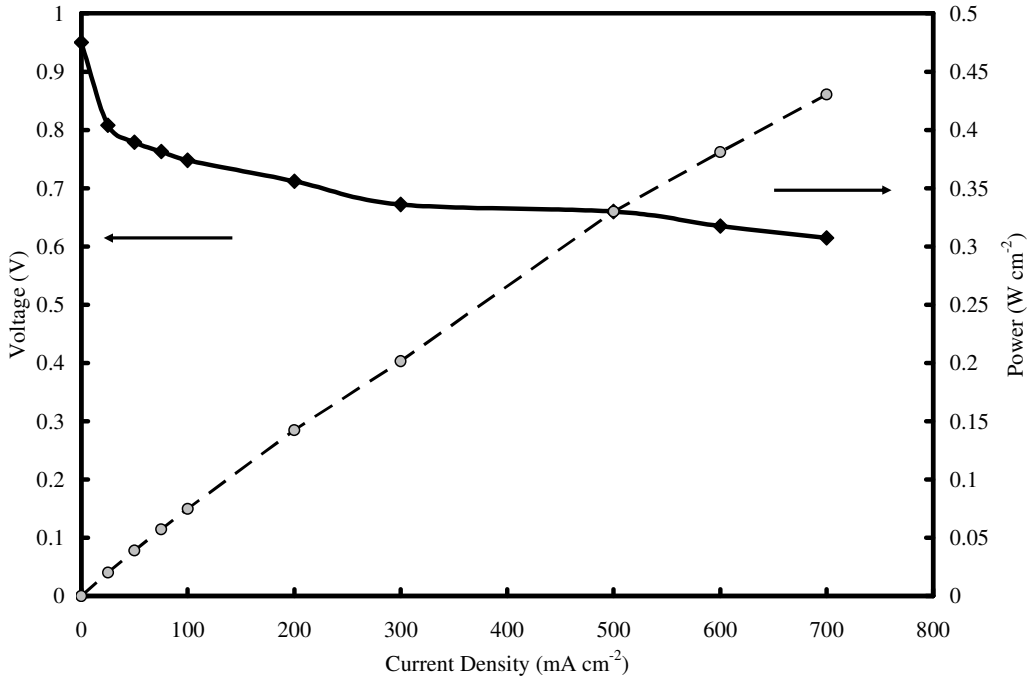

Power data used in the above Figure is as follows:

Current Density mA cm^{-2}	Power W cm^{-2}
0	0
25	0.0202
50	0.03895
75	0.057225
100	0.0748
200	0.1424
300	0.2016
500	0.33
600	0.381
700	0.4305

The power from the stack is given by:

$$P_{FC} = n_{cell} V_{cell} i_{cell} A_{geo}$$

Since the power for one cell is given by

$$P_{cell} = V_{cell} i_{cell} A_{geo} = \frac{P_{FC}}{n_{cell}} = \frac{2064W}{400} = 5.16W$$

thus

$$V_{cell} i_{cell} = \frac{P_{FC}}{n_{cell} A_{geo}} = \frac{5.16W}{400cm^2} = 0.0129 \frac{W}{cm^2}$$

Using the fuel cell power curve the current density for a given power density can be linearly interpolated from the data. For the above power density the corresponding current density would be expected to fall between 0 and 25 mA cm^{-2}.

Thus,

$$i_{cell_2} = \left(\frac{i_3 - i_1}{P_3 - P_1} \right) (P_2 - P_3) + i_3 = \left(\frac{25 - 0}{0.0202 - 0} \right) (0.0129 - 0.0202) + 25 = 15.96 \frac{mA}{cm^2}$$

APPENDIX D – DISCUSSION OF ERROR AND REPEATABILITY

D 1 Error in cumulative fluoride release curves

Cumulative fluoride release curves represent the backbone of the modeling work in this thesis and as such the error in their measurement must be addressed. There are two main sources of error; a) Water mass measurement and b) fluoride concentration.

a) Water measurement uncertainty arises from the sensitivity of the scale used. In the measurements done here scale accuracy was approximately +/- 0.05g.

b) Uncertainty in fluoride ion concentration measurements was evaluated by repeating measurements on random samples. Results showed that average variability was below +/- 3%.

Overall, since water measurements were typically greater than 10g, even at the lowest relative humidity settings, the measurement uncertainty is less than 1%, and therefore has a negligible impact on fluoride release curves. On the other hand, the uncertainty in fluoride concentration is much more significant. A +/- 3% uncertainty translates into a +/- 3% uncertainty in Total cumulative fluoride release values. Figure **** shows the results for Cells 1 – 3 and 6 with this uncertainty shown as error bars. It is clear that the differences between each curve is greater than the uncertainty implying that each cell was different.

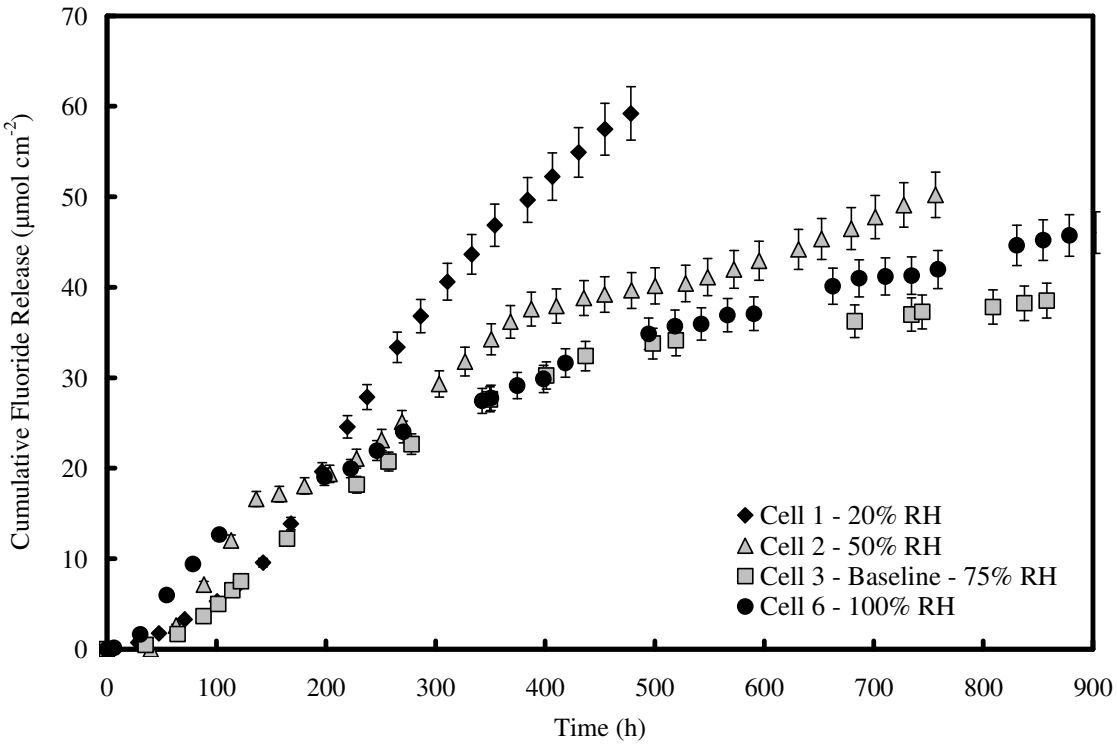

Shows the influence of this variability on the cumulative fluoride release results from Cells 1 – 3 and 6.

D 2 Voltage measurements

Voltage measurements shown in this thesis were typically voltage measurements from every 5 hours. Variability in voltage measurements were estimates by examining voltage measurements over 5 hour periods. In the worst case, measurements during the transient voltage degradation phase, variability over a 5 hour period was as low as 1.5 mV. This quantity is negligible compared to the measured voltages, thus it can be said that differences in voltage measurements shown in this thesis are the results of differences within the cells and not due to measurement uncertainty.

D 3 Comments on Cell – Cell Repeatability of cumulative fluoride release curves

Cumulative fluoride release data formed the basis of the modeling effort in the work presented in this thesis. As such, it is necessary to have confidence in the cumulative fluoride release curves to have confidence in the model. The following discussion examines the cell-cell repeatability of the data presented in this thesis. Due to the length

of time necessary to build and run each cell, also considering fuel cell test stand downtime, it was not possible to perform replicate experiments for each fuel cell test condition.

Even if time and cell materials were available, creating a true replicate is much more difficult than it appears. It is not enough to simply obtain a new membrane and repeat the cell conditions. Cell to cell variability in cumulative fluoride release curves, at specific operational conditions, is impacted by variability in material properties such as the membrane permeability. Since the proposed model attempts to account for the specific permeability of each membrane tested, a true replicate is one where not only cell operational conditions are repeated, but where material properties are also repeated.

One true replicate cell was done, Cell 4, and is discussed in Chapter 5. This cell had the same hydrogen permeability as Cell 3, the baseline cell, and was also operated at the same conditions of 75% RH and 90°C cell temperature. Unfortunately, an unavoidable issue with durability testing are cell stoppages and interruptions. As discussed in Chapter 5, interruptions in testing are suspected of impacting the cumulative fluoride release curves resulting in a curve for Cell 4 that did not perfectly overlay with the results from Cell 3. However, simulation results for Cell 3, when applied to Cell 4 with consideration of interruptions, showed excellent agreement with the data. This implies that had Cell 4 been able to operate without interruption, that the data would have matched the data from Cell 3. A second set of cells, Cells 5 and 6, were also operated at the same conditions. However, reliable fluoride release curves are not available for Cell 5 so comments about replication cannot be made.

Thus, with the exception of Cell 3 and 4, there were no other opportunities to reproduce cumulative fluoride release data. The result is that to gain confidence in the interpretation of the data one must rely on trends. The impact of initial hydrogen crossover and the effect of current density are two such trends.

APPENDIX E – MATLAB CODE

The following Matlab code models the fluoride release behaviour during an OCV test.

E 1 Main Program

The main program initializes all the necessary variable to solve the differential equations related to fluoride production and release. The code below represents the final second order model. Once variables are initialized they are passed to a function called ode23s which solves systems of stiff differential equations.

```
clc
clear

DeltaCath0 = 0.00075;   %inital cathode thickness
DeltaAn = 0.00075;      %anode thickness
P = 2.06e-8;            %permeability
H2P = 100;              %hydrogen partial pressure
K1 = 2.9e-2;            %degradation constant
K2 =4.7e-7;             %fluoride production constant
DGDL = 4.2e-9;          %fluoride diffusion constant through the
                        GDL/MPL/Cat layers
DIONA= 1.2e-10;         %fluoride diffusion constant through the
                        electrolyte layer
DelG = 0.0004;

Fo(1,204)=0;            %Initialize fluoride concentrations
DelT = 3600;            %Time increment

[t,y] = ode23s(@derr3, …
[0:DelT:3600000],[100,Fo],[],DeltaCath0,DeltaAn,P,H2P,K1,K2,…
DGDL,DIONA,DelG);

t = t./3600;


%use results to determine fluoride release rates at the GDL/channel

AFlux = y(:,3).*(DGDL/DelG);
CFlux = y(:,204).*(DGDL/DelG);

Melectrolyte = y(:,1);  % Percent of cathode electrolyte remaining with
t

%calculation of cumulative release
CumuA(1)=AFlux(1)*DelT;
```

```
CumuC(1)=CFlux(1)*DelT;

for k = 2:1:length(t)
    CumuA(k)=CumuA(k-1)+AFlux(k)*DelT;
    CumuC(k)=CumuC(k-1)+CFlux(k)*DelT;
end

CumuA = CumuA';
CumuC = CumuC';
```

E 2 Functions

The following function “derr3” calculated the time derivative of fluoride concentration at each spatial point. Method of lines is used to solve the differential equations.

```
function yprime = derr3(t,y,DeltaCath0,DeltaAn,P,H2P,K1,K2,
DGDL,DIONA,DelG,FRAC);

%y is a vector of sixe 205 with the following components
%y(1)= fraction of cathode electrolyte remaining
%y(2 - 205)= fluoride concentrations in the MEA

%K1 = Reaction rate constant for electrolyte degradation
%K2 = Conversion of electrolyte to fluoride
%DGDL = Diffusion Coiefficient of Fluoride ions through the GDL
%DIONA = Diffusion coefficient of F- through the anode electrolyte and
%reinforcement layer

%DelG = Space step size in the GDL

%need to determine the cathode thickness and hydrogen permeation rates

DeltaCath = y(1)*DeltaCath0/100;
DeltaTOT = DeltaCath + DeltaAn;

pFrac = 1;

H2Flux = P*H2P*pFrac/DeltaTOT;
O2Flux = H2P*.21*P/2.6/DeltaTOT;

yprime(1)=-1*abs(K1*H2Flux^2*y(1));

%Fluoride Generation

NF = -1*K2*yprime(1);

%Concentration at platinum band/ generation point

y(103)= (NF + y(102)*DIONA/DeltaTOT + y(104)*DGDL/DelG)/(DIONA/DeltaTOT
+ DGDL/DelG);
```

```
%Calculate the change in fluoride concentration in the MEA

yprime(2) = 0;%Anode GDL/Channel


for i = 3:1:101
    yprime(i)= DGDL*(y(i-1)-2*y(i)+y(i+1))/(DelG^2);
end

yprime(102)= (1/DeltaTOT)*((DIONA*(y(103)-y(102))/DeltaTOT)-
(DGDL*(y(102)-y(101))/DelG));

yprime(103) =0;

for j = 104:1:204
    yprime(j) = DGDL*(y(j-1)-2*y(j)+y(j+1))/(DelG^2);
end

yprime(205)=0;%Cathode GDL/Channel


yprime = yprime';
```